

Contract No. DTFACT-15-D-00007
Delivery Order 005 NAPTF Support
Deliverable 4.9.2.6.2: CC8 Phase 4 Strength/Fatigue
Traffic Test Report – Inner Lane

Submitted on February 12, 2021

Prepared by GDIT
with Horizon Engineering Consulting, LLC

TABLE OF CONTENTS

	Page
1. INTRODUCTION	1
2. DESIGN AND CONSTRUCTION OF TEST SECTION	1
3. DESCRIPTION OF TESTING METHODS AND EQUIPMENT	2
3.1 TESTING EQUIPMENT	2
3.2 TEST DESCRIPTION	2
3.2.1 STAGE 1 – CRACK INITIATION	5
3.2.2 STAGE 2 – CRACK PROPAGATION	8
3.2.3 TEST PROCEDURE	10
4. FULL-SCALE TEST	10
4.1 STATIC LOAD TEST (NORTH)	10
4.2 MOVING LOAD TEST (NORTH AND SOUTH)	13
5. BEHAVIOR OF TEST AREA UNDER TRAFFIC	17
5.1 DISTRESS MAPPING	17
5.2 SUMMARY OBSERVATION	17
6. PRELIMINARY DATA ANALYSIS	19
6.1 CHARACTERIZATION OF CRACK PROPAGATION	19
6.1.1 DISTRESS DATA	19
6.1.2 INSTRUMENTATION DATA	22
6.2 PAVEMENT EVALUATION	28
6.2.1 PCC SLAB MODULUS	28
6.2.2 HWD DEFLECTION	29
6.3 PCC SLAB CRACKING STRENGTH	43
7. ADVANCED DATA ANALYSIS	46
7.1 FAILURE MECHANISM	46
7.1.1 PAVEMENT DEFORMATION ENERGY FOR CRACK CHARACTERIZATION	46
7.1.2 INTERNAL STRAIN ENERGY IN PCC SLAB FOR CRACK CHARACTERIZATION	51
7.1.3 TENSILE STRESS RATIO	53
7.2 EFFECT OF CONCRETE FLEXURAL STRENGTH AND SLAB THICKNESS ON FATIGUE LIFE	56
7.3 EFFECT OF SUBGRADE STRENGTH ON FATIGUE LIFE	56
7.4 COMPARISON OF NOTCHED VERSUS UNNOTCHED SLABS	57
7.5 FIELD EXPERIMENT VERSUS FAARFIELD	57

8. CC8 S/F TEST PAUSE AND TRAFFIC RESUMPTION	58
8.1 SLAB CURLING MONITORING	58
8.2 INSTRUMENTATION VERIFICATION	65
8.3 UPDATED BASELINE HWD AND PSPA TESTS	67
8.4 VISUAL INSPECTION OF SLAB CONDITION	68
8.5 RECOMMENDATION ON TRAFFIC RESUMPTION	71
9. CONCLUSIONS	72
9.1 INSTRUMENTATION AND FIELD TESTING	72
9.2 CRACKING STRENGTH	72
9.3 MOVING LOAD TESTS	72
9.4 FIELD EXPERIMENT VERSUS FAARFIELD	73
10. REFERENCES	74
Appendix A – Summary of Seating Load Pattern	
Appendix B – CC8 Phase 4 Strength Fatigue Distress Maps	
Appendix C – CC8 Phase 4 Strength Fatigue Distress Map Written Log	
Appendix D – Embedded Strain Gauge (EG) Data Analyzed for Crack Characterization	

LIST OF FIGURES

Figure	Page
Figure 1. Rigid Pavement Failure Model in FAARFIELD (Reproduced from Guo et al. 2008)	1
Figure 2. Slab Groups in CC8 Phase 4 – S/F Test Area	3
Figure 3. Initial Gear Configuration used for CC8 Phase 4 S/F Tests on Inner Lanes	4
Figure 4. Position of D NAPTV Module for Static Load Tests	6
Figure 5. Aircraft Gear Configuration for FEAFAA Simulations: (a) S module, and (b) D module	7
Figure 6. NAPTV Module Positions for Moving Load Test	9
Figure 7. Static Load Test on the North Inner Lane, Slab SF2N - Strain vs. Load	10
Figure 8. Tensile Strain vs. Load using D Module, North Inner Lane: (a) SF1N (12 inch),	11
Figure 9. Tensile Strain vs. Load using S Module, North Inner Lane: (a) SF1N (12 inch),	12
Figure 10. Moving Load Test	13
Figure 11. Current Distress Map for Inner Lanes (Groups 1-4, Last Updated: March 19, 2020)	20
Figure 12. Current Distress Map for Inner Lanes (Groups 5-8, Last Updated: March 19, 2020)	21
Figure 13. Response of Top EG in SF2N (12-inch PCC Slab)	22
Figure 14. Response of Top EG in 9-inch PCC Slabs: (a) SF5N, (b) SF6N	23
Figure 15. Response of Bottom EG in SF4N (9-inch PCC Slab)	24
Figure 16. Response of Bottom EGs in 9-inch PCC slabs: (a) SF7N, (b) SF8N	25
Figure 17. NAP Trends in 9-inch PCC Slabs: (a) SF7N, (b) SF8N	26
Figure 18. Response of Top and Bottom EGs in 9-inch PCC slabs: (a) SF7N, (b) SF8N	27
Figure 19. PSPA Slab Modulus: (a) North Inner Lanes (Group 1 & 3: 12 inch), (b) North Inner Lanes (Group 5 & 7: 9 inch), (c) South Inner Lanes (Group 2 & 4: 12 inch), (d) South Inner Lanes (Group 6 & 8: 9 inch)	28
Figure 20. Slab Center Deflection Basins, North Inner Lanes	30
Figure 21. Slab Center Deflection Basins, South Inner Lanes	31
Figure 22. ISM vs. Cumulative Passes for Inner Lanes: (a) North (Group 1 & 3), (b) North (Group 5 & 7), (c) South (Group 2 & 4), (d) South (Group 6 & 8)	33
Figure 23. Corner-to-Center Deflection Ratio vs. Cumulative Passes for Inner Lanes: (a) North (Group 1 & 3), (b) North (Group 5 & 7), (c) South (Group 2 & 4), (d) South (Group 6 & 8)	34
Figure 24. Change in Slab Temperature over the Course of Trafficking: (a) Average Slab Temperature, (b) Temperature Differential (Top-Bottom)	35
Figure 25. Example of Void Detection in Corner 8SW of Slab SF8S	36
Figure 26. Intercept vs. Cumulative Passes for Inner Lanes: (a) North (Group 1 & 3), (b) North (Group 5 & 7), (c) South (Group 2 & 4), (d) South (Group 6 & 8)	37
Figure 27. Backcalculated Moduli of P-501MR vs. Cumulative Passes for Inner Lanes:	39
Figure 28. Backcalculated Moduli of P-306MR vs. Cumulative Passes for Inner Lanes:	40
Figure 29. Backcalculated Moduli of P-154M vs. Cumulative Passes for Inner Lanes:	41
Figure 30. Backcalculated Moduli of P-152M vs. Cumulative Passes for Inner Lanes:	42
Figure 31. Load-induced Strain during Static Load Tests on SF1N: (a) Load vs. Strain, (b) Change in Neutral Axis Position	44
Figure 32. Load-induced Strain during Static Load Tests on SF5N: (a) Load vs. Strain, (b) Change in Neutral Axis Position	45
Figure 33. Pavement Deformation Energy on 12-inch Thick Slabs in North Inner Lanes: (a) SF1N, (b) SF2N, (c) SF3N, (d) SF4N	47

Figure 34. Pavement Deformation Energy on 12-inch Thick Slabs of South Inner Lanes: (a) SF1S, (b) SF2S, (c) SF3S, (d) SF4S	48
Figure 35. Pavement Deformation Energy on 9-inch Thick Slabs on North Inner Lanes: (a) SF5N, (b) SF6N, (c) SF7N, and (d) SF8N	49
Figure 36. Pavement Deformation Energy on 9-inch Thick Slabs on South Inner Lane: (a) SF5S, (b) SF6S, (c) SF7S, (d) SF8S	50
Figure 37. Derivation of Bending Moment from Strain Profile	51
Figure 38. Change in Internal Strain Energy Over the Course of Trafficking: (a) Slab SF7N, (b) Slab SF8N	52
Figure 39. Change in Total Tensile Stress Over the Course of Trafficking: (a) SF7N, (b) SF8N	54
Figure 40. Change in Tensile Stress Ratio Over the Course of Trafficking: (a) SF7N, (b) SF8N	55
Figure 41. Corner Displacement in 12-inch Thick Slabs: (a) SF1N, (b) SF4N, (c) SF1S, (d) SF4S	60
Figure 42. Corner Displacement in 9-inch Thick Slabs: (a) SF5N, (b) SF8N, (c) SF5S, (d) SF8S	62
Figure 43. Daily Variation in Slab Temperature, August 18-20, 2020: (a) North, (b) South	63
Figure 44. Corner Displacement vs. Temperature Differential: (a) 12-inch Slabs, (b) 9-inch Slabs	65
Figure 45. Maximum HWD Deflection at Center of Slabs: (a) North, and (b) South	67
Figure 46. Slab Modulus from PSPA Testing at the Center of Slabs: (a) North, and (b) South	68
Figure 47. Shrinkage Cracks on Slab SF4N	68
Figure 48. Joint Faulting Measurement: (a) Field Measurement, (b) Faulting Interpretation, (c) Measurement Locations	69
Figure 49. Surface Elevation Mapping: (a) Placement of Straight Edge, (b) Surface Measurement	70
Figure 50. Slab Surface Elevation Map: (a) North (SF3N and SF4N), (b) South (SF5S and SF6S)	71

LIST OF TABLES

Table	Page
Table 1. Summary of Slab Groups	4
Table 2. Summary of CC8 S/F Traffic Tests	5
Table 3. Summary of CC8 S/F Inner Lane Traffic Tests	6
Table 4. Summary of Static Load Test Results	12
Table 5. Determination of Traffic Loads	14
Table 6. Traffic History of Moving Load Test on Inner Lanes	15
Table 7. Pavement Deterioration History of Inner Lanes	18
Table 8. Summary of PSPA Modulus (First and Last Round of Testing)	29
Table 9. Summary of Material Properties for Back-calculation	38
Table 10. Summary of Load-induced Maximum Fiber Strain, Stress, and Stress Ratio	46
Table 11. Summary of Estimated Residual Stresses	53
Table 12. Summary of Stress Ratio Analysis	56
Table 13. Load-Induced Stresses (Subgrade with CBR 7-8 vs Subgrade with CBR 3-4)	57
Table 14. FAARFIELD Predicted Fatigue Life Allocated to Each Stage	58
Table 15. Assessment of Gauge Functionality for Traffic Resumption	66
Table 16. Summary of Joint Faulting Measurement	70

LIST OF ACRONYMS

ASTM	American Society for Testing Materials
CBR	California Bearing Ratio
CC6	Construction Cycle 6
CC8	Construction Cycle 8
CV	Coefficient of Variation
D	Dual (two-wheel)
DF	Design Factor
ECS	Eddy Current Sensors
EG	Embedded Strain Gauge
FAA	Federal Aviation Administration
FAARFIELD	FAA Rigid and Flexible Iterative Elastic Layered Design
FEAFAA	Finite Element Analysis - FAA
HWD	Heavy Weight Deflectometer
ID	Identifier
ISM	Impact Stiffness Modulus
NAPTF	National Airport Pavement Test Facility
NAPTV	National Airport Pavement Test Vehicle
PCC	Portland Cement Concrete
PSPA	Portable Seismic Properties Analyzer
R	Concrete Flexural Strength
S	Single (single wheel)
SCI	Structural Condition Index
S/F	Strength/Fatigue

1. INTRODUCTION

Full-scale tests of Phase 4 of Construction Cycle 8 (CC8) are aimed at determining the cracking strength and fatigue life of concrete slabs designed and built to Federal Aviation Administration (FAA) standards (FAA, 2017, 2018); hence this phase is designated the Strength/Fatigue (S/F) test.

CC8 S/F tests at the National Airport Pavement Test Facility (NAPTF) are conducted on four lanes of slabs. The previous report on CC8 S/F covered traffic on the two outer lanes. This report documents the continuation of full-scale tests on the remaining 2 inner lanes. A discussion on the research need for the S/F test can be found in the CC8 S/F Test Report – Outer Lane.

The Structural Condition Index (SCI) is the summation of structural distresses from the Pavement Condition Index (PCI) survey. The FAA rigid pavement design is based on the failure model proposed by Rollings in 1988 (Rollings, 1988), which uses the SCI as a measure of pavement performance (see figure 1) (FAA, 2017). The primary objective of the CC8 S/F test is to isolate the three stages of the bottom-up cracking mechanism in rigid pavements and estimate the fatigue life contribution of all three stages in the failure model.

The series of full-scale tests were designed to obtain data from individual slabs regarding: (1) slab cracking strength for comparison to ASTM C78 (ASTM, 2018); (2) bottom-up crack propagation in notched slabs (Stage 2 only); (3) crack initiation and propagation in unnotched slabs (Stages 1 and 2); and (4) the trade-off between concrete flexural strength (R) and slab thickness as both factors affect fatigue life. In addition, the effect of subgrade strength is considered by including two California Bearing Ratio (CBR) values, 3-4 and 7-8.

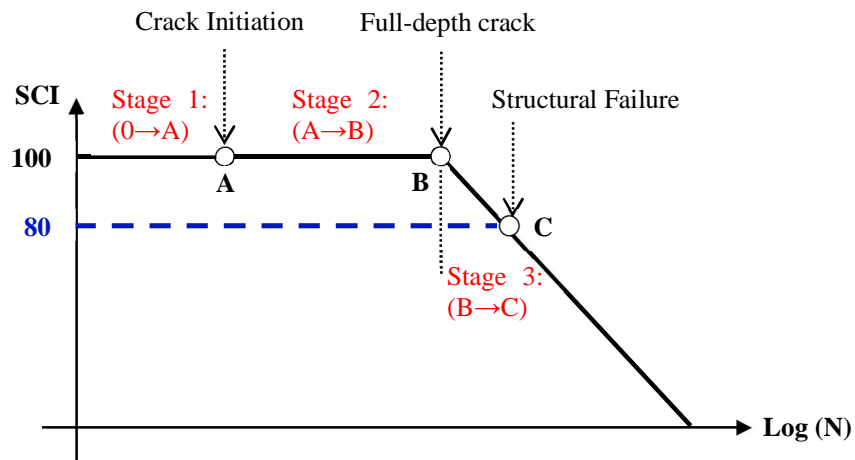


Figure 1. Rigid Pavement Failure Model in FAARFIELD (Reproduced from Guo et al. 2008)

2. DESIGN AND CONSTRUCTION OF TEST SECTION

Figure 2 shows the plan view of the test area. There is a total of thirty-two 15 × 15 ft. slabs, 16 on each side of the test area centerline. These 32 slabs were divided into 8 groups of four, as indicated

by the red dashed lines in the figure, based on combinations of (a) slab thickness, (b) design flexural strength R ; and (c) subgrade CBR. The black horizontal dashed line on the south side represents the notch location. The notch is intended to induce crack initiation at the bottom of slabs, directly under the traffic path. Neither longitudinal nor transverse joints were dowelled to prevent load transfer between slabs. Table 1 summarizes slab thickness, design flexural strength (R), and subgrade strength of each slab group.

The cross-section of slab groups 1-4 consists of 12.1 inch P-501MR (cement concrete pavement) on 6 inch P-306MR (lean concrete base course) on 13.7 inch P-154MR (granular subbase course). The structure is supported on a prepared P-152MR (subgrade) clay with CBR 7-8. The cross-section for slab groups 5-8 consists of 9 inch P-501MR on 6 inch P-306MR on 16.7 inch P-154MR. The structure of groups 5-6 and groups 7-8 is supported on P-152MR clay of CBR 7-8 and 3-4, respectively. A general overview of construction and instrumentation of the CC8 S/F test area was provided in the CC8 S/F Test Report – Outer Lane (HEC, 2020). Also, more detailed information can be found in the CC8 Construction Report (Tomlinson, et al. 2018).

3. DESCRIPTION OF TESTING METHODS AND EQUIPMENT

3.1 TESTING EQUIPMENT

General features of the National Airport Pavement Test Vehicle (NAPTV) were previously described in the CC8 S/F Test Report – Outer Lane (HEC, 2020). For comparison purposes, both static and moving load tests on the inner lanes were originally planned with a two-wheel (D) module (Figure 33). Due to the limited wheel load capacity of the D module, static load tests on the north inner lanes were later on completed using single wheel (S) module. All moving load tests were initially conducted using D module.

3.2 TEST DESCRIPTION

As shown in figure 1, rigid pavement failure progresses through stages. Stage 1 is the initiation of a crack in a new or intact pavement. The CC8 S/F experiment started with stationary-load crack initiation tests to determine the cracking strength of selected slabs. For four slabs on the north inner lanes (SF1N, SF2N, SF5N and SF6N), the static load was initially conducted using a D module, with the tires spaced 34 inch apart (i.e., distance between inner tire edges). After reaching maximum load capacity with no indication of crack initiation from embedded strain gauge (EG) responses, the static load test on these four slabs had to be completed using an S module, which can attain wheel loads up to 150,000 lbs. The remaining slabs on the north (SF4N, SF4N, SF7N and SF8N) were not pre-cracked, so in those slabs the crack initiation (Stage 1) was intended to be achieved “naturally” by the moving gear load.

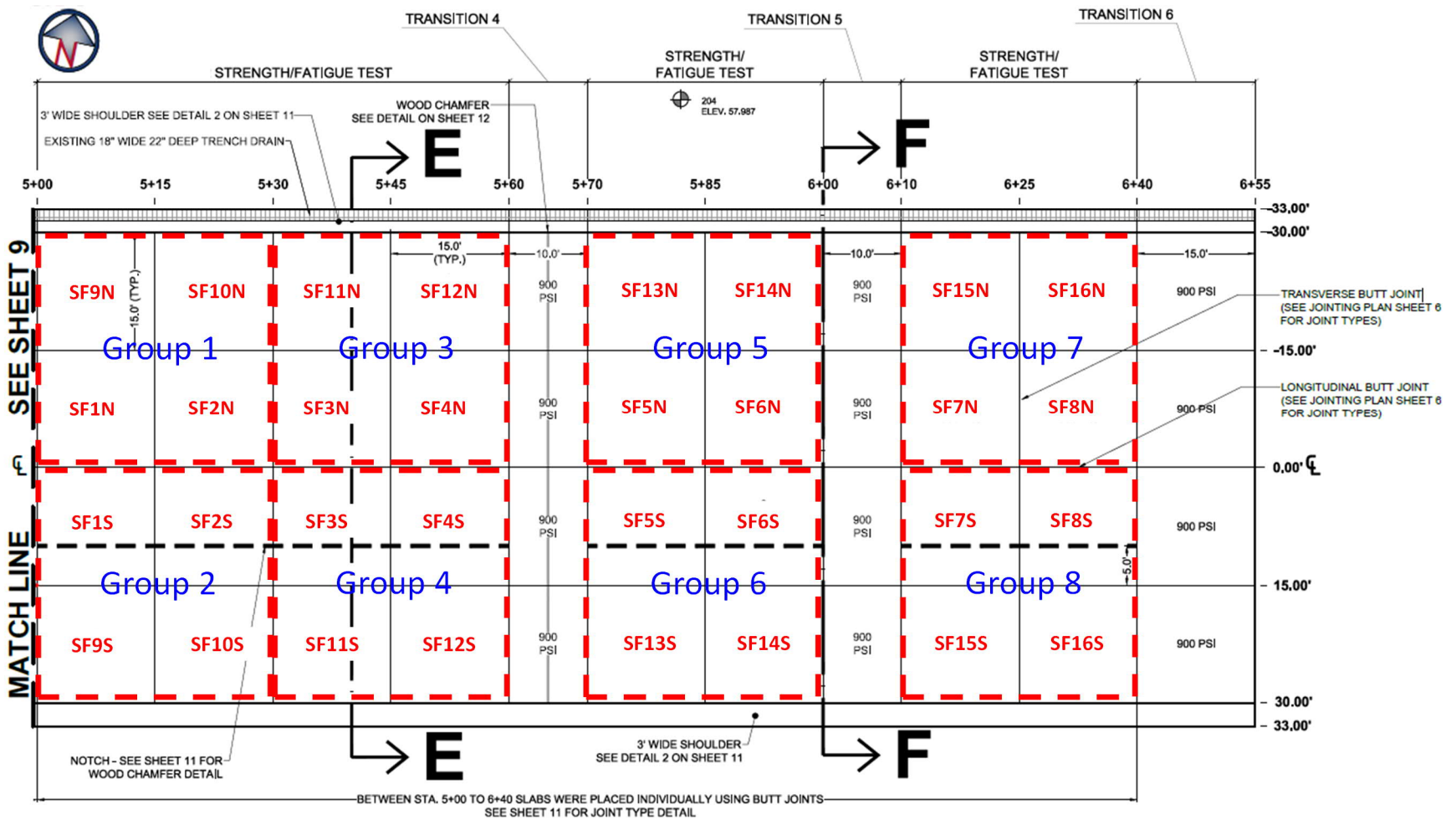
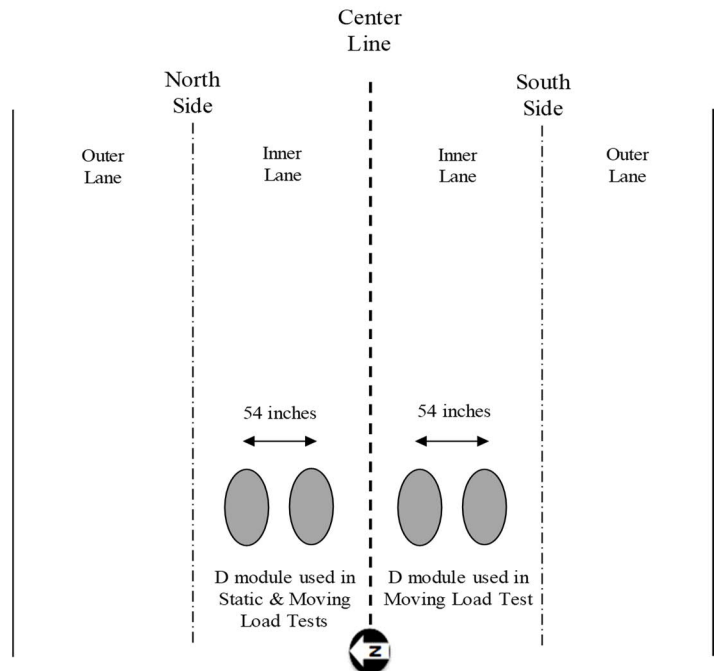


Figure 2. Slab Groups in CC8 Phase 4 – S/F Test Area

Table 1. Summary of Slab Groups

Group	Test Item	Lane	Notched / Unnotched	Slab Thickness (inch)	Flexural Strength R (psi)	CBR (%)
1	North	Inner and Outer	Unnotched	12	650	7-8
2	South	Inner	Notched	12	650	7-8
2	South	Outer	Unnotched	12	650	7-8
3	North	Inner and Outer	Unnotched	12	650	7-8
4	South	Inner	Notched	12	650	7-8
4	South	Outer	Unnotched	12	650	7-8
5	North	Inner and Outer	Unnotched	9	900	7-8
6	South	Inner	Notched	9	900	7-8
6	South	Outer	Unnotched	9	900	7-8
7	North	Inner and Outer	Unnotched	9	900	3-4
8	South	Inner	Notched	9	900	3-4
8	South	Outer	Unnotched	9	900	3-4



**Since maximum load capacity under D module was reached, static load tests on north inner lanes were ultimately completed with S module.*

Figure 3. Initial Gear Configuration used for CC8 Phase 4 S/F Tests on Inner Lanes

The eight notched slabs on the south inner lane (SF1S-SF8S) were treated as pre-cracked, due to the weakened plane formed by the notch. It was assumed that for the notched slabs there was no Stage 1, and all load-related damage would be concentrated in Stages 2 and 3. After the completion of stationary load tests for crack initiation, the test proceeded to apply moving loads for crack propagation in pre-cracked slabs on the north and notched slabs on the south, and crack initiation and propagation in non-pre-cracked slabs on the north. For comparison purposes, all moving load tests on inner lanes were conducted using the D module. All applied traffic was zero-wander (i.e., traffic applied over a single transverse position) due to the simplicity of quantifying the failure mechanism (Guo et al., 2012). The vehicle speed was limited to 2.5 mph. The traffic tests conducted during CC8 S/F experiment are summarized in table 2.

Table 2. Summary of CC8 S/F Traffic Tests

Crack Initiation					Crack Propagation			
Group	Test Item	Lane	Static Load	Moving Load	Group	Test Item	Lane	Moving Load
1, 5	North	Inner	D ¹	-	1, 3, 5, 7	North	Inner	D
3, 7	North	Inner	-	D	2, 4, 6, 8	South	Inner	D

¹Since maximum load capacity under D module was reached, static load tests were completed with S module.

3.2.1 STAGE 1 – CRACK INITIATION

During Stage 1, selected concrete slabs were brought from a new condition to the point where bottom-up cracks initiate by applying static and moving loads.

3.2.1.1 STATIC LOAD CRACK INITIATION

Static load tests were performed to initiate bottom-up cracks at transverse joints on the north inner lane. Static load tests were initially conducted on slabs SF1N, SF2N, SF5N and SF6N, using a D module. After reaching maximum load capacity with no indication of bottom-up cracking from EG responses, cracking loads were then achieved using the S module which allowed further increasing the wheel load. As shown in figure 4, the NAPTV was positioned such that the front edge of the tire print (S module) or one of the tire prints (D module) was aligned with the transverse joint, and directly over the transverse EG pair of interest. This position produces the maximum tensile stress at the slab bottom (Guo et al., 2012).

The initial wheel load of 5,000 lbs was applied, held for approximately 10s, and then released. During this interval, strain gauge responses (e.g., EG-N-FS-II-5/6 in slab SF1N for D module in figure 4) were acquired at a rate of 20 Hz. The wheel load was then increased in 2,500 lbs increments and the procedure repeated until strain gauge responses indicated a rupture at the slab bottom. The final wheel load (cracking load) for the tested slab was noted. The load sequence was repeated on the opposite side of the slab in the same wheel path. The locations for crack initiation test and the EGs to monitor are provided in table 3.

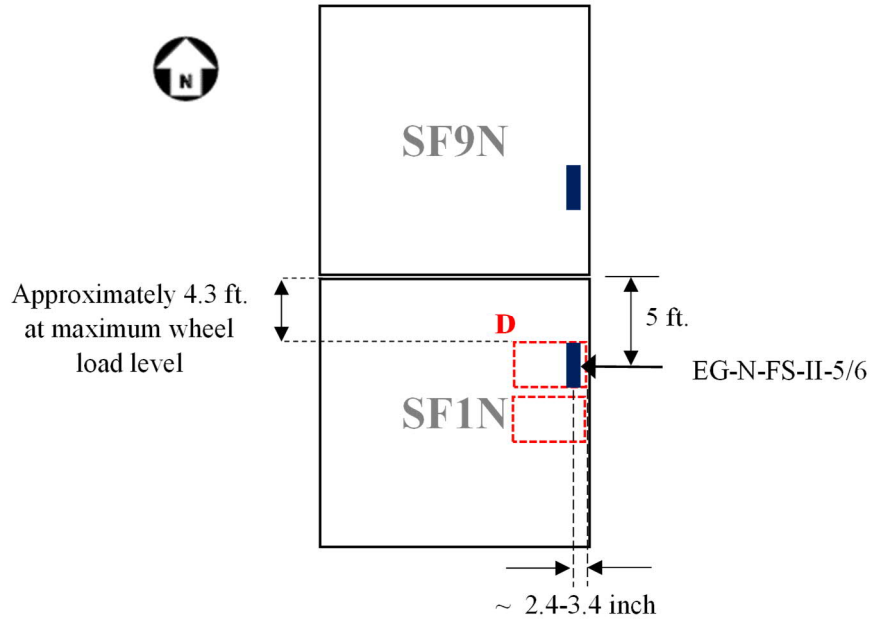


Figure 4. Position of D NAPTIV Module for Static Load Tests

Table 3. Summary of CC8 S/F Inner Lane Traffic Tests

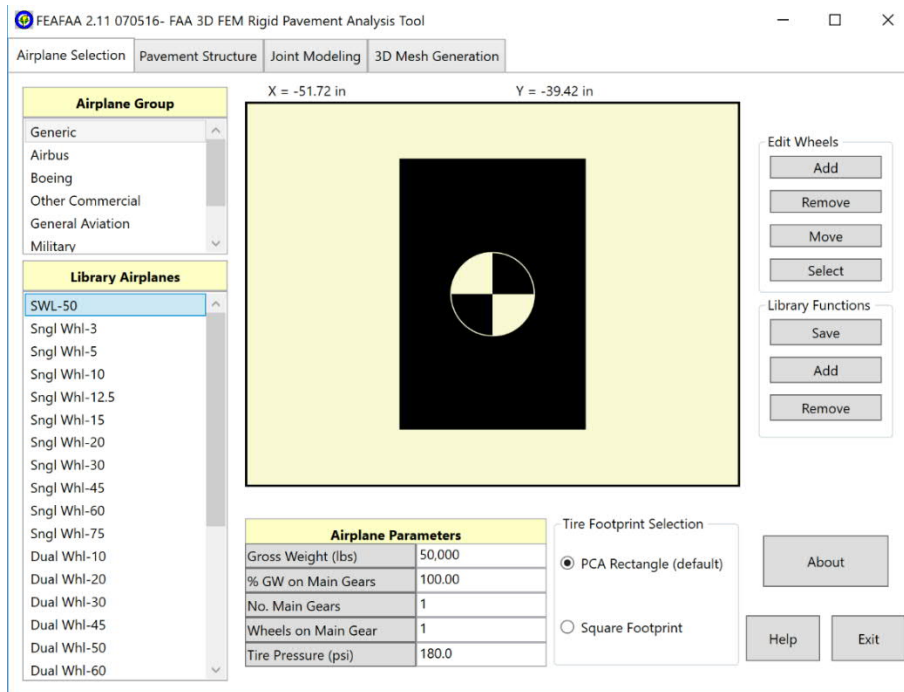
Group	NAPTIV Module	Slab	EG to Monitor	Transverse Joint ¹
1	D	SF1N	-	STA 5+00
			EG-N-SF-II-6	STA 5+15
	D	SF2N	EG-N-SF-II-8	STA 5+15
			-	STA 5+30
5	D	SF5N	-	STA 5+70
			EG-N-SF-II-38	STA 5+85
	D	SF6N	EG-N-SF-II-40	STA 5+85
			-	STA 6+00

Prior to the initiation of full-scale tests, the theoretical wheel load magnitude required to initiate bottom-up cracks along transverse joints was estimated by simulation using Finite Element Analysis – FAA (FEAFAA) v2.11. The free edge stress was calculated assuming:

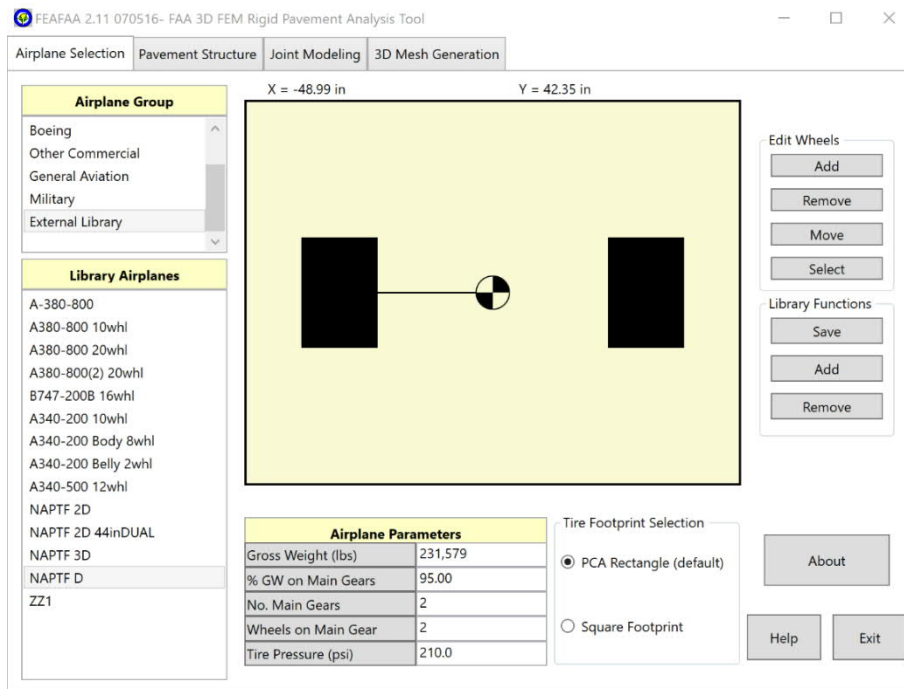
- Aircraft gear configurations: SWL-50 (figure 5a) and NAPTIV D (figure 5b);
- As-built pavement structure; and
- Layer properties of standard FAA materials

The initial wheel load of 50,000 lbs was incrementally increased by 1,000 lbs until the calculated maximum free edge stress had reached the flexural strength of lab-cured concrete beams. Theoretical cracking loads of 54,000 lbs and 63,000 lbs that would result in a stress ratio of 1.0 were determined for groups 1-4 (12-inch slabs) and 5-8 (9-inch slabs), respectively. These

theoretical values represented 50% and 71% of the actual average cracking load for groups 1-4 (with target $R=650$ psi) and 5-8 (with target $R=900$ psi), respectively, as determined from static load test results (section 4.1).



(a)



(b)

Figure 5. Aircraft Gear Configuration for FEAFAA Simulations: (a) S module, and (b) D module

3.2.1.2 MOVING LOAD

Prior to the initiation of full-scale tests, the FAARFIELD rigid pavement failure model (Brill, 2010) was used to estimate the level of traffic required to attain “first crack” condition. The details on the calculation method were previously documented in the CC8 S/F Test Report – Outer Lane (HEC, 2020). It was initially found that at 80% of cracking load, the FAARFIELD failure model predicted single digit coverages causing initial rupture at the bottom of slab. The analysis was later updated using the load-induced strain obtained from the moving load test. Results of the updated analysis are discussed in section 7.5.

Zero-wander traffic was applied to both north and south side for the moving load tests. Although the entire inner lane on the north side was trafficked with D module, only groups 1 and 3 were instrumented to monitor crack initiation. Following tracks N2 and S2 in figure 6, the NAPTIV carriages were positioned such that the module traveled directly above the EG pairs of interest. Note that tracks N2 and S2 are specific for this test and are not related to any wander patterns used in previous construction cycles at the NAPTF to approximate a normal distribution of aircraft traffic.

Laboratory beam fatigue test conducted during CC6 identified 0.8 as a suitable stress ratio (i.e., edge stress to flexural strength) for attaining crack propagation within a reasonable number of passes while not exceeding the project time frame (Guo et al., 2012). The procedures developed for the earlier CC6 Strength Test were followed to set traffic loads at 80% of the average cracking loads from the static tests. Trafficking continued until the strain responses indicated rupture at the gauge location.

3.2.2 STAGE 2 – CRACK PROPAGATION

Once bottom-up cracks were initiated, additional trafficking was executed to complete Stage 2, characterized by the development of a full-length and full-depth crack. The Stage 2 failure mechanism was quantified by a rolling wheel test at 80% of the bottom-up cracking load. On both the north and south side, the D module was used to propagate cracks to the surface on inner lanes. The vehicle speed was 2.5 mph traveling in both West to East (W→E) and East to West (E→W) directions at the transverse gear positions, as shown in figure 6.

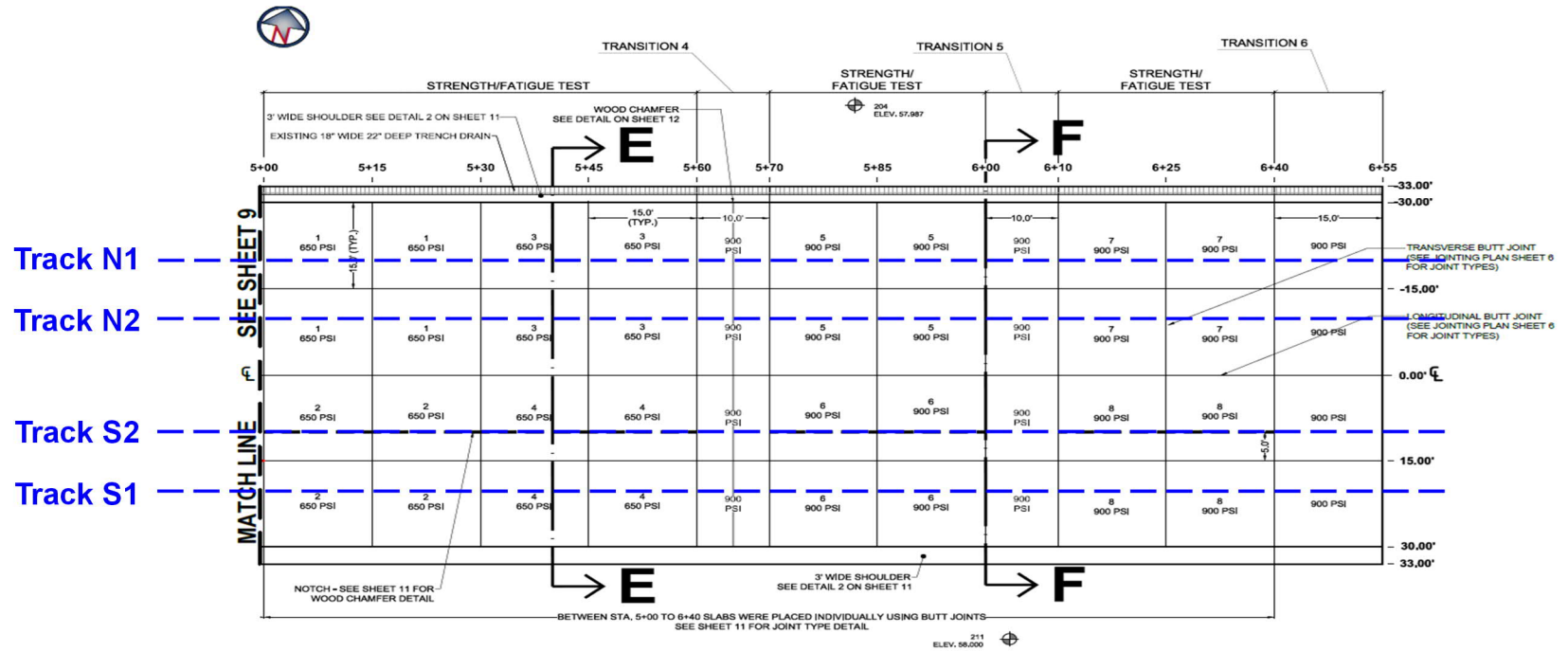


Figure 6. NAPTV Module Positions for Moving Load Test

3.2.3 TEST PROCEDURE

The detailed test procedure can be found in the CC8 S/F Test Report – Outer Lane.

4. FULL-SCALE TEST

The full-scale tests on the inner lanes were conducted in two phases: static and moving load testing. The static load test was aimed at attaining the initiation of bottom-up cracking (Stage 1) in selected slabs of the north inner lanes. The notched slabs on the south were treated as pre-cracked, due to the weakened plane formed by the notch. The moving load test aimed at achieving both crack initiation and propagation (Stage 1-3) in the non-pre-cracked slabs of the north inner lane. In pre-cracked and notched slabs on both north and south side, respectively, the moving load test was intended to cover only crack propagation (Stage 2 and 3).

4.1 STATIC LOAD TEST (NORTH)

During static load tests on the north inner lane, strain gauge data were collected over two days, August 22-23, 2018. Twelve-inch thick slabs SF1N and SF2N, and 9-inch thick slabs SF5N and SF6N were initially subjected to the static load using D module. After reaching maximum load capacity (i.e., 75,000 lbs) with no indication of bottom-up cracking from transverse EG responses, cracking loads were then achieved using the S module which allowed further increasing the wheel load.

Figure 7 shows an example of a static load test to initiate a bottom-up crack in slab SF2N. For this test, the NAPT V S module was positioned as described in section 3.2.1.1 and illustrated in figure 4. The initial wheel load of 5,000 lbs was applied, held for approximately 10s, and then released. The wheel load was then increased in 2,500 lbs increments and the procedure repeated until the response of transverse gauge EG-N-SF-II-8 indicated a rupture at the slab bottom. The relationship observed between the recorded strain and applied load in figure 7 was approximately linear at low load levels. The relationship flattens at approximately 90,000 lbs before turning highly nonlinear at an inflection point corresponding to 110,000 lbs, which indicates the crack formation.

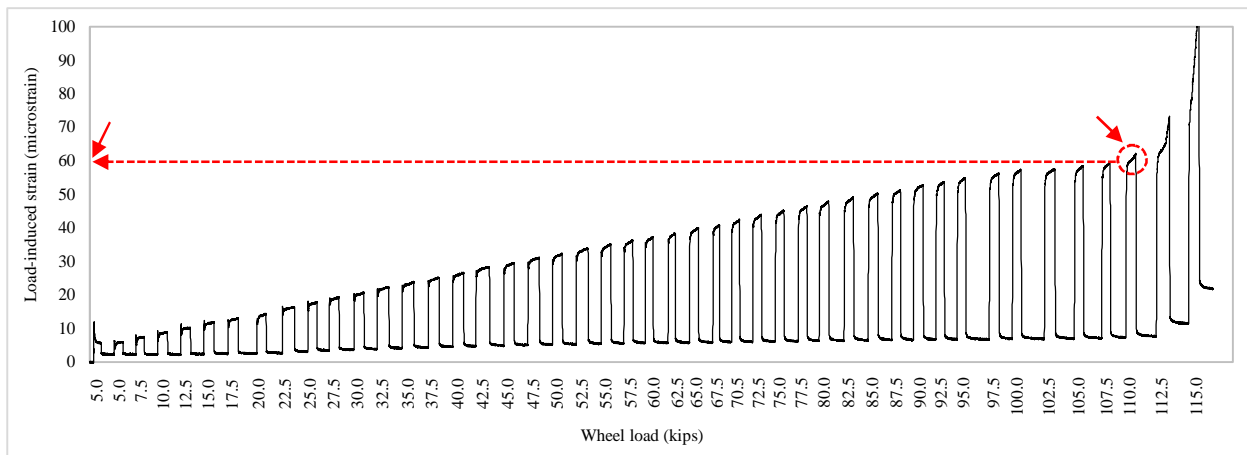


Figure 7. Static Load Test on the North Inner Lane, Slab SF2N - Strain vs. Load

Figure 8 shows the relation between tensile strain and wheel load for 12 inch and 9 inch-thick slabs in the north inner lane, respectively. Up to the maximum load capacity with D module (i.e., 75,000 lbs), no indication of bottom-up cracking was observed from transverse EG responses. Figure 9 shows the relation between tensile strain and S module wheel load for the same slabs. Table 4 summarizes both cracking loads and strains from static load tests using the S module.

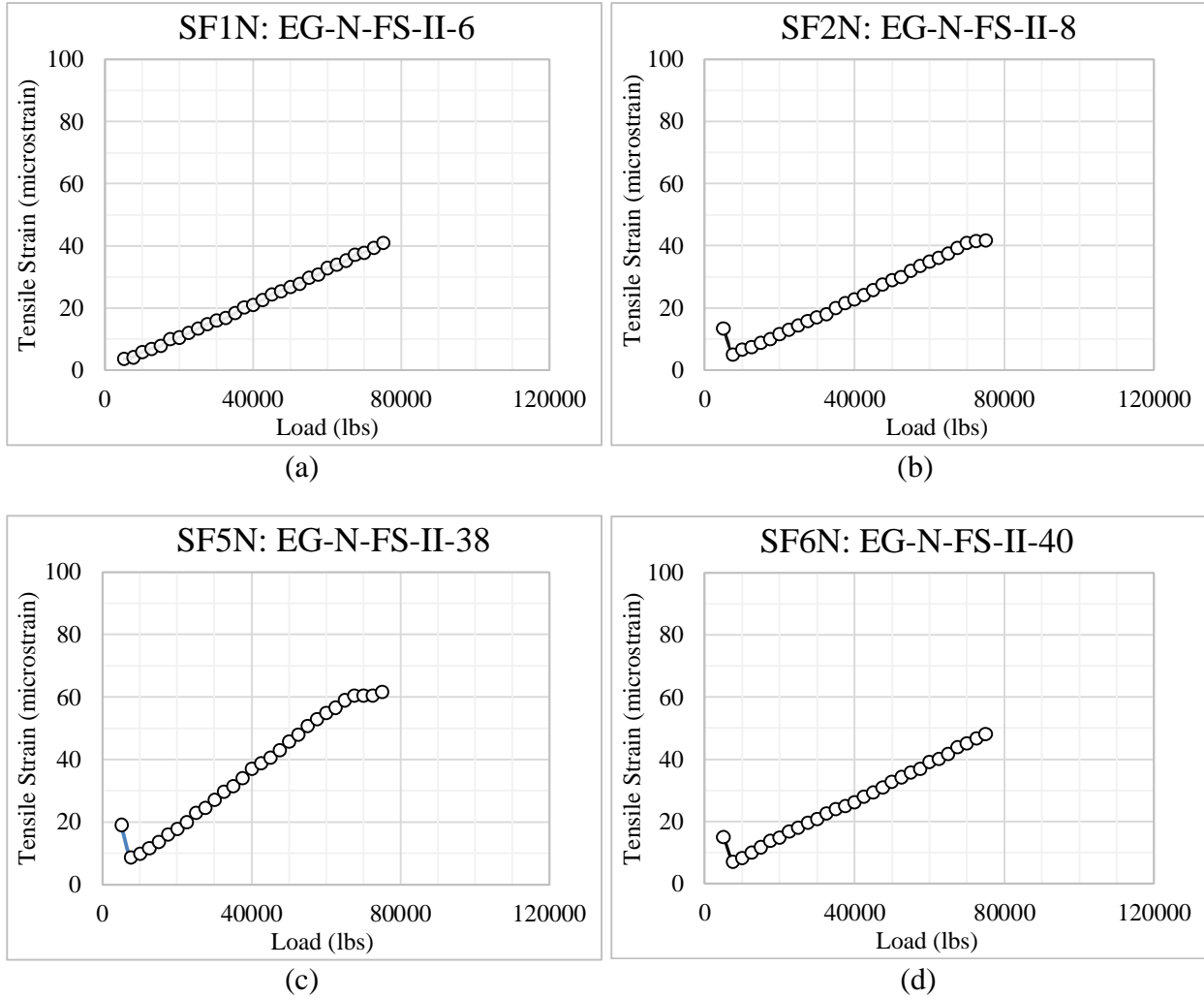


Figure 8. Tensile Strain vs. Load using D Module, North Inner Lane: (a) SF1N (12 inch), (b) SF2N (12 inch), (c) SF5N (9 inch), (d) SF6N (9 inch)

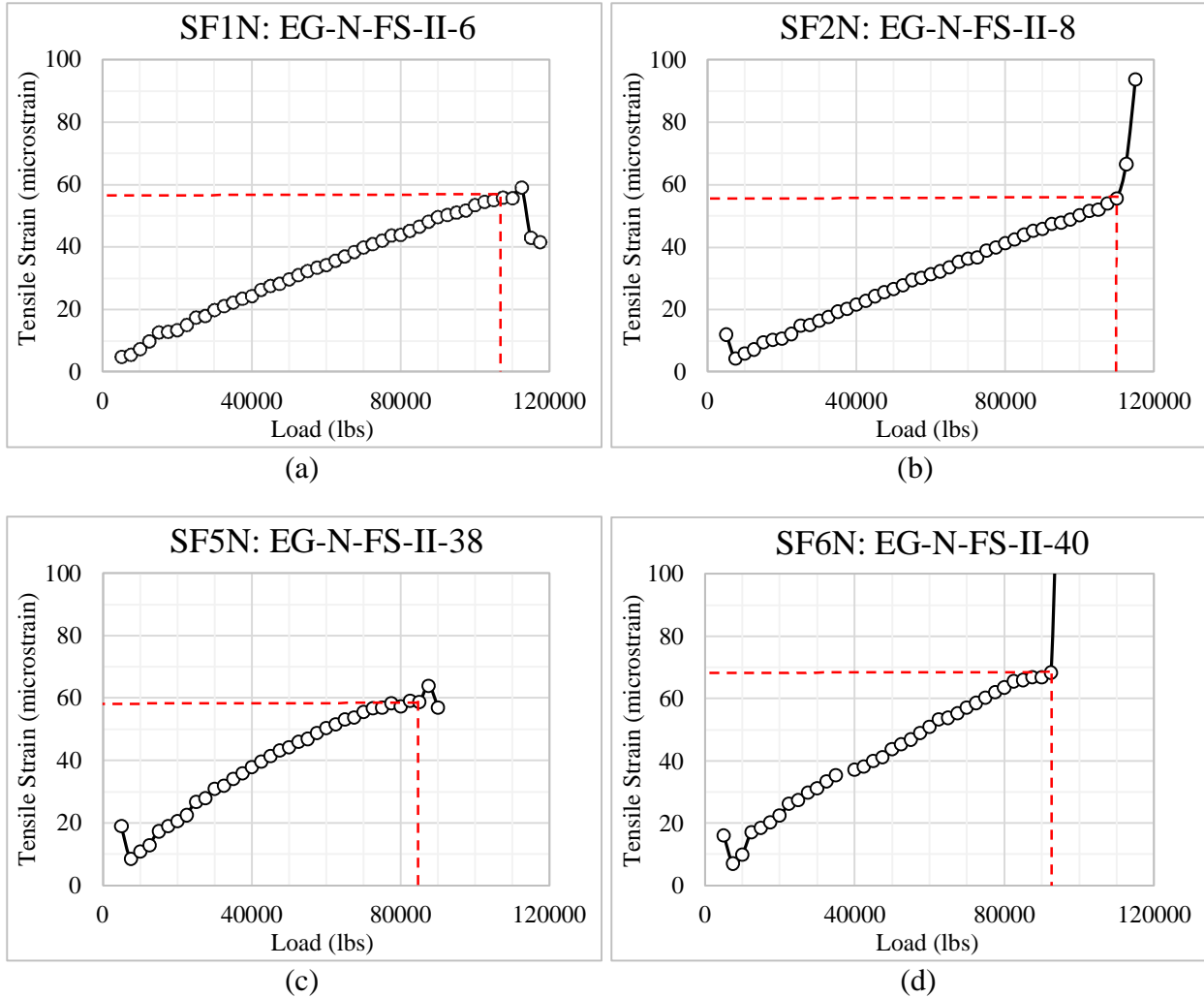


Figure 9. Tensile Strain vs. Load using S Module, North Inner Lane: (a) SF1N (12 inch), (b) SF2N (12 inch), (c) SF5N (9 inch), (d) SF6N (9 inch)

Table 4. Summary of Static Load Test Results

Slab ID	Thickness (inch)	R (psi)	Cracking Load (lbs)	Cracking Strain ¹ (microstrain)
SF1N	12	650	107,500	55.8
SF2N			110,000	55.6
SF5N	9	900	85,000	58.8
SF6N			92,500	68.3

¹See CC8 S/F Test Report – Outer Lane (HEC, 2020) for additional detail on the instrumentation.

4.2 MOVING LOAD TEST (NORTH AND SOUTH)

Upon completion of static load tests for crack initiation, the test proceeded by applying moving loads for crack propagation on slabs SF1N, SF2N, SF5N, and SF6N (north inner lane). In the case of non-pre-cracked slabs SF3N, SF4N, SF7N and SF8N (north inner lane), the crack initiation was first achieved “naturally” by the moving gear load and then followed by the crack propagation phase. In the case of notched slabs SF1S-SF8S (south outer lane), the moving load test comprised only the crack propagation phase.

Prior to initiation of the moving load traffic tests, 50 passes were applied to both the north and south inner lanes on July 15, 2019 as part of preparation efforts for CC9 data collection. Moving load traffic tests on the inner lanes began on October 16, 2019. As illustrated in figure 10, the moving load test with zero-wander was conducted simultaneously on the north and south inner/outer lanes using the NAPT module, at a nominal tire pressure of 220 psi.

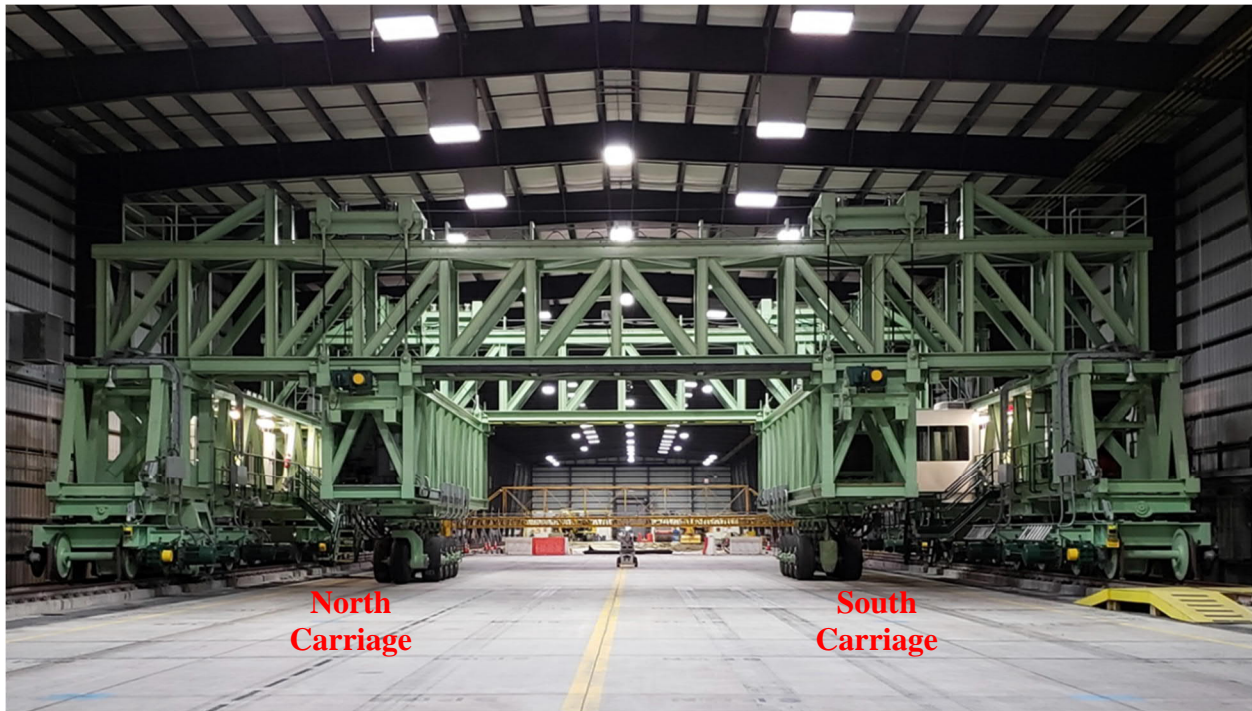


Figure 10. Moving Load Test

Traffic loads equivalent to 80% of the average bottom-up cracking load were equally distributed between the D module wheels (i.e., 40% per wheel) and applied on tracks N2 and S2 (figure 6). Table 5 summarizes the determination of traffic loads. A total of 25,000 passes have been applied to both the north and south inner lanes as of March 6, 2020. Table 6 shows the moving load traffic test history for the inner lanes.

Table 5. Determination of Traffic Loads

Slab ID	Thickness (inch)	Cracking Load (lbs)	Average Cracking Load (lbs)	80% of Average Cracking Load ¹ (lbs)
SF1N	12	107,500	108,750	87,000
SF2N		110,000		
SF5N	9	85,000	88,750	71,000
SF6N		92,500		

¹ For the moving load tests, 80% of the average cracking load was equally distributed between the two wheels of *D* module.

Table 6. Traffic History of Moving Load Test on Inner Lanes

Day No	Date	Passes		Cumulative Passes	
		North	South	North	South
1	10/16/19	170	170	170	170
2	10/17/19	376	376	546	546
3	10/18/19	292	292	838	838
4	10/23/19	514	514	1352	1352
5	10/24/19	510	510	1862	1862
6	10/25/19	310	310	2172	2172
7	10/28/19	508	508	2680	2680
8	10/29/19	524	524	3204	3204
9	10/30/19	524	524	3728	3728
10	10/31/19	512	512	4240	4240
11	11/01/19	250	250	4490	4490
12	11/04/19	504	504	4994	4994
13	11/05/19	524	524	5518	5518
14	11/06/19	426	426	5944	5944
15	11/07/19	456	456	6400	6400
16	11/12/19	466	466	6866	6866
17	11/13/19	476	476	7342	7342
18	11/14/19	480	480	7822	7822
19	11/15/19	244	244	8066	8066
20	11/18/19	524	524	8590	8590
21	11/19/19	492	492	9082	9082
22	11/20/19	434	434	9516	9516
23	11/21/19	504	504	10020	10020
24	11/25/19	492	492	10512	10512
25	11/26/19	498	498	11010	11010
26	11/27/19	418	418	11428	11428
27	12/02/19	456	456	11884	11884
28	12/05/19	364	364	12248	12248
29	12/09/19	292	292	12540	12540
30	12/10/19	372	372	12912	12912
31	12/12/19	170	170	13082	13082
32	12/13/19	254	254	13336	13336
33	12/16/19	442	442	13778	13778
34	12/17/19	292	292	14070	14070
35	12/18/19	478	478	14548	14548

Table 6 (continued)

Day No	Date	Passes		Cumulative Passes	
		North	South	North	South
36	12/19/19	252	252	14800	14800
37	12/20/19	220	220	15020	15020
38	12/23/19	466	466	15486	15486
39	12/26/19	374	374	15860	15860
40	12/27/19	170	170	16030	16030
41	12/31/19	432	432	16462	16462
42	01/02/20	480	480	16942	16942
43	01/03/20	270	270	17212	17212
44	01/06/20	482	482	17694	17694
45	01/07/20	482	482	18176	18176
46	01/08/20	196	196	18372	18372
47	01/09/20	472	472	18844	18844
48	01/10/20	246	246	19090	19090
49	01/13/20	458	458	19548	19548
50	01/14/20	344	344	19892	19892
51	01/15/20	474	474	20366	20366
52	01/16/20	520	520	20886	20886
53	01/17/20	250	250	21136	21136
54	02/24/20	382	382	21518	21518
55	02/25/20	526	526	22044	22044
56	02/26/20	512	512	22556	22556
57	02/27/20	110	110	22666	22666
58	02/28/20	248	248	22914	22914
59	03/02/20	474	474	23388	23388
60	03/03/20	338	338	23726	23726
61	03/04/20	514	514	24240	24240
62	03/05/20	428	428	24668	24668
63	03/06/20	332	332	25000	25000

5. BEHAVIOR OF TEST AREA UNDER TRAFFIC

5.1 DISTRESS MAPPING

Daily distress surveys were conducted in accordance with ASTM D5340 (ASTM, 2012). Visual distress surveys were documented in two ways: a scale map and a written log. The distress map shows all distresses to scale and keys each distress to a pass number, date of observance, station number, and slab ID. Distresses are color coded and numbered for reference to the written log. Appendix B contains all CC8 S/F distress maps. The written log records all the distress information chronologically. The written log records the date, pass number, type of distress, distress number (which can be cross-referenced to the distress map), the location of the distress, and any relevant notes. Appendix C contains the complete written log. Additional detail on the distress survey methods can be found in the CC8 S/F Test Report – Outer Lane.

5.2 SUMMARY OBSERVATION

The primary objective of the CC8 S/F test is to isolate the three phases of the bottom-up cracking mechanism and estimate the fatigue life contribution of each stage (see figure 1). Distress surveys were the tool to track the number of passes required by slabs to attain: (a) the first appearance of surface distresses (i.e., formation and full-depth progression of bottom-up cracks), and (b) the full-length propagation of longitudinal cracks (i.e., crack extends to both ends of the slab). In addition, the surveys documented the formation of secondary distresses (e.g., diagonal cracks).

Table 7 presents the pavement deterioration history for the inner lanes. Table 7 compiles all surface deterioration events from first appearance of the crack to full-length completion. CC8 S/F traffic test paused on March 19, 2020 due to the COVID-19 pandemic and facility shutdown. After 25,000 cumulative passes with the D module, no sign of surface distress was observed on the inner lane slabs, except transition slab T3-1N.

Table 7. Pavement Deterioration History of Inner Lanes

Day No	Date	Cumulative Passes		Distress Observations
		North	South	
1	10/16/19	170	170	Traffic commencement
3	10/18/19	838	838	Visual inspection showed a new diagonal crack on transition slab: T3-1N
63	03/06/20	25000	25000	End of trafficking with D module
64	03/18/20	25350	25350	Beginning of trafficking with S module
65	03/19/20	25838	25838	Traffic Pause

6. PRELIMINARY DATA ANALYSIS

6.1 CHARACTERIZATION OF CRACK PROPAGATION

6.1.1 DISTRESS DATA

The cumulative passes applied with D module on both north and south inner lanes are 25,000 as of March 6, 2020. Prior to the moving load tests, 50 passes were applied on July 15, 2019 to both north and south inner lanes as a separate effort in preparation for CC9 data collection. This resulted in an unintended crack on SF3S (12-inch thick, $R=650$ psi and CBR 7-8) along the inner wheel path. After the traffic test commenced on October 16, 2019, only one diagonal crack was recorded on T3-1N (i.e., transition slab at west end of CC8 S/F test area). This distress was observed on October 18, 2019 after 838 cumulative passes. Neither north nor south inner lane slabs (i.e., on the actual CC8 S/F test area) has shown any additional surface distress. To date, isolating the three phases of fatigue failure (i.e., crack initiation, full-depth and full-length crack propagation) is not possible due to the lack of performance data. Figures 11 and 12 show current distress maps for slab groups 1-4 and 5-8, respectively.

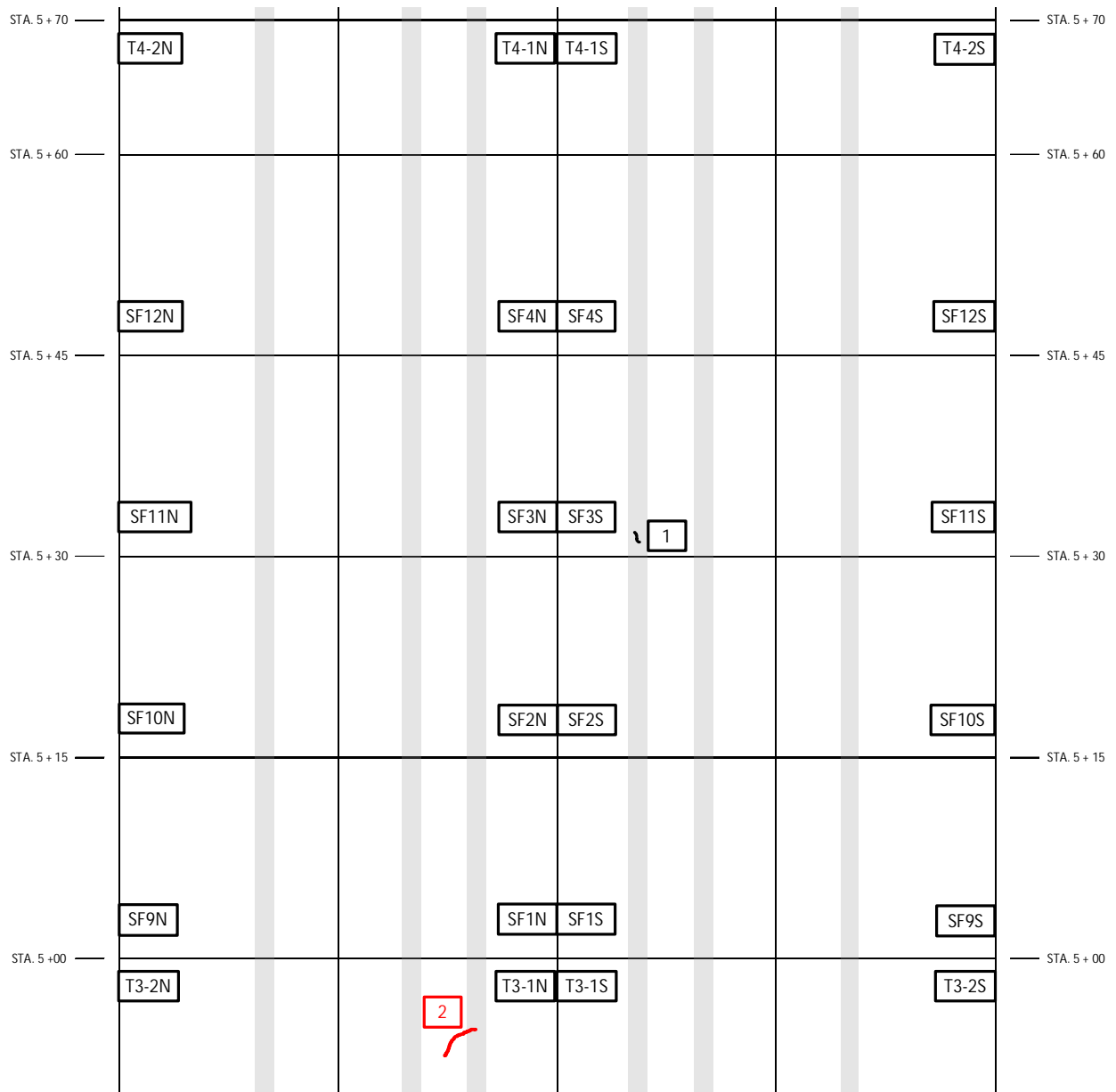


Figure 11. Current Distress Map for Inner Lanes (Groups 1-4, Last Updated: March 19, 2020)

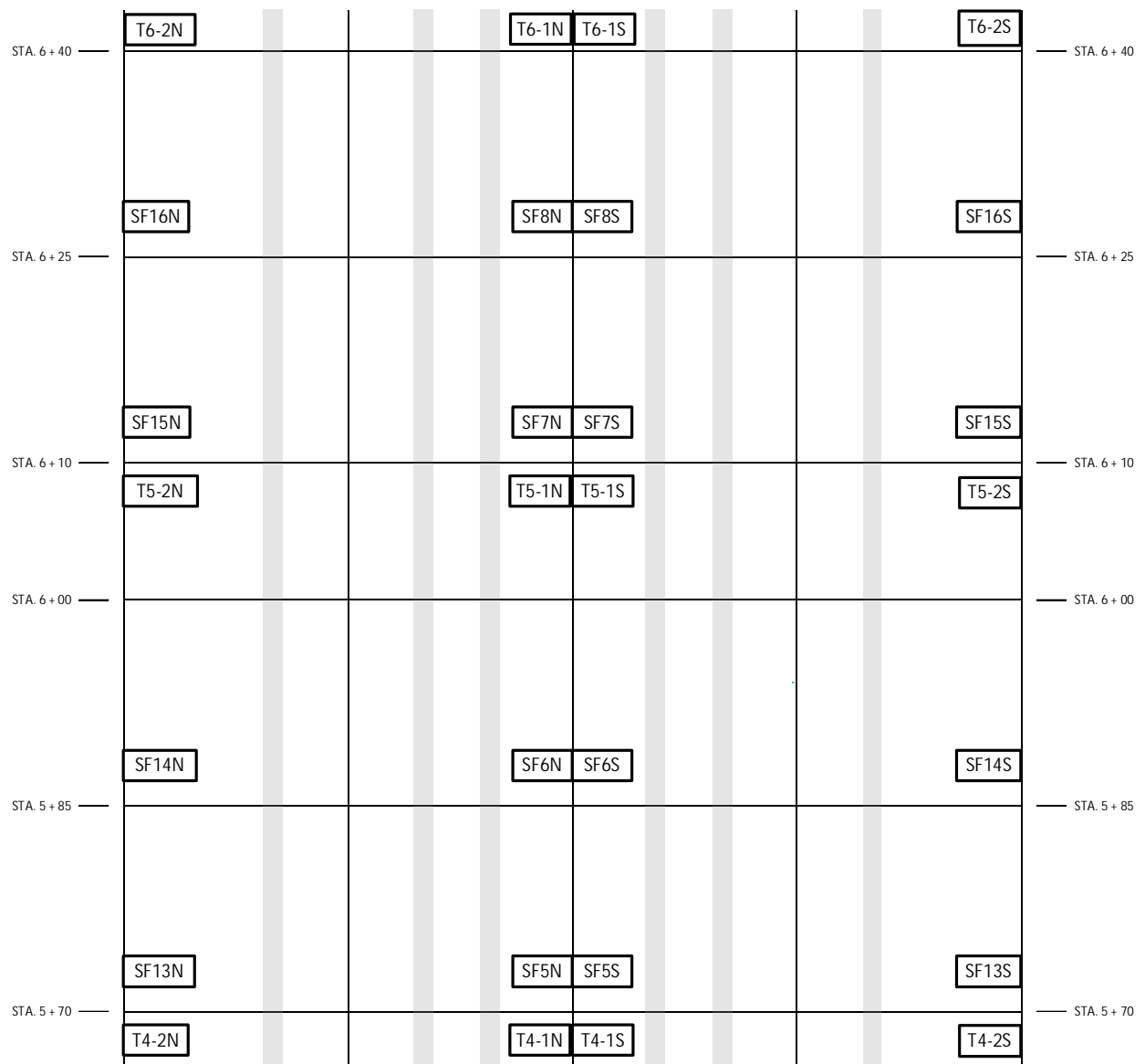


Figure 12. Current Distress Map for Inner Lanes (Groups 5-8, Last Updated: March 19, 2020)

6.1.2 INSTRUMENTATION DATA

The strains measured by transverse EGs along the inner wheel path were monitored in real-time throughout traffic testing. After completion of the static load tests, the bottom EGs in the pre-cracked slabs SF1N, SF2N, SF5N, and SF6N were no longer expected to provide insight on full-depth propagation. It was then decided to use only top EGs for characterizing crack propagation (i.e., full-depth and full-length) during the moving load test. Also, the top EG in slab SF1N became malfunctioning during the static load test and was excluded from the daily monitoring.

Figure 13 shows as example the top EG response from slab SF2N (i.e., 12-inch thick slab). A gradual increase in negative strain possibly due to initial stabilization of the pavement was observed at the beginning of trafficking. Following the initial increase, the strain response was fairly stable except for an observable fluctuation around cumulative pass 23,000. This fluctuation could be indication of full-depth propagation. Figure 14(a) and (b) show the top EG response of 9-inch thick slabs SF5N and SF6N, respectively. Compared to slab SF2N, the peak negative strains in slabs SF5N and SF6N were more consistent.

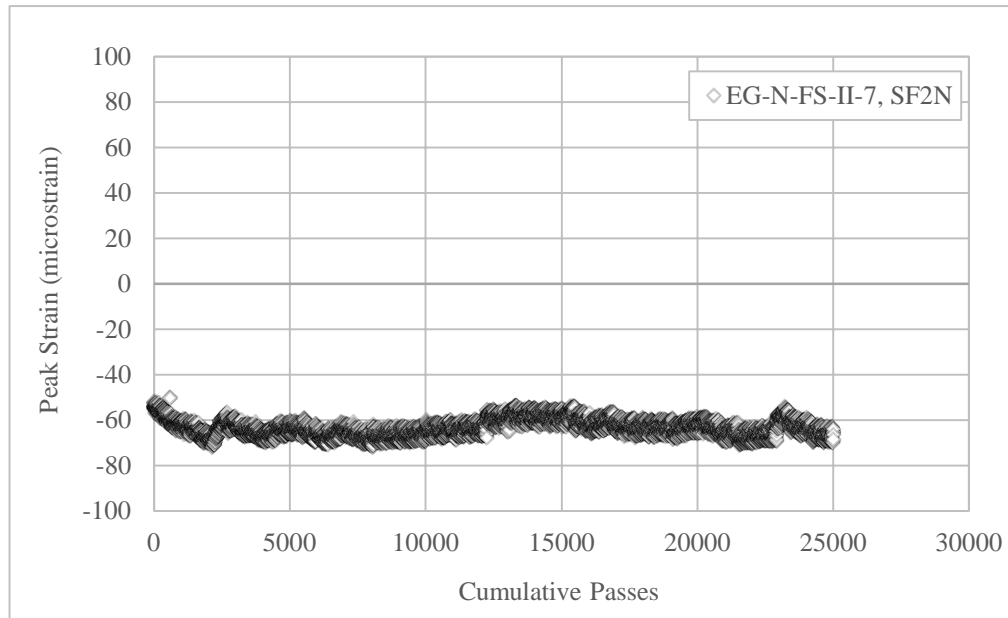
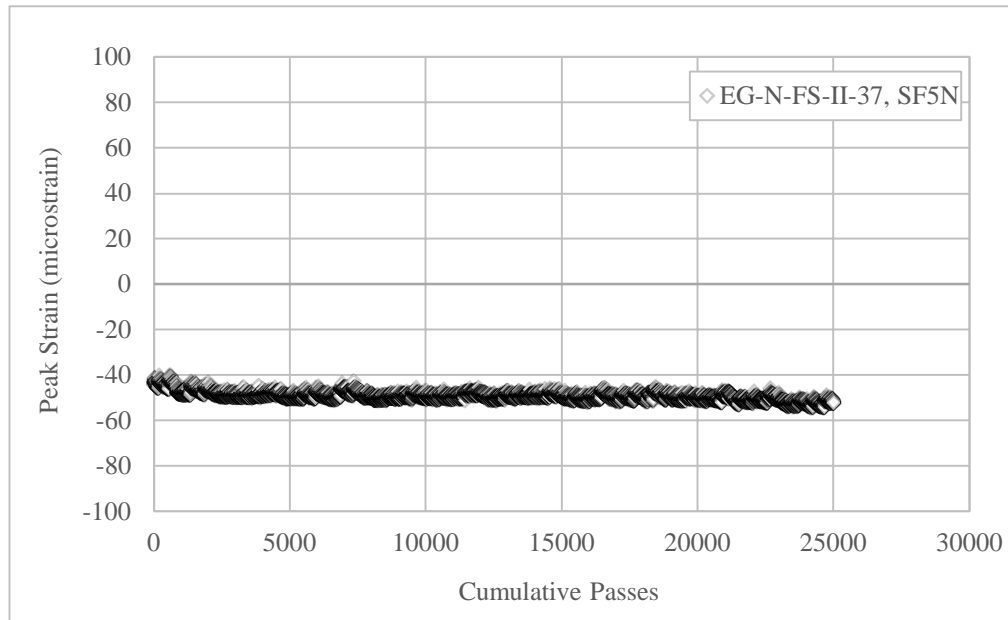
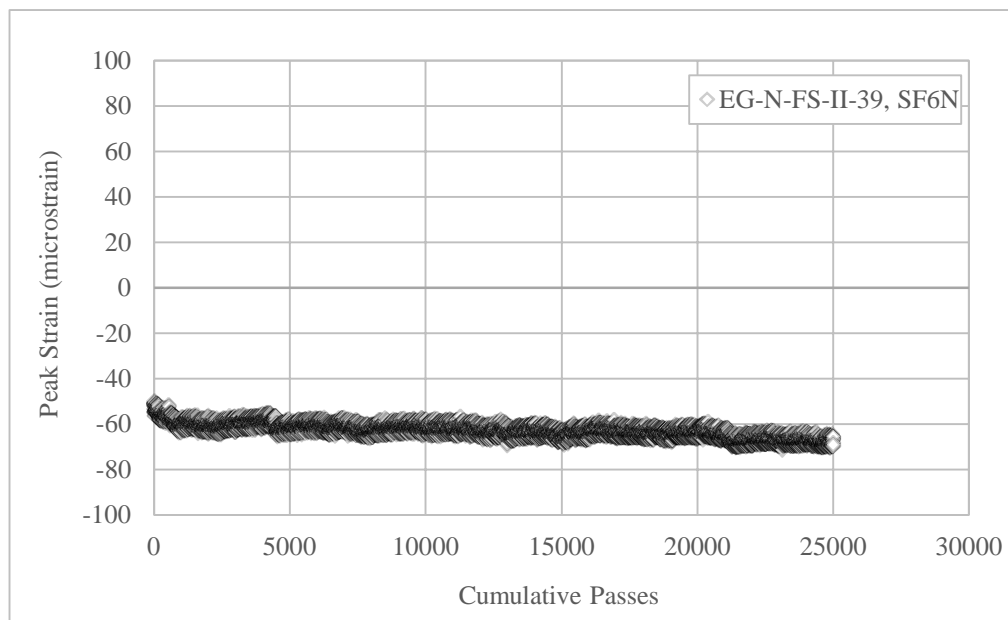


Figure 13. Response of Top EG in SF2N (12-inch PCC Slab)



(a)



(b)

Figure 14. Response of Top EG in 9-inch PCC Slabs: (a) SF5N, (b) SF6N

Since south inner lane slabs SF3N, SF4N, SF7N, and SF8N were not pre-cracked, the positive response of both top and bottom EGs were about or below the maximum cracking strain levels observed during static load tests (see table 4). Only the response of bottom EGs were monitored for characterizing bottom-up crack initiation during the moving load test. The bottom EG of slab SF3N became malfunctioning prior to the traffic test and therefore, it was excluded from daily monitoring.

Figure 15 shows as example the bottom EG response from slab SF4N that had a thickness of 12 inches. The peak positive strain was initially inconsistent but became fairly stable later on. No signs of bottom-up crack initiation were observed over the 25,000 cumulative passes applied with D module.

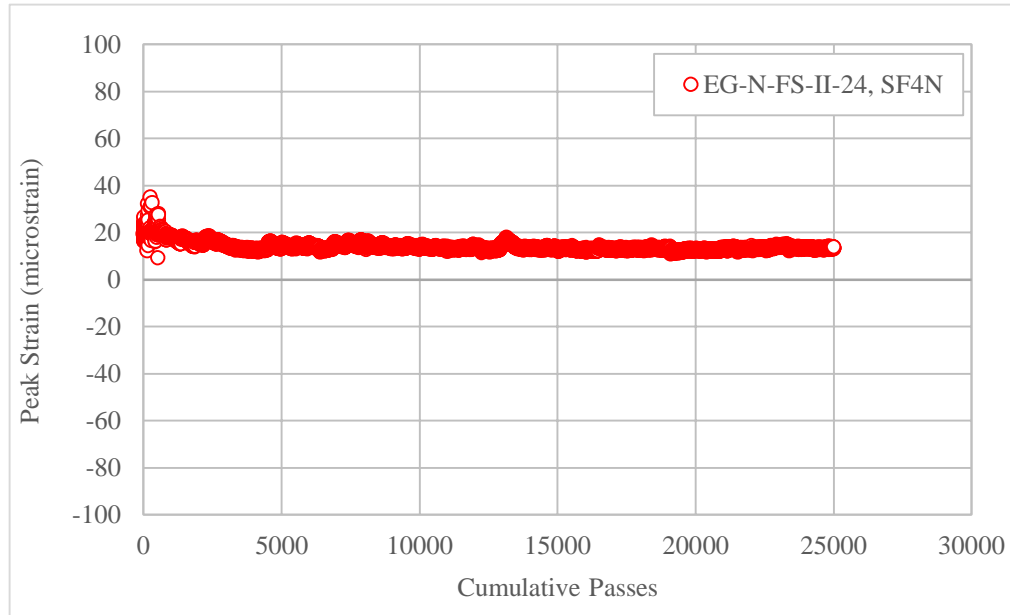


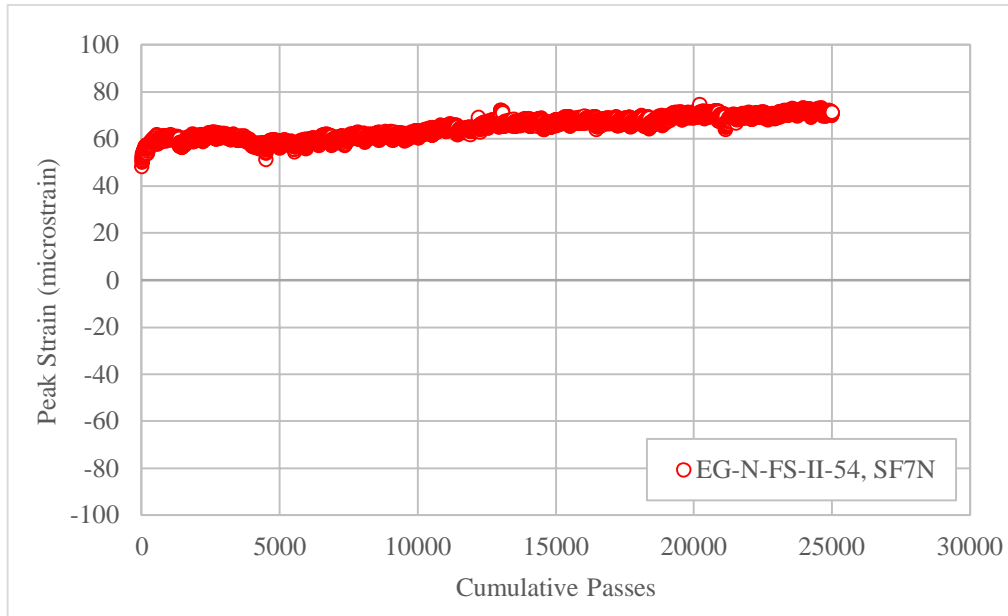
Figure 15. Response of Bottom EG in SF4N (9-inch PCC Slab)

Figure 16(a) and (b) show the bottom EG responses of 9-inch thick slabs SF7N and SF8N, respectively. Slab SF7N shows a rapid increase in peak positive strain at the beginning of trafficking possibly due to initial stabilization of the pavement. Later, a slight drop in peak positive strain observed after approximately 4,000 cumulative passes was followed by a gradual increasing trend. Unlike 12-inch slab SF4N, both slab SF7N and SF8N generally exhibit a gradual increase in peak positive strain over the course of trafficking. Note that the peak positive strain in SF7N is higher compared to SF8N. This suggests that with additional traffic, SF7N may show surface distress earlier than SF8N.

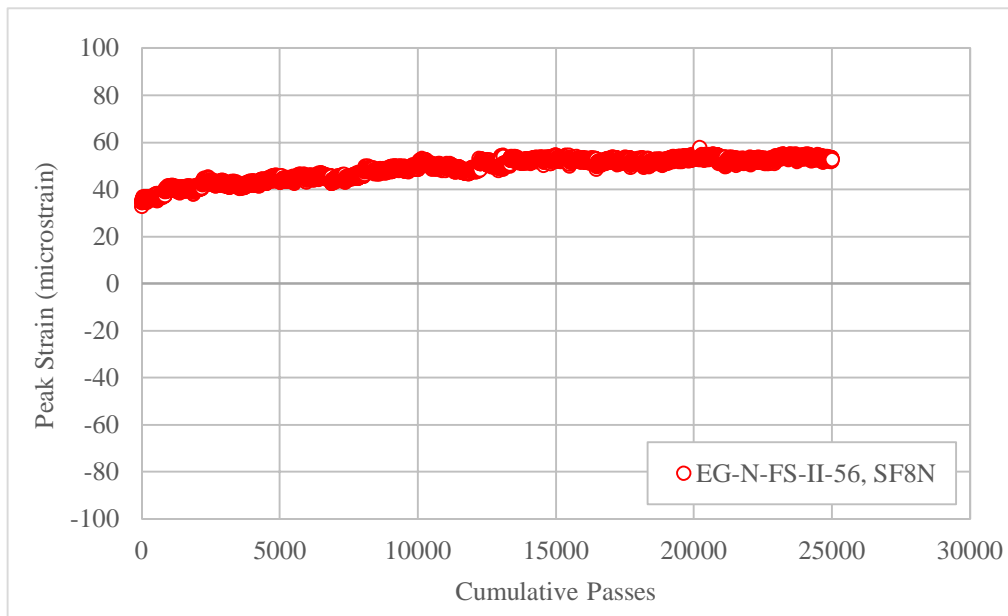
The neutral axis position (NAP) is defined as the location within the slab where the strains induced by moving load change from compression to tension. The NAP was calculated for SF7N and SF8N (i.e., using top and bottom EG responses) to perform in-depth characterization of bottom-up crack initiation. It is expected that changes in NAP observed over the course of trafficking will provide indication of crack initiation and propagation. Note that the NAP is measured relative to the pavement surface. Figure 17(a) and (b) show the change in NAP over the course of trafficking for SF7N and SF8N, respectively. The NAP for SF7N remained relatively constant throughout trafficking. For SF8N, an increasing trend at a generally slow rate can be observed. In both cases, the NAP gives no sign of crack initiation.

In figure 18 (a) and (b), the top and bottom EG peak responses are plotted for slabs SF7N and SF8N, respectively. For SF7N, the peak response of top (negative) and bottom (positive) EGs were of similar magnitude (figure 18(a)). For SF8N, the top EG peak response was greater in magnitude

than the bottom which is consistent with the NAP in this slab being generally higher than that of SF7N. The bottom EG peak response in none of these two slabs indicates crack initiation.

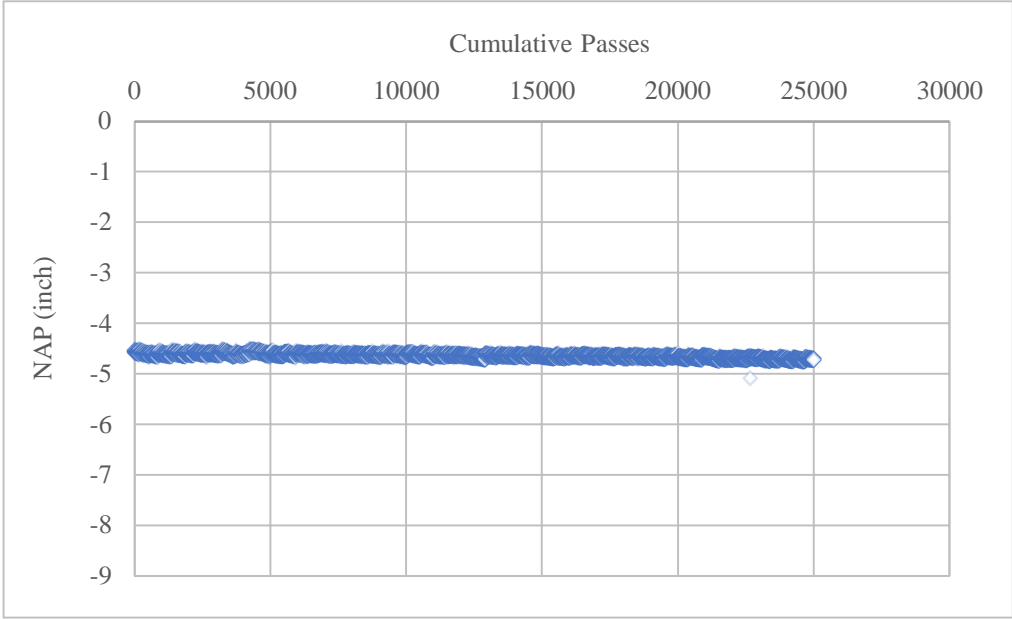


(a)

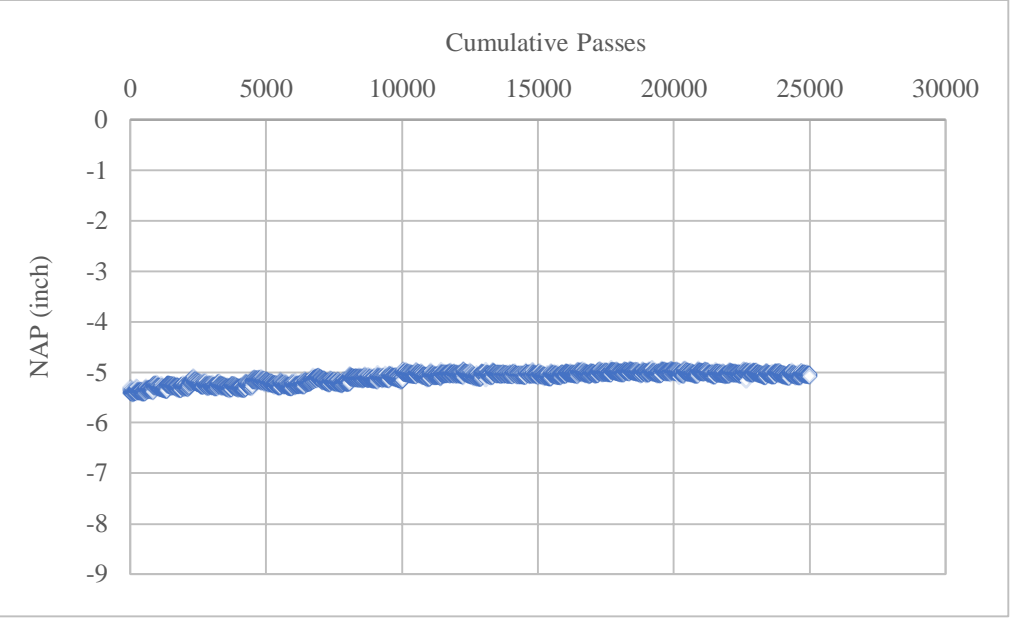


(b)

Figure 16. Response of Bottom EGs in 9-inch PCC slabs: (a) SF7N, (b) SF8N

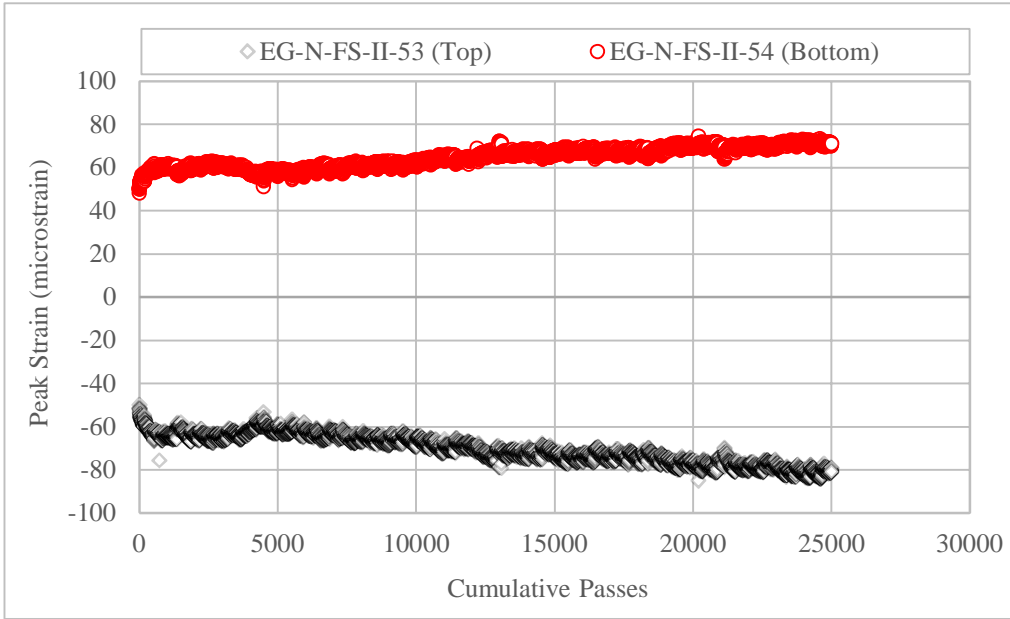


(a)

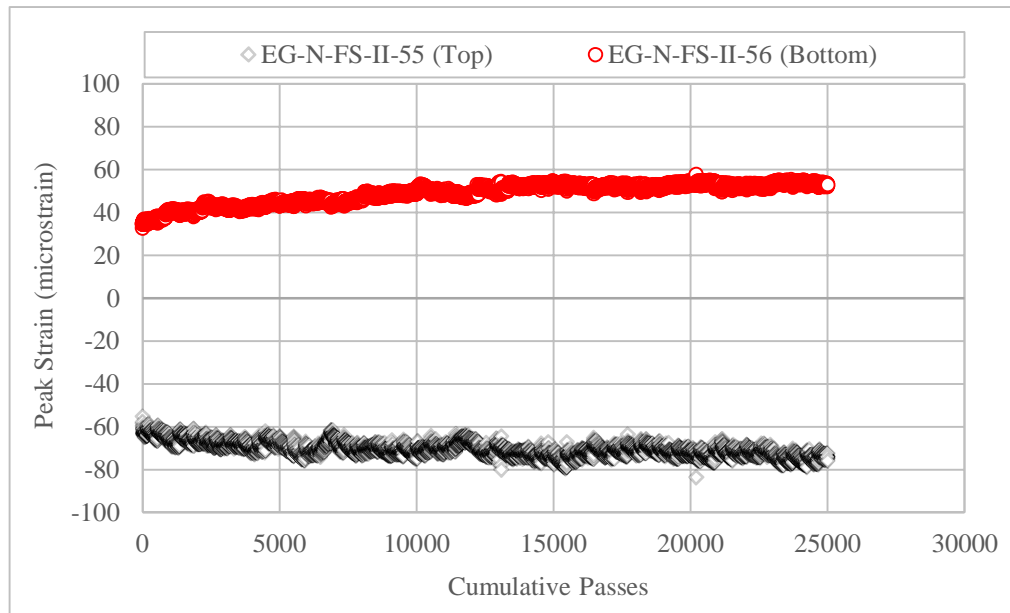


(b)

Figure 17. NAP Trends in 9-inch PCC Slabs: (a) SF7N, (b) SF8N



(a)



(b)

Figure 18. Response of Top and Bottom EGs in 9-inch PCC slabs: (a) SF7N, (b) SF8N

6.2 PAVEMENT EVALUATION

6.2.1 PCC SLAB MODULUS

PSPA tests were performed on inner lanes to assess the change in slab modulus over the course of trafficking. Figure 19(a)-(d) show the change in slab modulus with cumulative passes. Neither the north nor south inner lane slabs show signs of modulus degradation indicating that slabs integrity remained unchanged. In the figures, 9-inch thick slabs exhibit slightly higher slab modulus compared to 12-inch thick slabs on both the north and south inner lane, possibly due to the difference in flexural strength.

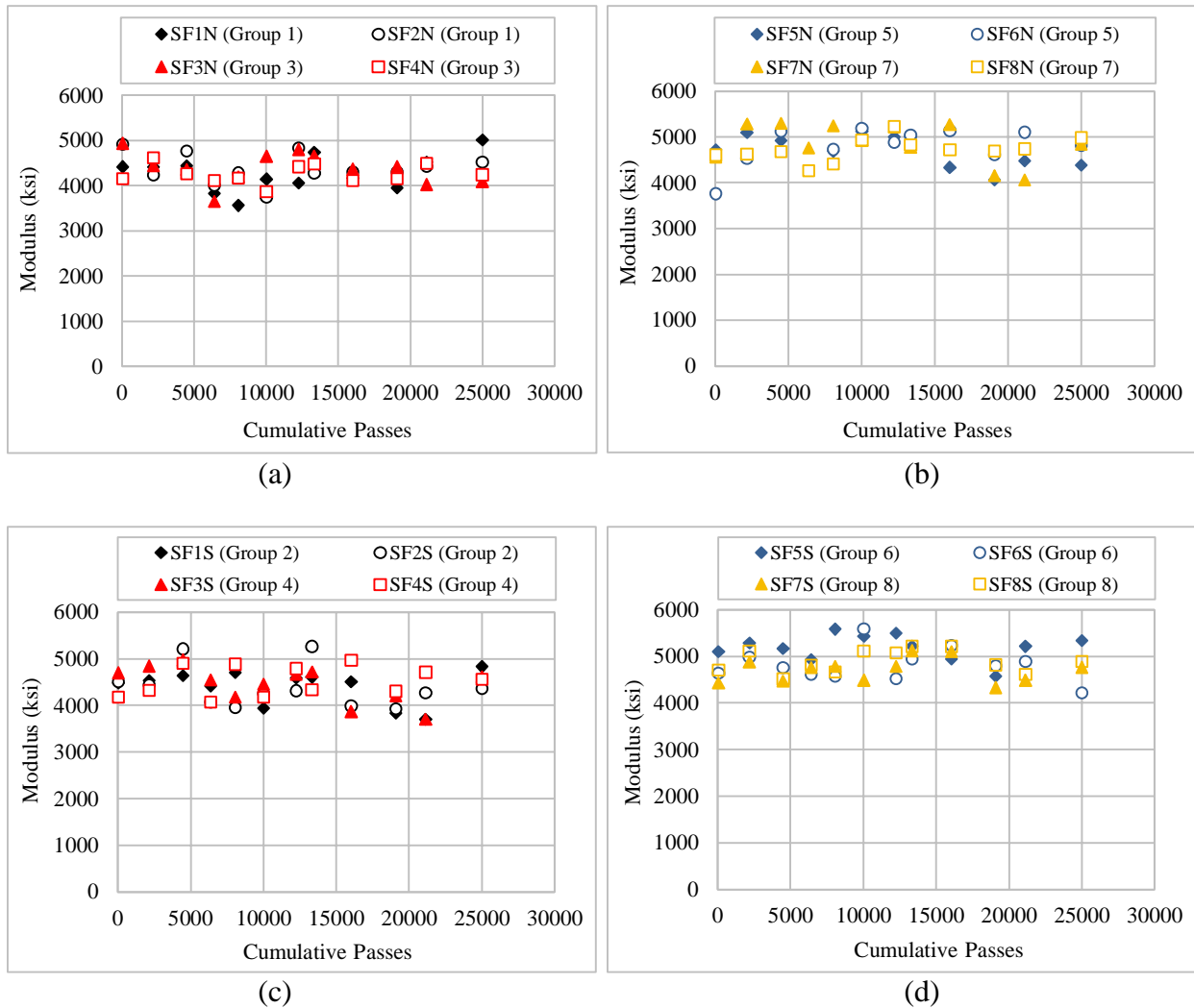


Figure 19. PSPA Slab Modulus: (a) North Inner Lanes (Group 1 & 3: 12 inch), (b) North Inner Lanes (Group 5 & 7: 9 inch), (c) South Inner Lanes (Group 2 & 4: 12 inch), (d) South Inner Lanes (Group 6 & 8: 9 inch)

Table 8 summarizes the average moduli from both the first and last round of PSPA testing. The distribution of slab modulus of both 12- and 9-inch slabs on north and south inner lanes was fairly

consistent, showing coefficient of variation (CV) below 10% in both the first and last round of PSPA testing. Based on the first round of PSPA testing, the average modulus of 9-inch slabs was slightly lower than that of 12-inch slabs on north inner lanes. On the south inner lanes, the average modulus of 9-inch slabs was slightly higher than that of 12-inch slabs. The last round of PSPA testing on 9-inch slabs exhibited slightly higher modulus compared to 12-inch slabs on both north and south inner lanes. Generally, no degradation of slab integrity was observed when comparing results between the first and last round of testing.

Table 8. Summary of PSPA Modulus (First and Last Round of Testing)

Test Item	Group	Slab ID	Thickness (inch)	R (psi)	First Round of Testing			Last Round of Testing ¹		
					Modulus (ksi)	Average (ksi)	CV ² (%)	Modulus (ksi)	Average (ksi)	CV ² (%)
North	1	SF1N	12	650	4417	4606	8.3	5007	4463	9.1
		SF2N			4915			4518		
	3	SF3N			4933			4089		
		SF4N			4158			4237		
	5	SF5N	9	900	4717	4412	9.9	4380	4754	5.5
		SF6N			3763			4810		
	7	SF7N			4565			4847		
		SF8N			4602			4980		
South	2	SF1S	12	650	4481	4467	4.9	4832	4594	4.2
		SF2S			4511			4367		
	4	SF3S			4700			4617		
		SF4S			4176			4562		
	6	SF5S	9	900	5107	4719	6.0	5338	4801	9.7
		SF6S			4640			4211		
	8	SF7S			4424			4767		
		SF8S			4706			4888		

¹ Final round of PSPA testing on the north and south was conducted on March 9, 2020

² Coefficient of Variation (CV)

6.2.2 HWD DEFLECTION

6.2.2.1 DEFLECTION BASIN

HWD tests were performed on a weekly basis at the center of all 16 S/F inner lane slabs and slab corners. Figures 20 and 21 show deflection basins normalized to 36,000-lbs HWD drops at slab centers for both north and south inner lanes, respectively. In general, the deflection basins of slabs on the south inner lanes showed more consistency over the course of trafficking compared to slabs on the north. Based on the magnitude of deflection, SF5S and SF6S were the weakest of the south inner lane. On the north inner lane, the deflection basin of slabs SF3N and SF4N exhibited a downward shift over the course of trafficking, indicating decrease in structural integrity. Slabs SF5N and SF6N showed the highest deflection values, which suggests these two were the weakest of the entire CC8 S/F test area.

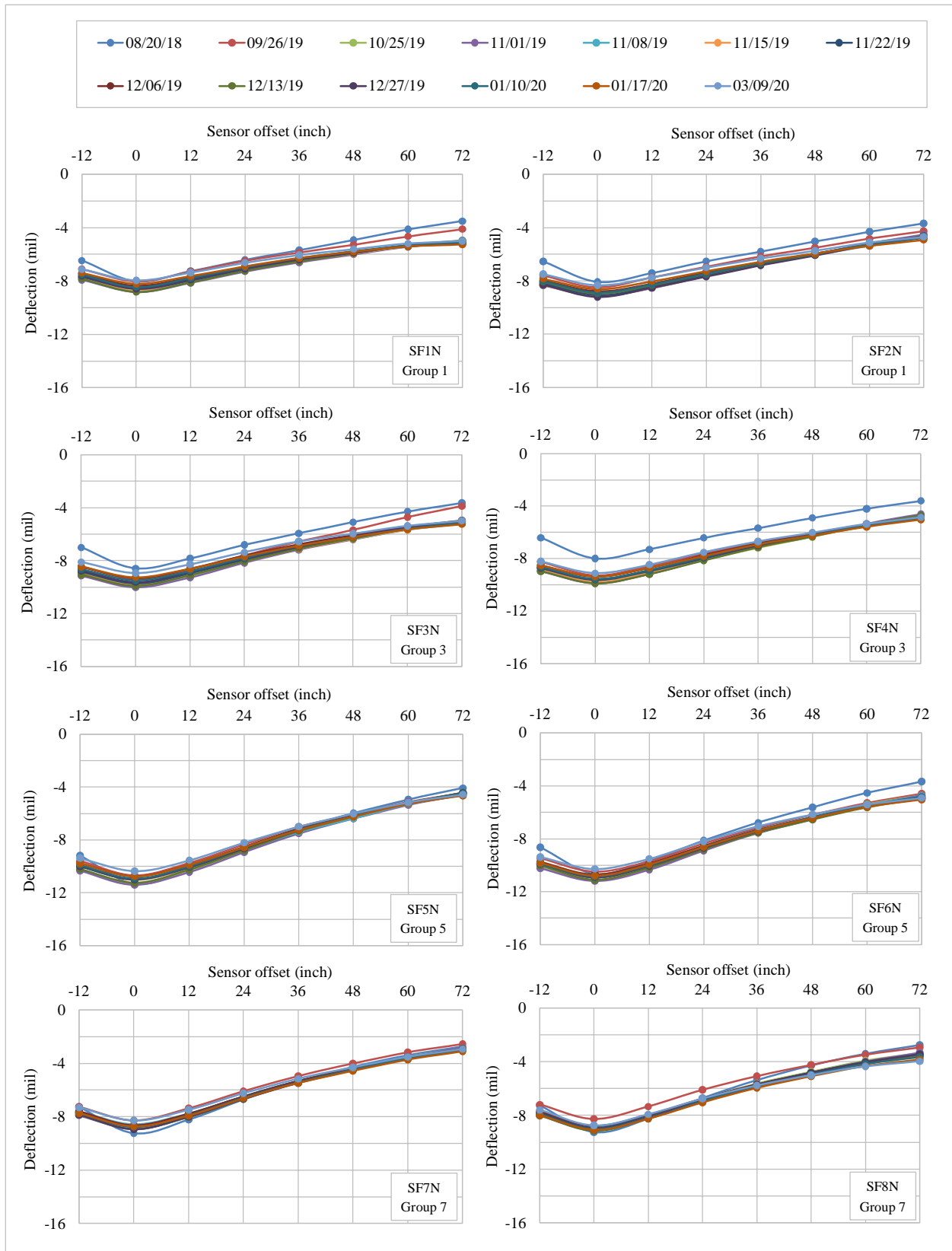


Figure 20. Slab Center Deflection Basins, North Inner Lanes

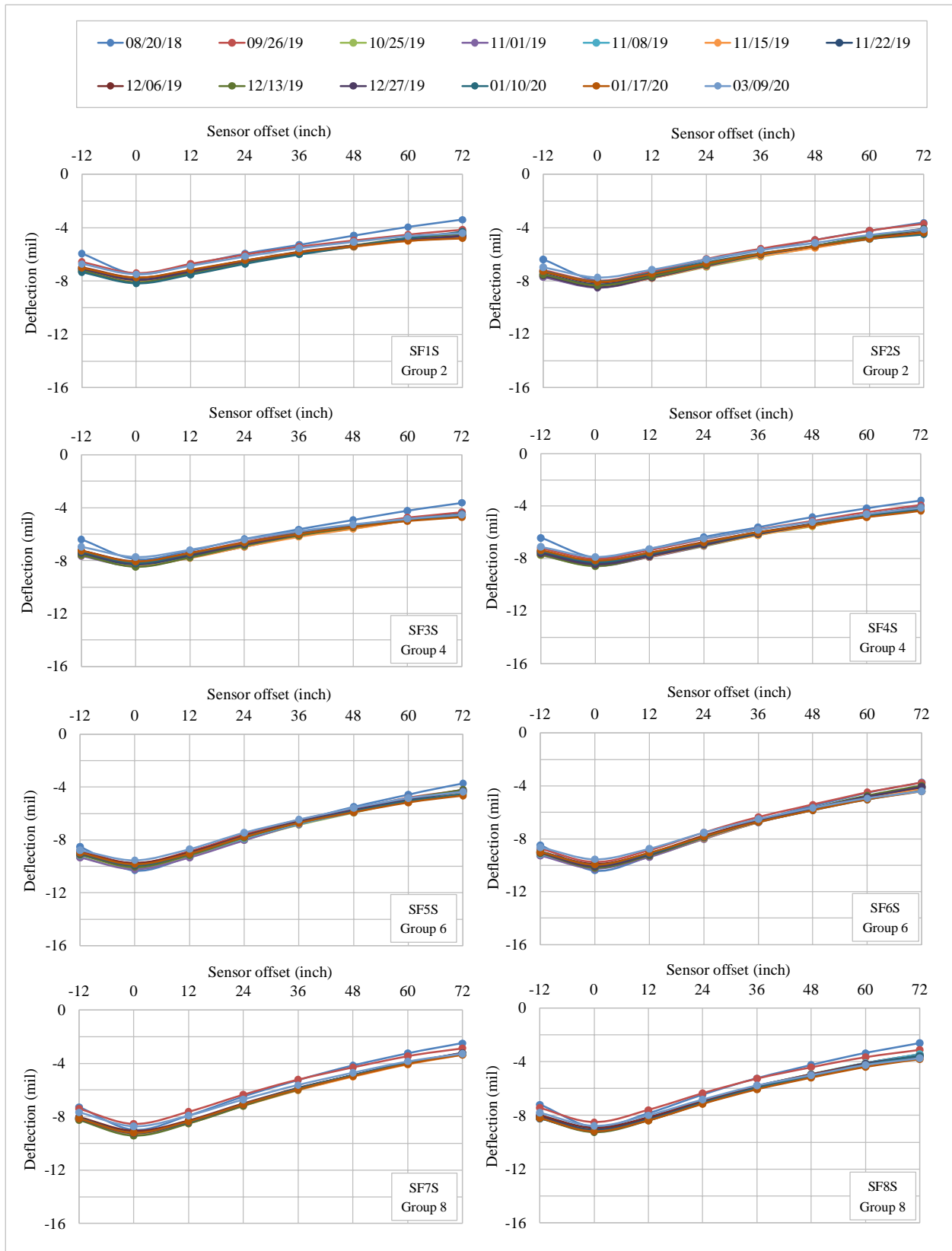


Figure 21. Slab Center Deflection Basins, South Inner Lanes

6.2.2.2 IMPULSE STIFFNESS MODULUS

Impulse Stiffness Modulus (ISM) is the ratio of HWD test load (P) to the maximum deflection (δ_{max}) at the center of the load plate. ISM was calculated at slab centers using only deflection data from HWD drops at nominal $P=36,000$ lbs. All δ_{max} data were first normalized to the nominal load and then ISM was obtained using the following equation:

$$ISM = \frac{P}{\delta_{max}} \quad (2)$$

Figures 22(a) and (b) illustrate the changes in ISM as a function of cumulative passes for 12- and 9-inch thick slabs on the north inner lane, respectively. In general, the ISM trends show no sign of degradation in slab integrity. The ISM of slabs in groups 5 and 7 (i.e., 9-inch thick slabs) showed more consistency over the course of trafficking compared to groups 1 and 3 (i.e., 12-inch thick slabs). Test area built over subgrade with CBR 3-4 (group 7) were expected to show lower ISM than the area built over subgrade with CBR 7-8 (groups 1, 3 and 5). However, in figure 22(b), slabs SF7N and SF8N (group 7) showed higher ISM than slabs SF5N and SF6N (group 5). This observation suggests that the effect of subgrade strength was possibly offset by strength variability in shallower layers (e.g., higher compressive strength of P-306MR observed for slab groups on subgrade with CBR 3-4 compared to groups on subgrade with CBR 7-8).

Figure 22(c) and (d) illustrate the changes in ISM for 12- and 9-inch thick slabs on the south inner lane, respectively. Overall, no sign of degradation in slab integrity was observed based on changes in ISM over the course of trafficking. Unlike for north inner lane slabs, the ISM between slabs was fairly consistent within every group on the south side. The ISM of groups 2 and 4 were higher than groups 6 and 8, indicating that 12-inch thick slabs on the south side possessed higher structural integrity than 9-inch thick slabs. Similar to the north inner lane, the south side built over subgrade with CBR 3-4 (group 8) showed higher ISM than the area built over subgrade with CBR 7-8 (group 6).

6.2.2.3 CORNER-TO-CENTER DEFLECTION RATIO

Corner-to-center deflection ratios corresponding to the highest HWD load (36,000 lbs) were determined. Every corner was identified using a three-character designation as follows:

1st Character: Slab Identification Number

2nd Character: Test Item (N or S)

3rd Character: Corner Orientation (E or W)

For instance, 1NE corresponds to the east corner of slab 1 on the north test item. The following corners were evaluated: 1NE, 2NW, 3NE, 4NW, 5NE, 6NW, 7NE, and 8NW (north inner lane); 1SE, 2SW, 3SE, 4SW, 5SE, 6SW, 7SE, and 8SW (south inner lane).

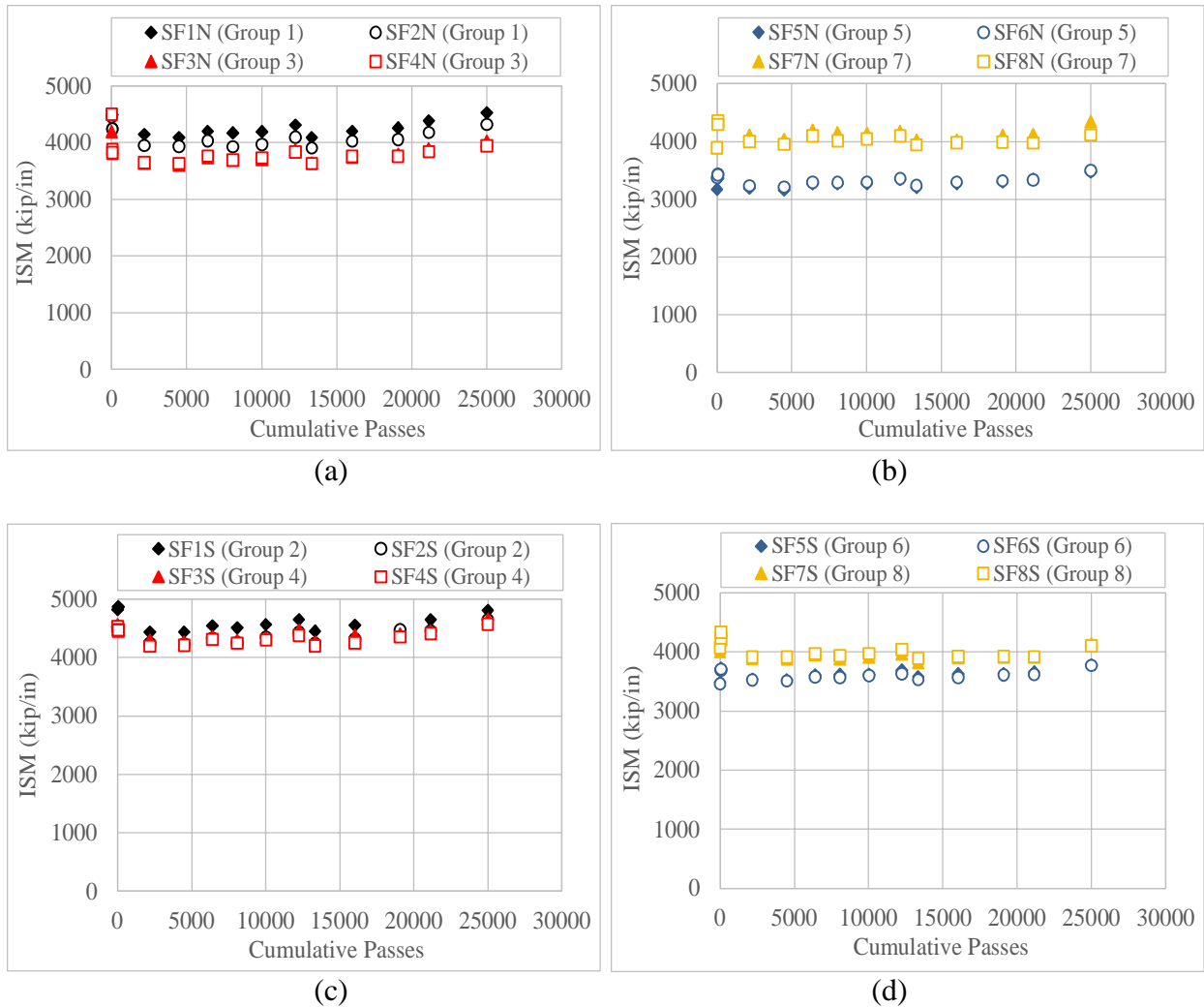


Figure 22. ISM vs. Cumulative Passes for Inner Lanes: (a) North (Group 1 & 3), (b) North (Group 5 & 7), (c) South (Group 2 & 4), (d) South (Group 6 & 8)

Notable changes in corner-to-center deflection ratio over the course of trafficking that are not associated to changes in slab temperature may provide indication of crack initiation/propagation. Figures 23(a)-(d) illustrate the change in corner-to-center deflection ratio over the course of trafficking. The trends of corner-to-center deflection ratio for 12-inch thick slabs (groups 1-4) were more uniform than those for 9-inch thick slabs (groups 5-8). The corner-to-center deflection ratios of slabs SF6N, SF1S, SF6S, and SF7S were relatively high compared to the rest of the slabs. It is speculated that localized deficiency of slab corner support resulting from construction variability can be a possible source for the observed high corner-to-center deflection ratios.

On both north and south inner lanes, a sustained increasing trend of corner-to-center deflection ratio can be observed for all slabs after cumulative pass 15,000. Figure 24 shows the change in slab temperature over the course of trafficking for both the north and south inner lanes. It should be noted that thermocouples were installed only in specific 12-inch slabs of the outer lanes (i.e., SF11N and SF11S). In figure 24(a), the average slab temperature reached a minimum after

approximately 15,000 cumulative passes and remained low thereafter. In figure 24(b), the slab temperature differential (i.e., top-bottom) generally fluctuates between positive and negative values up to about cumulative pass 15,000 and showed a decreasing trend thereafter up to about 21,000 passes, which is consistent with the increasing trend of corner-to-center deflection ratio. Since no thermocouple data are available for 9-inch slabs, the final change in temperature differential at 25,000 passes is only reflected in 12-inch slabs (i.e., groups 1-4). Changes in slab temperature trigger curling and warping cycles, which explains the observed variation in corner-to-center deflection ratio.

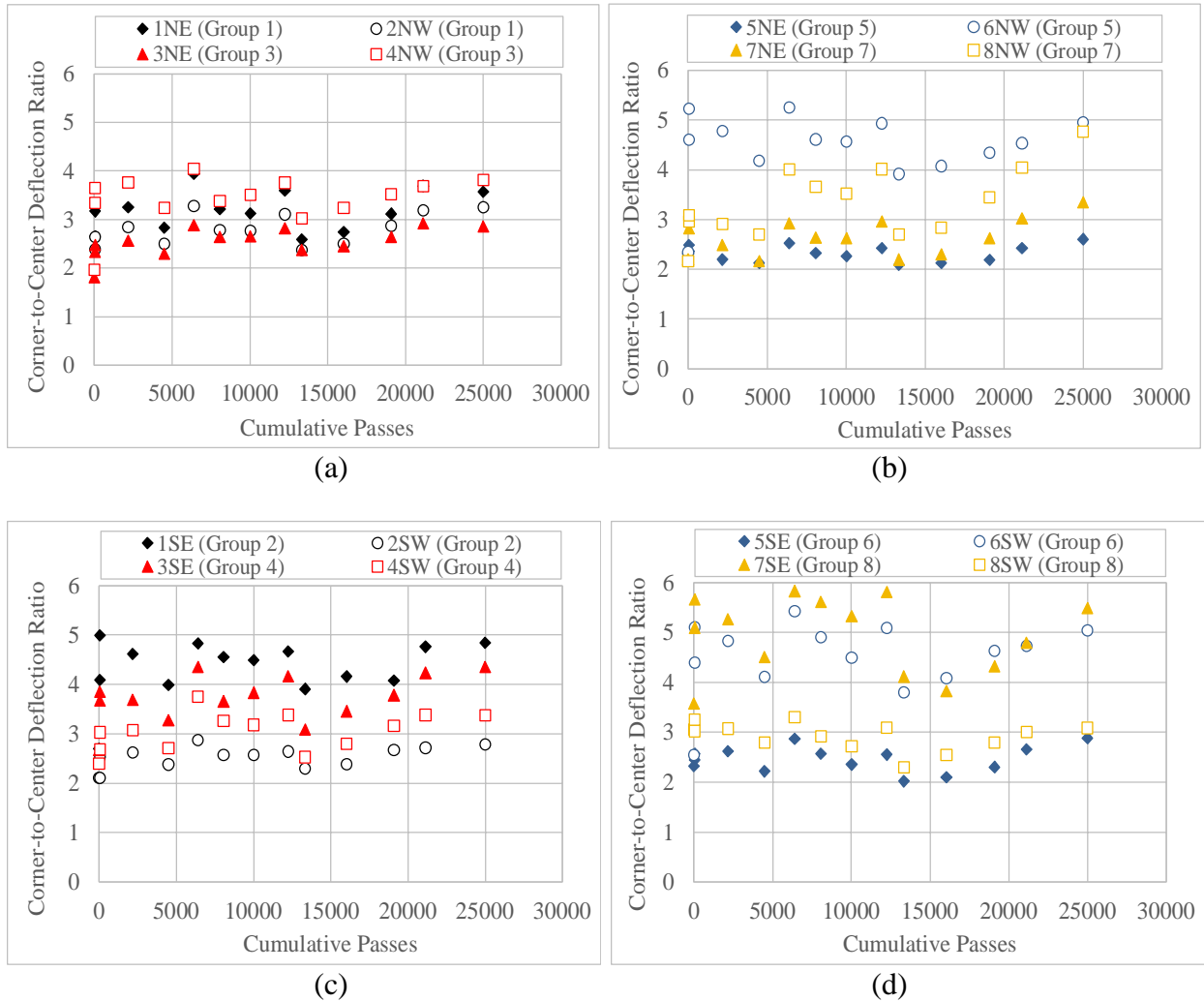
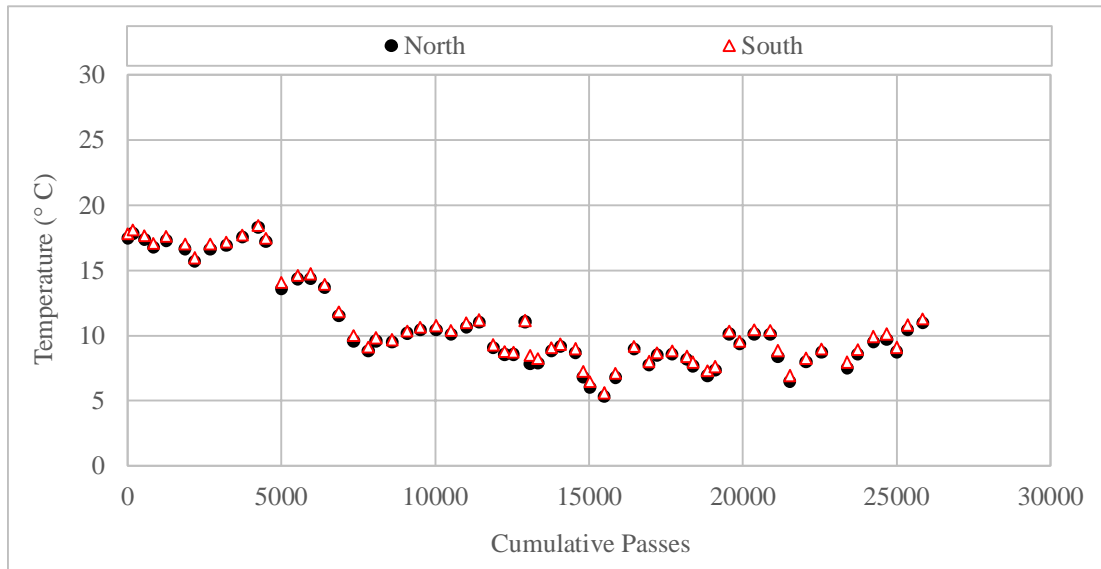
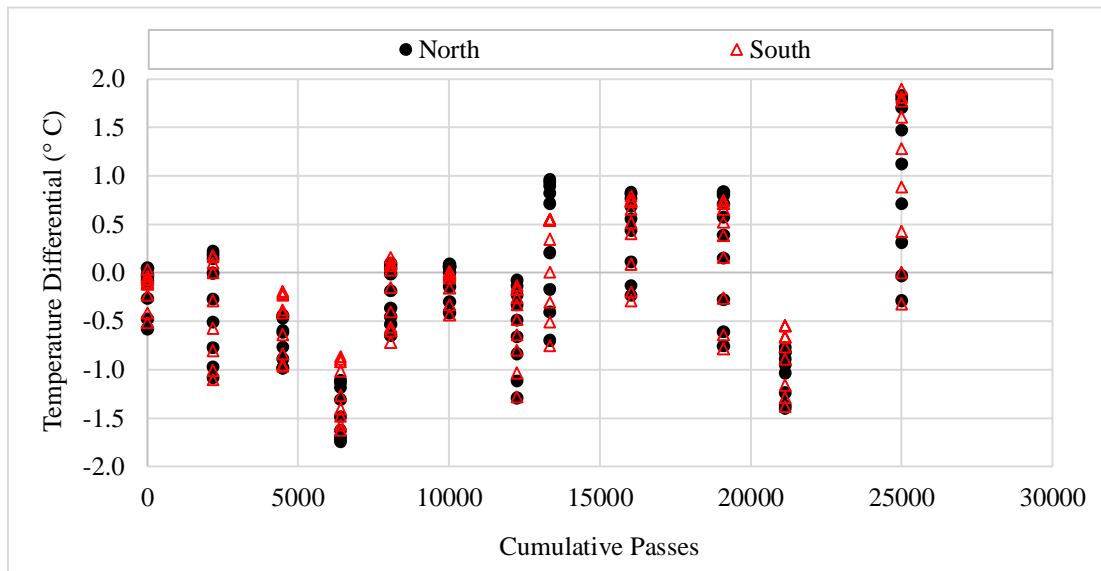


Figure 23. Corner-to-Center Deflection Ratio vs. Cumulative Passes for Inner Lanes: (a) North (Group 1 & 3), (b) North (Group 5 & 7), (c) South (Group 2 & 4), (d) South (Group 6 & 8)



(a)



(b)

Figure 24. Change in Slab Temperature over the Course of Trafficking: (a) Average Slab Temperature, (b) Temperature Differential (Top-Bottom)

6.2.2.4 VOID ANALYSIS

Slab support conditions are key element of the performance of rigid pavements. The occurrence of surface distresses such as corner breaks, joint faulting, and slab cracking can all result from loss of support. Figure 25 presents an example of maximum deflection at slab corner (D_0) versus HWD loads, from corner 8SW of slab SF8S. Intercept values greater than zero along the vertical axis, indicate the possible presence of voids (or gaps between the slab bottom and top of the base course).

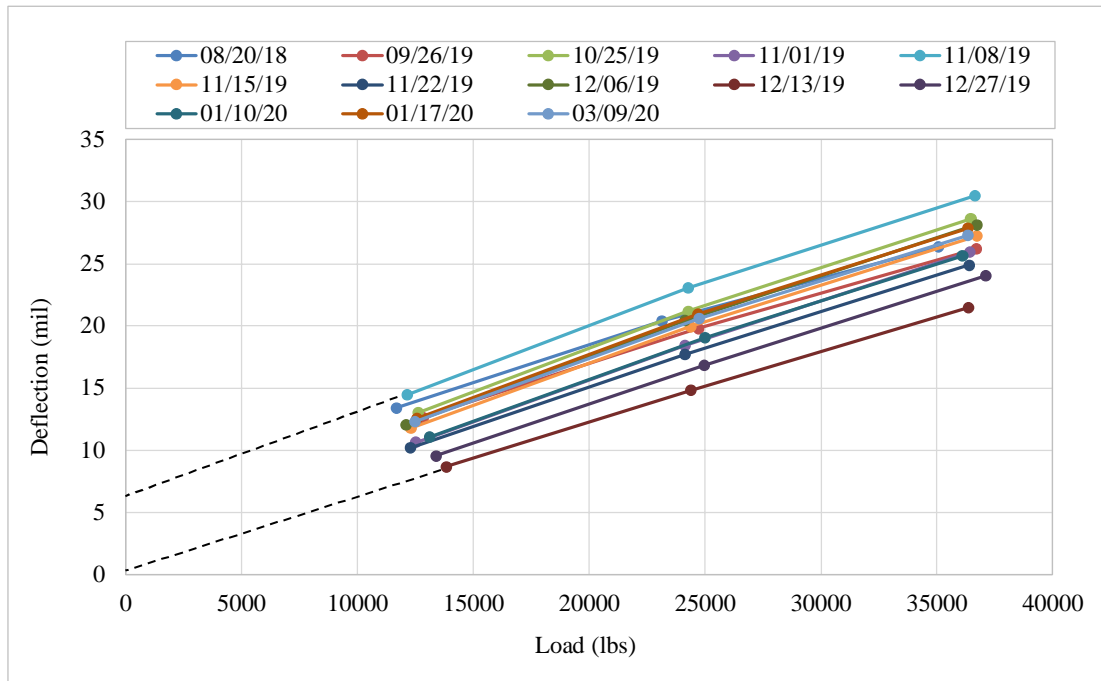


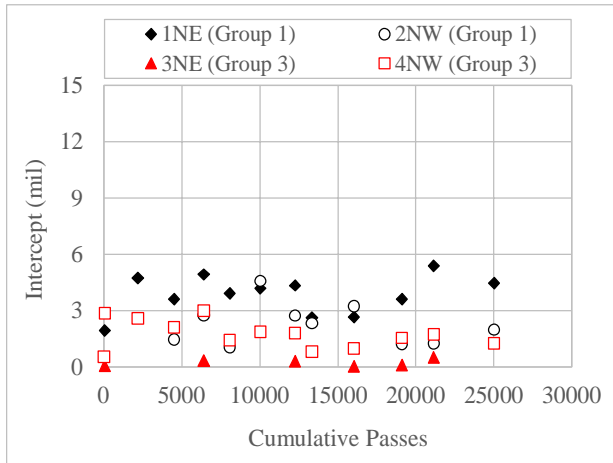
Figure 25. Example of Void Detection in Corner 8SW of Slab SF8S

Figures 26(a)-(d) illustrate the variation in intercept values (i.e., theoretical deflection at zero load) over the course of trafficking for 12- and 9-inch thick slabs along both the north and south inner lanes. Overall, the initial intercept values from the corners of 12-inch thick slabs were smaller compared to the corners of 9-inch thick slabs. This indicates that the initial support conditions provided by layers underlying 12-inch thick slabs were stronger than 9-inch thick slabs on both the north and south side. Before cumulative pass 15,000, the intercept value of most slabs showed an inconsistent variation. After cumulative pass 15,000, an increasing trend was generally observed for most of the slabs on both the north and south inner lanes up to about 21,000 passes. The observed trends are fairly consistent with those of corner-to-center deflection ratio in figure 23. The changes in intercept values can be attributed to changes in slab temperature differential.

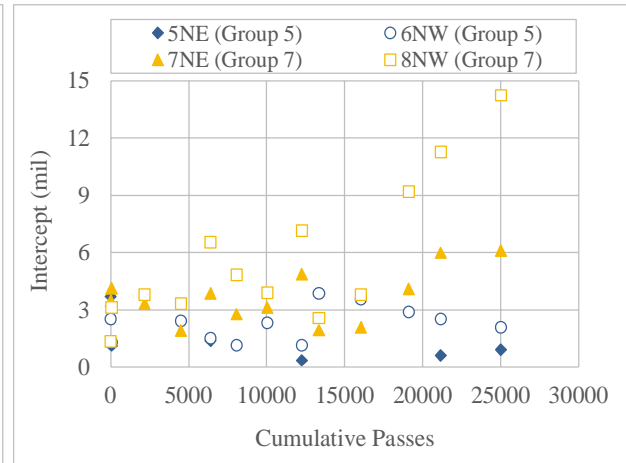
6.2.2.5 BACKCALCULATION OF LAYER MODULI

PSPA modulus only provides indication of stiffness for the surface PCC slab, while ISM from HWD deflection provides the combined stiffness of the pavement section. The layer moduli of individual pavement layers were back-calculated from slab center deflection basins using BAKFAA v3.1.0 software. Table 9 summarizes the pavement structure and material properties for back-calculation. FAARFIELD default moduli were assigned to the subbase and subgrade.

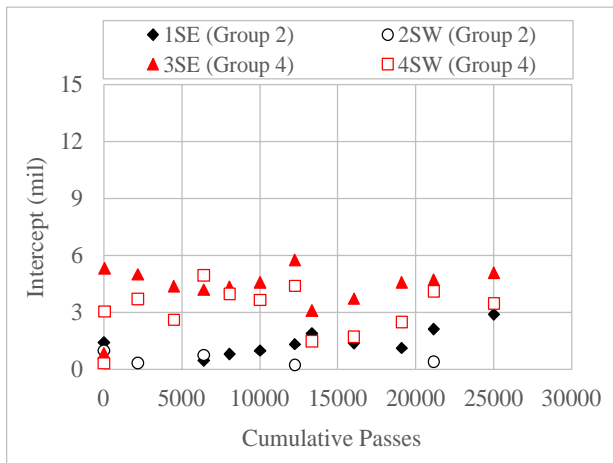
Representative layer moduli for slab groups with similar cross-section, *R*-value, and subgrade stiffness were obtained by averaging the values of individual slabs within the groups. Figures 27-30 illustrate the changes in back-calculated modulus as a function of cumulative passes for the PCC slab, base, subbase, and subgrade. Throughout the 25,000 cumulative passes applied by March 6, 2020, the back-calculated modulus trends for all four pavement layers show no clear sign of degradation in structural integrity.



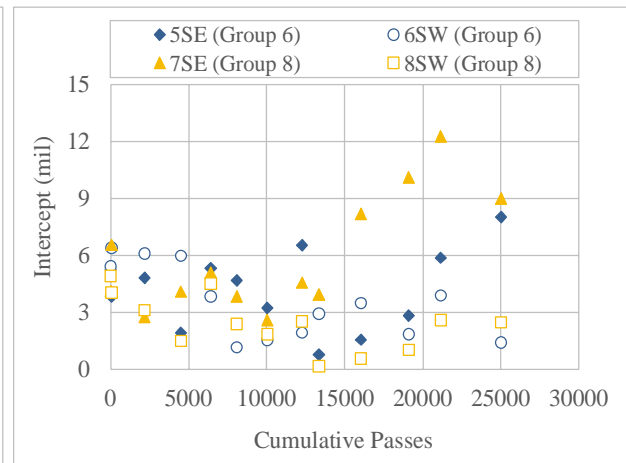
(a)



(b)



(c)



(d)

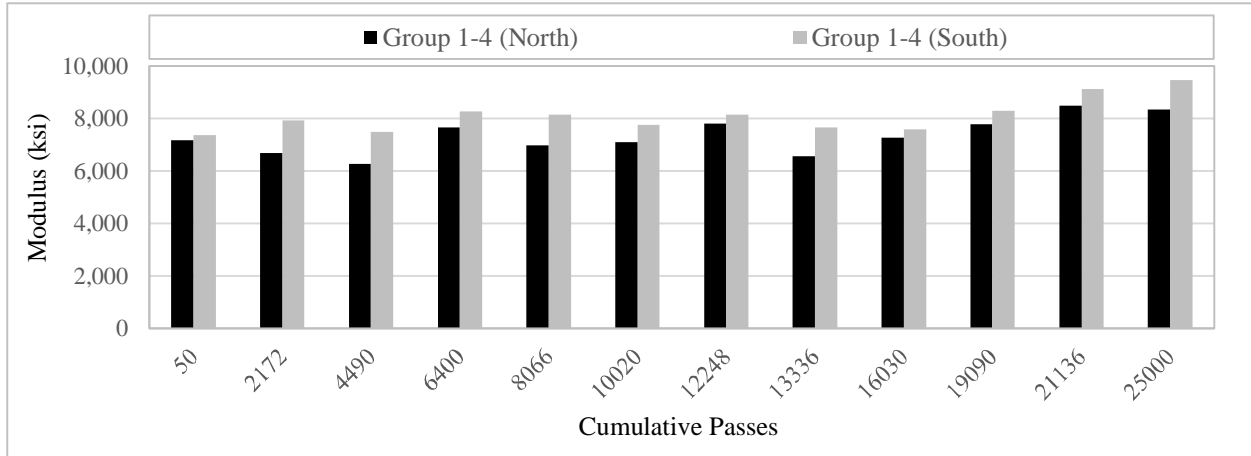
Figure 26. Intercept vs. Cumulative Passes for Inner Lanes: (a) North (Group 1 & 3), (b) North (Group 5 & 7), (c) South (Group 2 & 4), (d) South (Group 6 & 8)

Table 9. Summary of Material Properties for Back-calculation

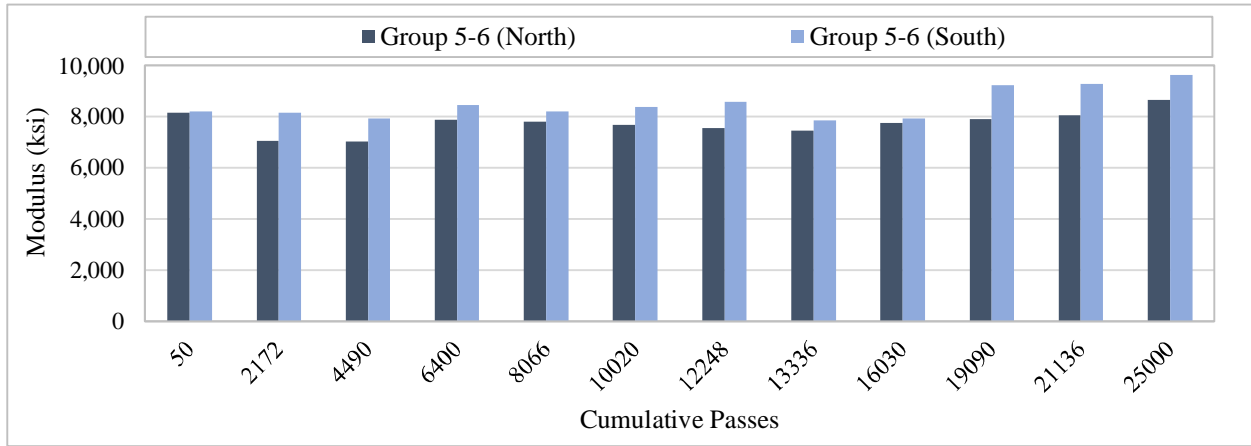
Pavement Layer	Group: 1-4				Group: 5-8			
	Seed Modulus (ksi)	Poisson's Ratio	Interface Condition	Thickness (in)	Seed Modulus (ksi)	Poisson's Ratio	Interface Condition	Thickness (in)
P-501MR	4000	0.15	0.0 ¹	12	4000	0.15	0.0 ¹	9
P-306MR	2000	0.2		6	2000	0.2		6
P-154M	20.24	0.35	1.0 ²	14	20.24	0.35	1.0 ²	17
P-152M	11.74	0.4		-	11.74	0.4		-

¹ fully-*unbonded*

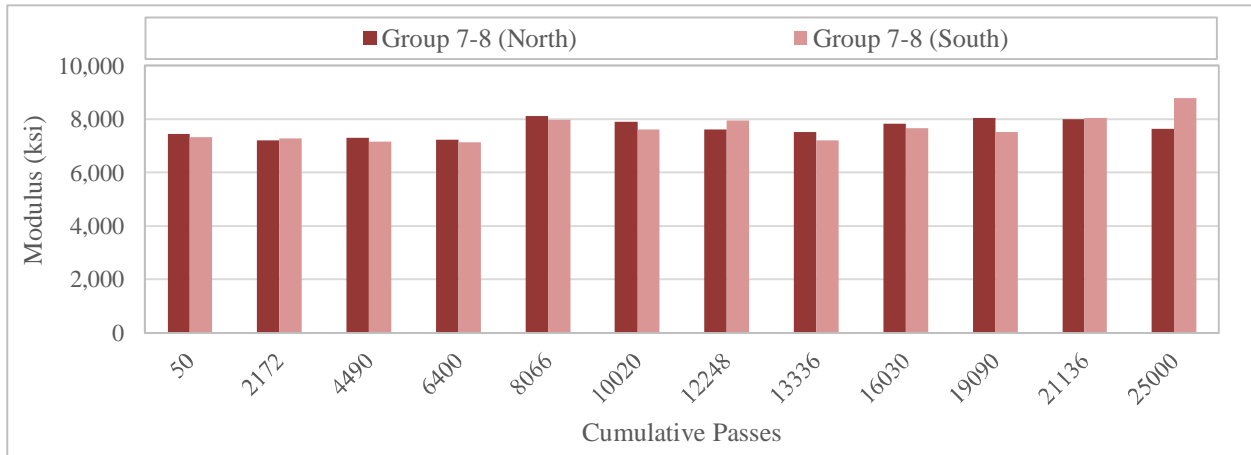
² fully-*bonded*



(a)

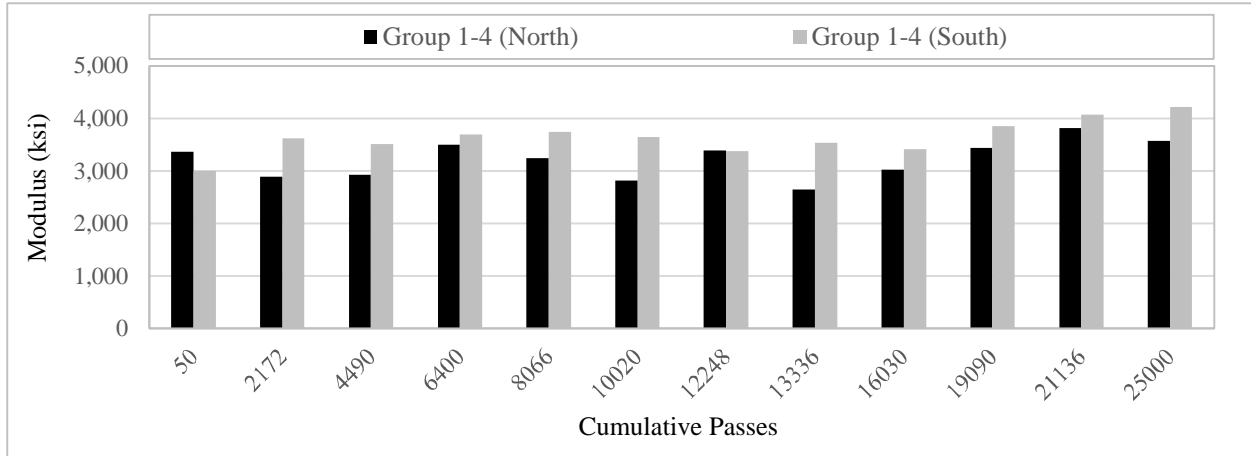


(b)

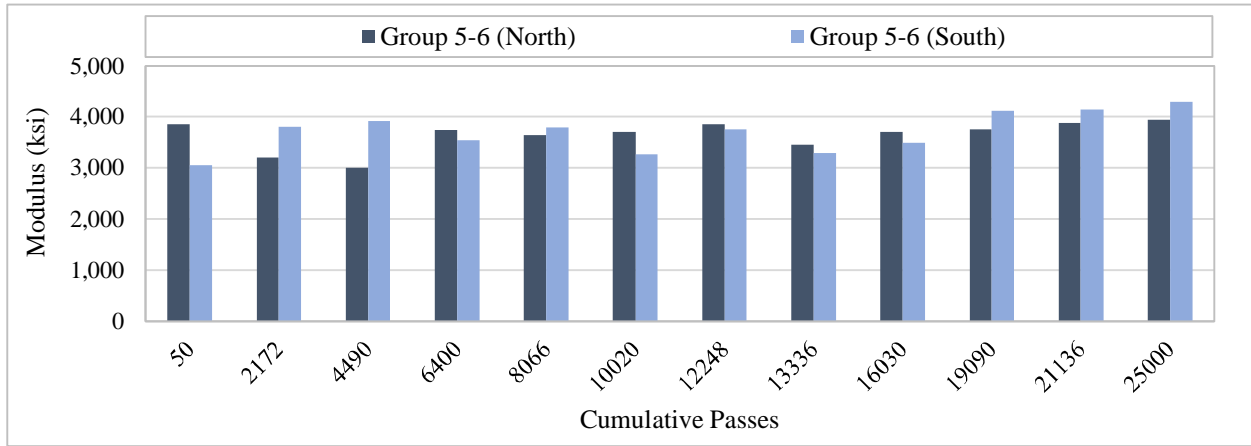


(c)

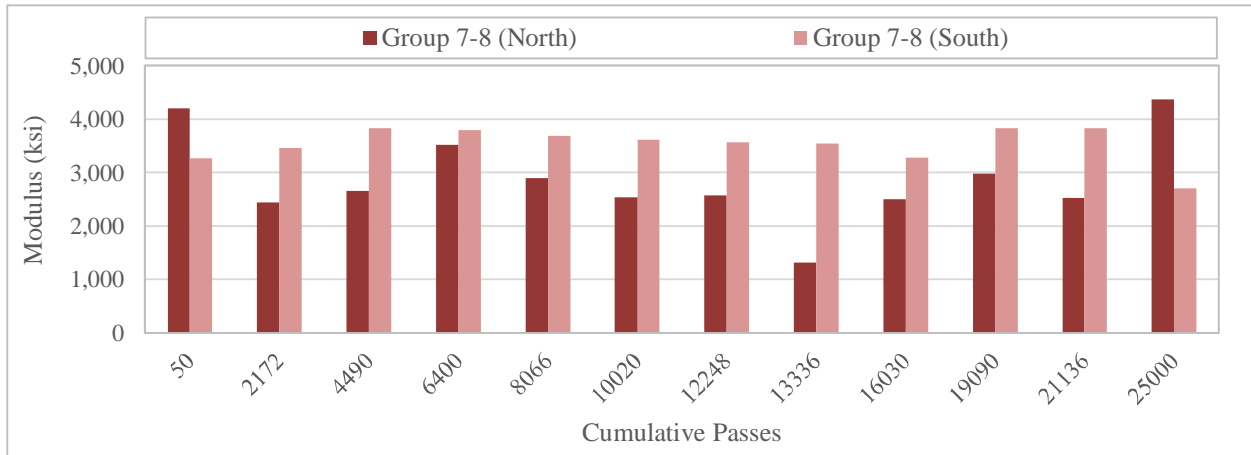
Figure 27. Backcalculated Moduli of P-501MR vs. Cumulative Passes for Inner Lanes:
 (a) Groups 1-4, (b) Groups 5 & 6, (c) Groups 7 & 8



(a)

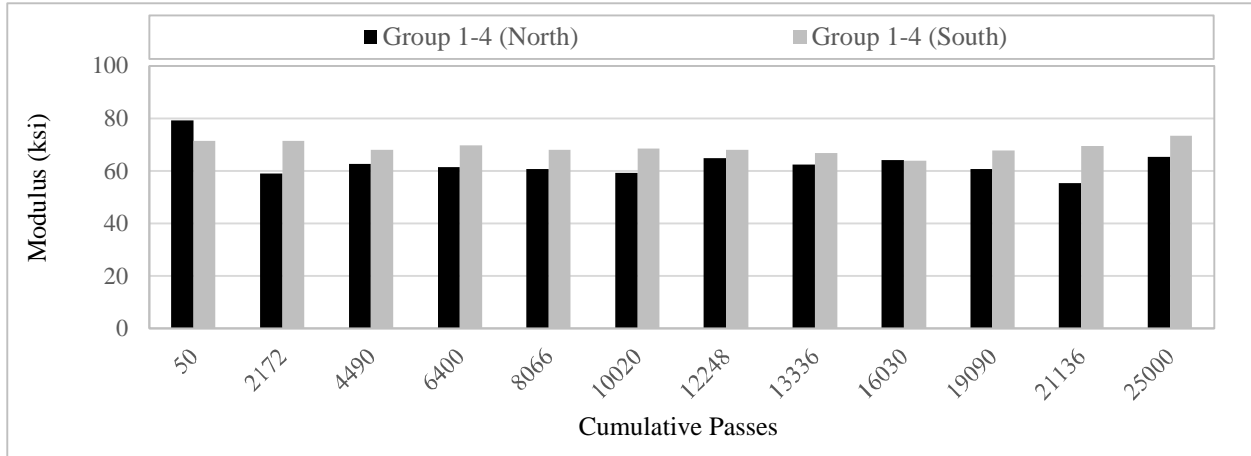


(b)

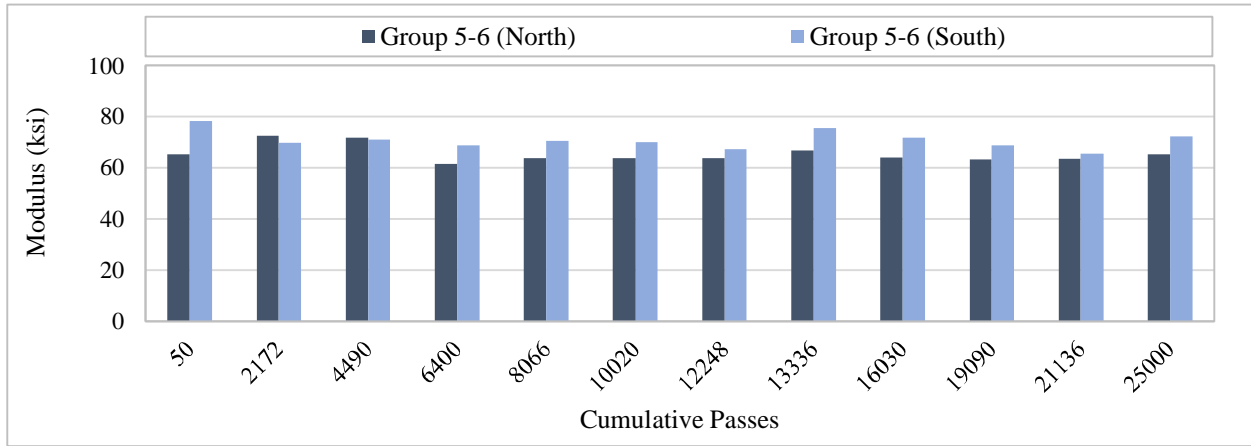


(c)

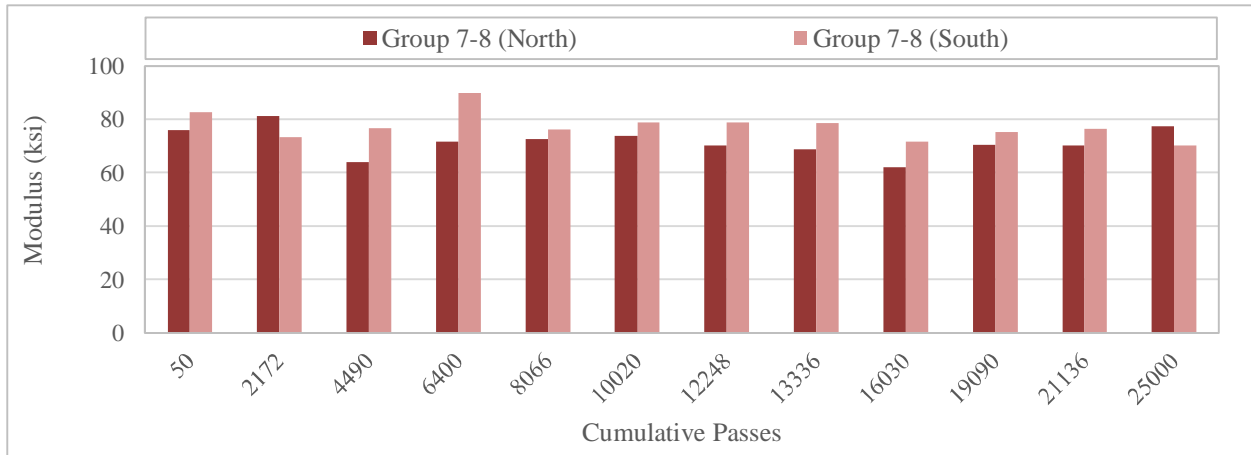
Figure 28. Backcalculated Moduli of P-306MR vs. Cumulative Passes for Inner Lanes:
 (a) Groups 1-4, (b) Groups 5 & 6, (c) Groups 7 & 8



(a)

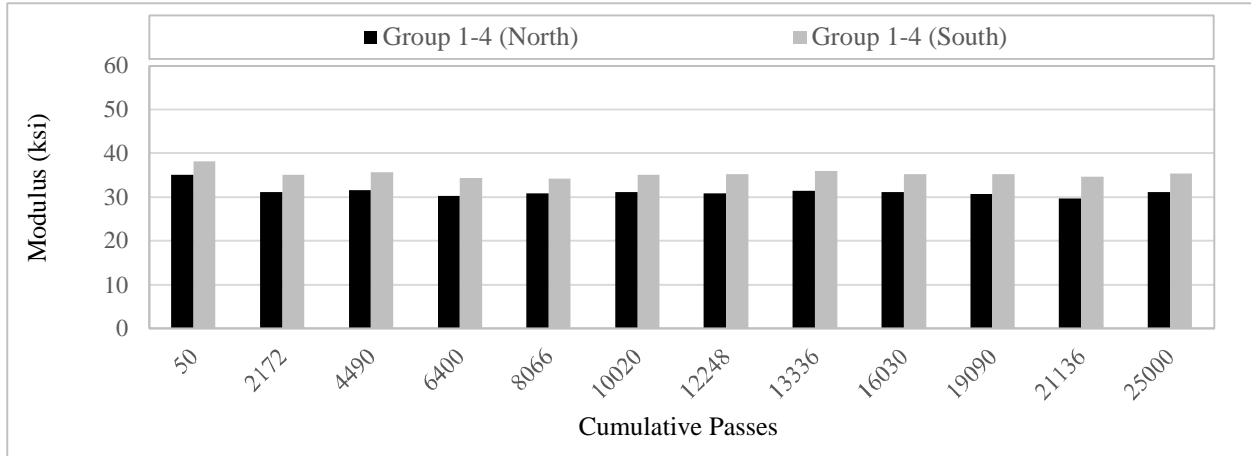


(b)

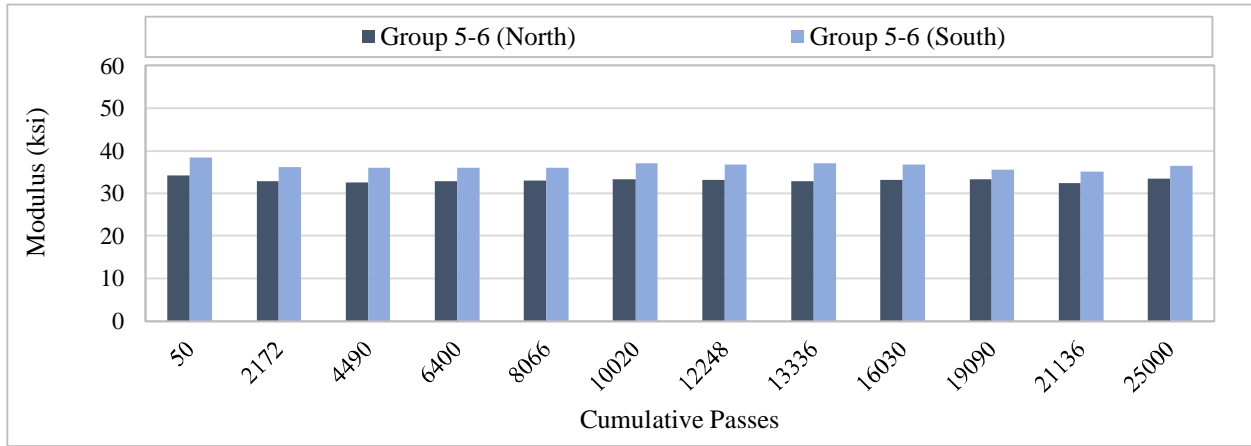


(c)

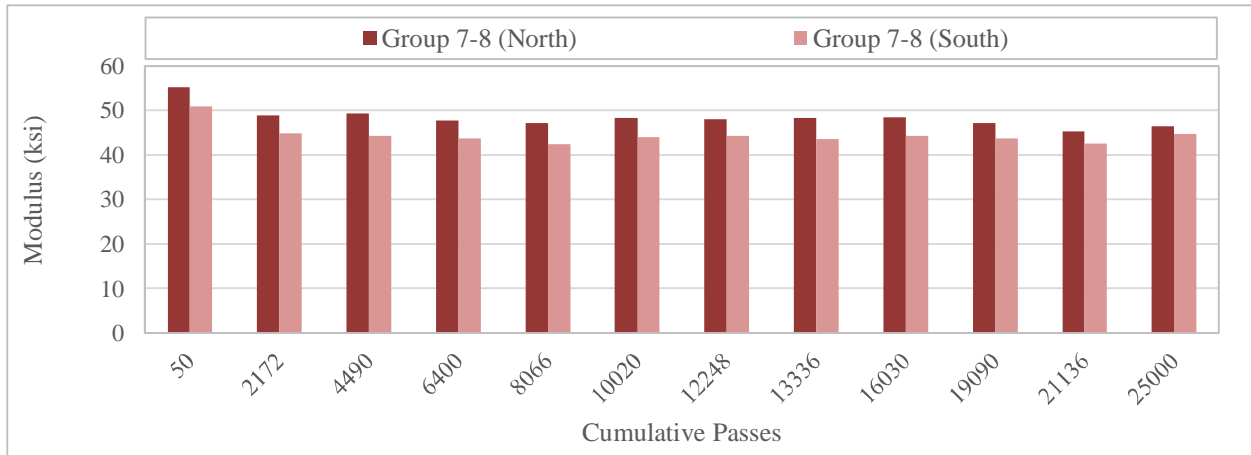
Figure 29. Backcalculated Moduli of P-154M vs. Cumulative Passes for Inner Lanes:
 (a) Groups 1-4, (b) Groups 5 & 6, (c) Groups 7 & 8



(a)



(b)



(c)

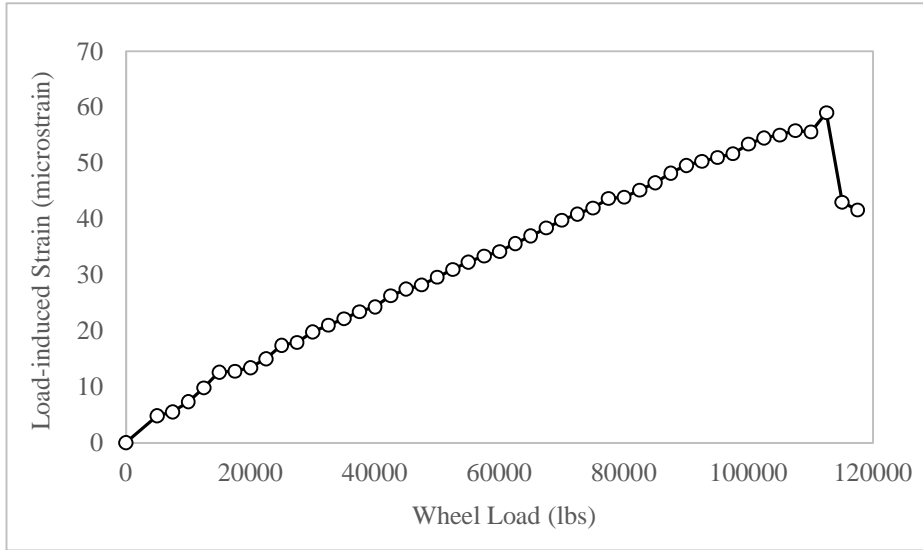
Figure 30. Backcalculated Moduli of P-152M vs. Cumulative Passes for Inner Lanes:
 (a) Groups 1-4, (b) Groups 5 & 6, (c) Groups 7 & 8

6.3 PCC SLAB CRACKING STRENGTH

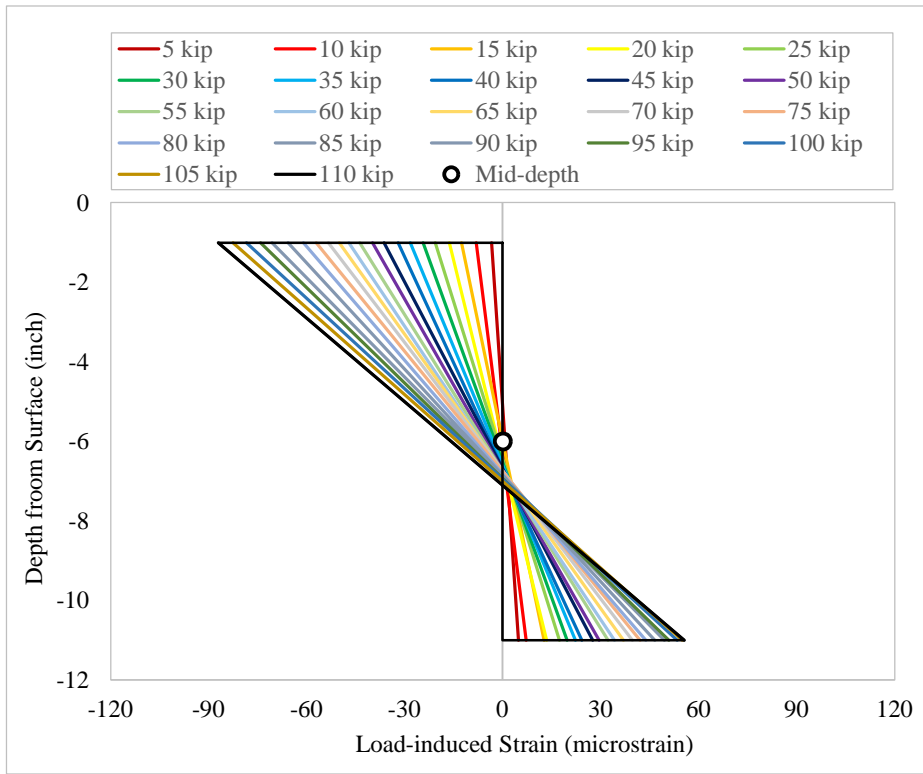
During static load tests, strain responses from bottom EGs were collected at every load increment. For demonstration, selected strain response histories indicating a rupture at the slab bottom are plotted in figure 31(a) and 32(a) for 12-inch and 9-inch slabs, respectively. On both charts, a progressive increase in strain at relatively steady rate is observed with increasing load. This increase continues until the trend is suddenly disrupted (i.e., spike or drop in the response), indicating the initiation of bottom-up crack. The corresponding strain profiles in figure 31(b) and 32(b) verify that in both cases the neutral axis started close to the mid-depth and moved downward with increasing loads until the point of rupture.

Given the known slab thickness and estimating the neutral axis position from the top and bottom strain gauge responses, the extreme fiber strain (bottom of slab) corresponding to the load just before rupture was computed. Then, the maximum load-induced extreme-fiber stress was estimated using the in-situ concrete modulus derived from PSPA test data. Table 10 summarizes the estimated load-induced stress at rupture. These stresses ranged from 309 psi to 372 psi and were unexpectedly low compared to the flexural strength R of field-cured beams determined from ASTM C78 (710 psi and 950 psi for 12-inch and 9-inch thick slabs, respectively). In fact, the apparent stress ratio of all slabs was below 55%, which theoretically should not produce rupture.

By contrast, the previous NAPTF CC6 Slab Strength Test documented cracking strains at the bottom of the PCC slab that ranged from 128 to 136 microstrains (Guo et al., 2012), which were in the expected range for concrete with R -value of 650 psi. The inconsistency between the CC6 and CC8 strength test results could be attributed to differences in some of the test parameters, specifically: the loading gear configuration (S in CC8 vs. 2D in CC6); the base material (lean concrete in CC8 vs. hot-mix asphalt treated base in CC6); and the joint type (undoweled construction joints in CC8 vs. doweled construction joints in CC6). Any analysis must consider that the total stress operating on the concrete slab, and which leads to the rupture, is the sum of the load-related stress and the built-in or residual stress (Guo et al., 2012). There is a strong likelihood that non-load-related tensile stresses may have developed in the CC8 slabs during the more than 400 days that elapsed between the concrete placement and the static load tests.

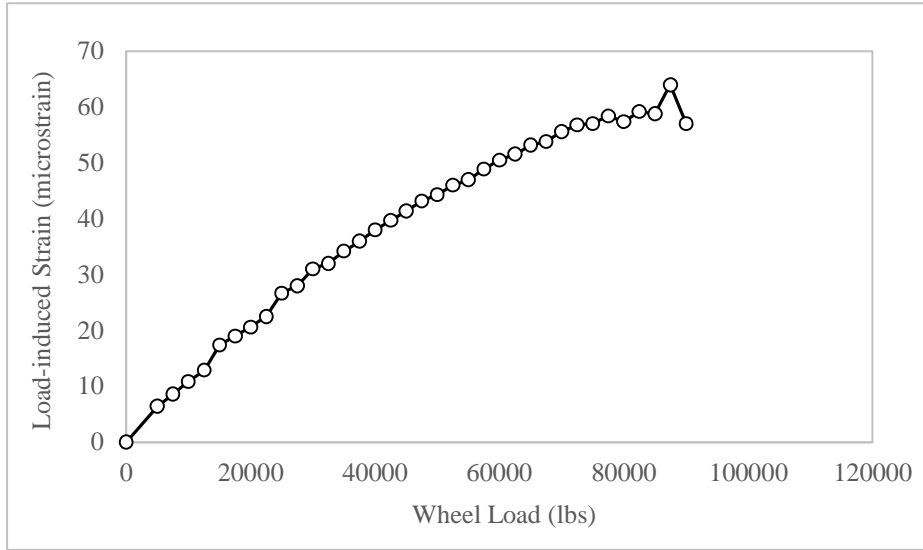


(a)

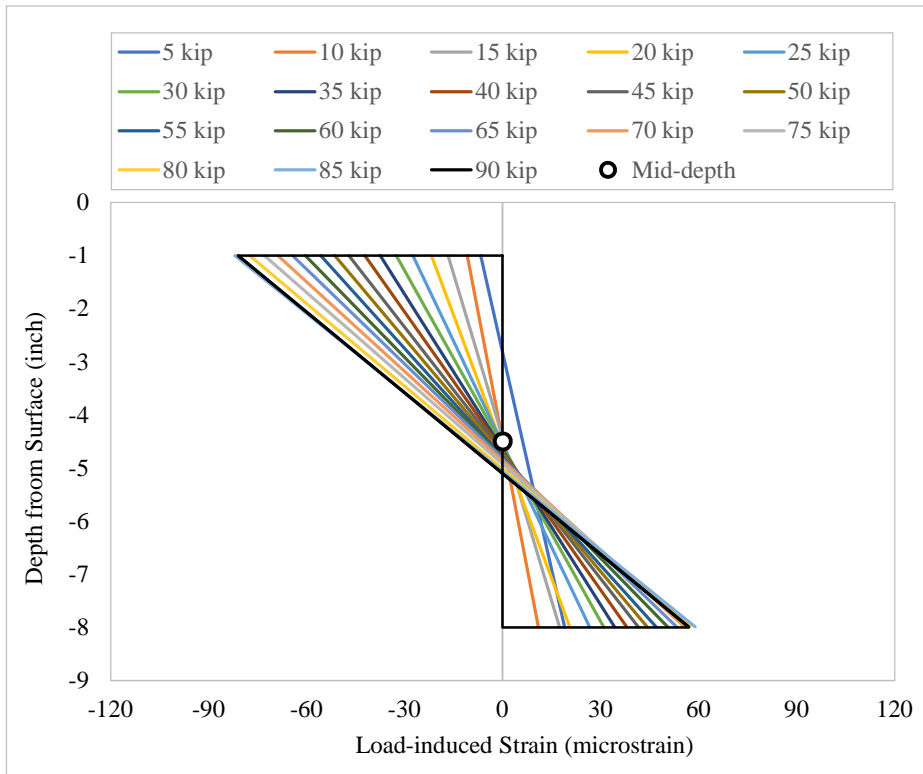


(b)

Figure 31. Load-induced Strain during Static Load Tests on SF1N: (a) Load vs. Strain, (b) Change in Neutral Axis Position



(a)



(b)

Figure 32. Load-induced Strain during Static Load Tests on SF5N: (a) Load vs. Strain, (b) Change in Neutral Axis Position

Table 10. Summary of Load-induced Maximum Fiber Strain, Stress, and Stress Ratio

Slab ID	Thickness (inch)	R-value (psi)	Maximum Fiber Strain (microstrain)	PSPA Modulus (ksi)	Maximum Fiber Stress (psi)	Stress Ratio
SF1N	12	650	70	4417	309	0.44
SF2N			71	4915	347	0.49
SF5N	9	900	79	4717	372	0.39
SF6N			90	3763	340	0.36

7. ADVANCED DATA ANALYSIS

7.1 FAILURE MECHANISM

Trafficking on the inner lanes of the CC8 S/F test area was paused on March 19, 2020 due to the COVID-19 pandemic. After 25,000 cumulative passes, no surface distresses were observed suggesting that only bottom-up crack initiation (Stage 1) may have been possible at that point. Three approaches are followed in an attempt to understand the failure mechanism: (a) HWD imposed pavement deformation energy for full-length longitudinal crack propagation; (b) internal strain energy for crack initiation and propagation; and (c) evaluation of tensile stress ratio.

7.1.1 PAVEMENT DEFORMATION ENERGY FOR CRACK CHARACTERIZATION

HWD load imposed pavement deformation energy can be simply calculated from the drop load (P) and surface maximum deflection (δ_{max}) at the center of the load plate. Energy calculation only included deflection data from HWD drops at nominal $P=36,000$ lbs. All δ_{max} data were first normalized to the nominal load and then energy was computed using the following expression:

$$Energy = \frac{1}{2} \times P \times \delta_{max} \quad (2)$$

Figures 33 (a)-(d) show the changes in HWD load imposed pavement deformation energy for 12-inch thick slabs on the north side. The initial values for the all the slabs ranged from 0.14 to 0.18 in-kip. No indication of changes in the pavement deformation energy trends was observed (i.e., drop or spike in energy values). This indicates that crack initiation either has not yet taken place or was not captured (if it occurred) by the energy trends.

Figures 34 (a)-(d) show the changes in HWD load imposed pavement deformation energy for the south side 12-inch thick slabs. Unlike north inner lane 12-inch slabs, the energy trends of 12-inch slabs on the south side show more consistency with a narrower range of initial values. Similar to north inner lane slabs, no indication of crack initiation can be observed in the trends.

Figures 35 and 36 show the changes in pavement deformation energy for 9-inch thick slabs on both the north and south side, respectively. On both the north and south side, non-uniformity in the energy level can be observed when comparing among slabs. However, the energy trends for slabs of both sides remained relatively constant over the course of trafficking. Again, this indicates

that most likely either crack initiation has not yet occurred or propagated into the vicinity of HWD testing locations.

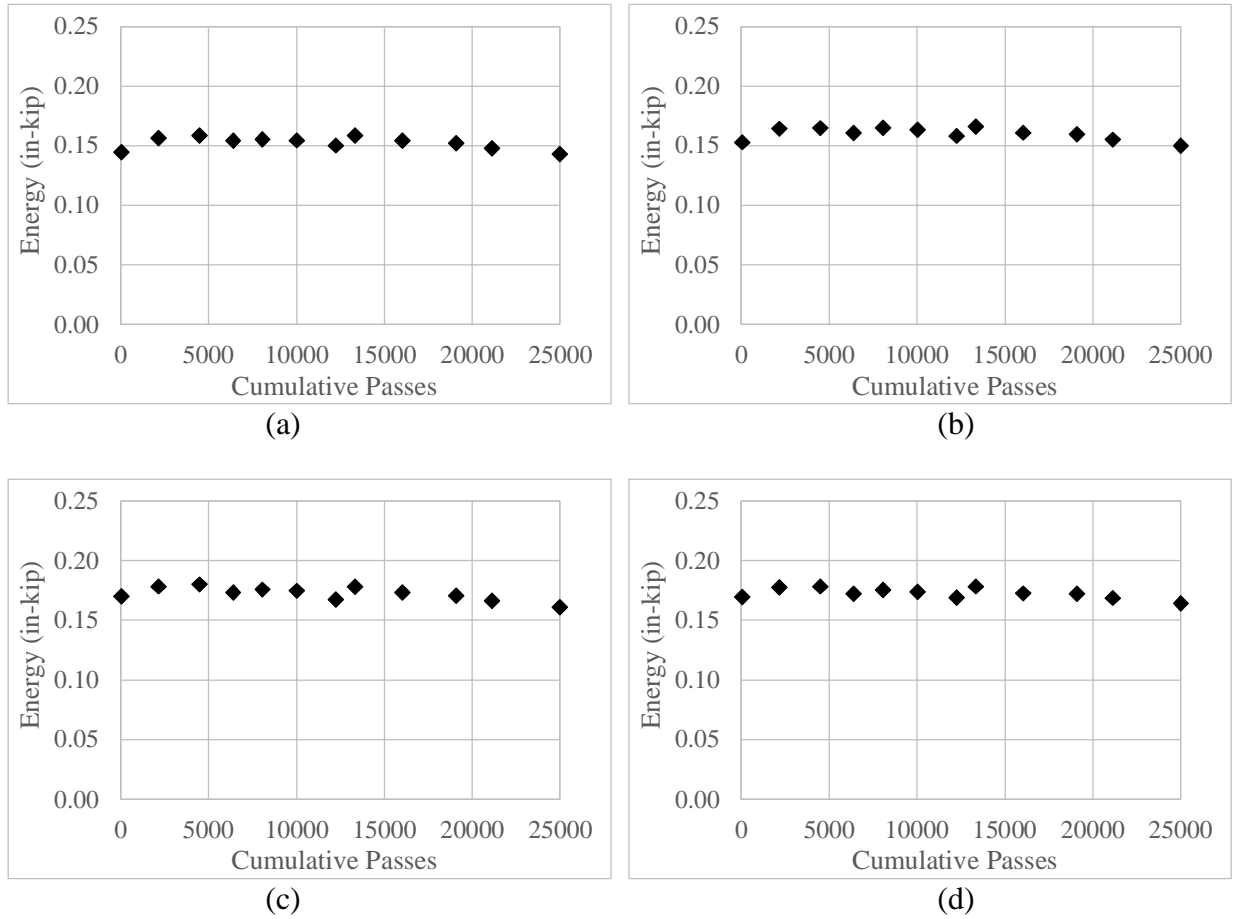
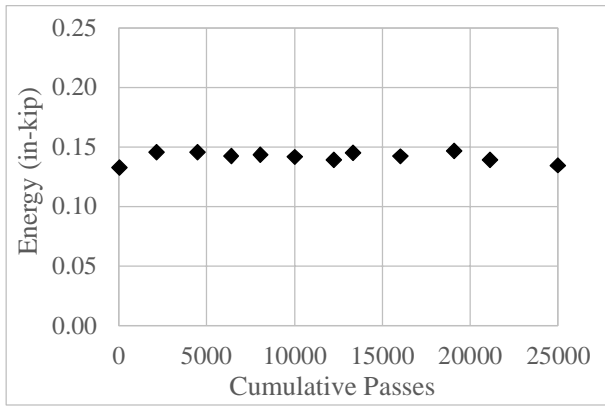
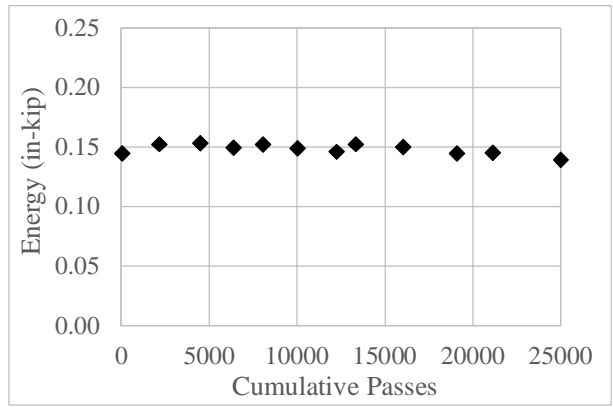


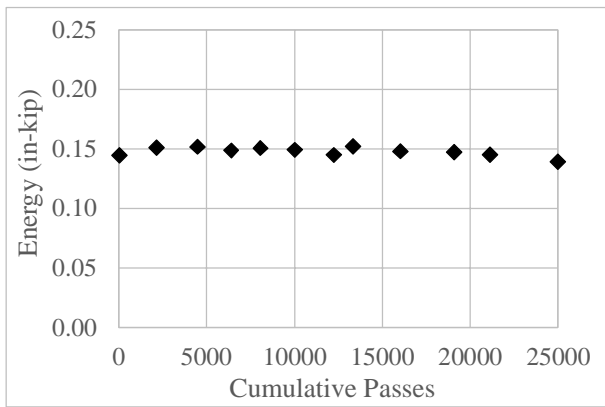
Figure 33. Pavement Deformation Energy on 12-inch Thick Slabs in North Inner Lanes: (a) SF1N, (b) SF2N, (c) SF3N, (d) SF4N



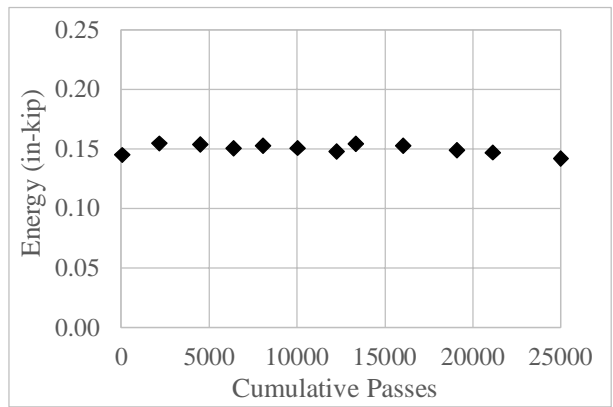
(a)



(b)

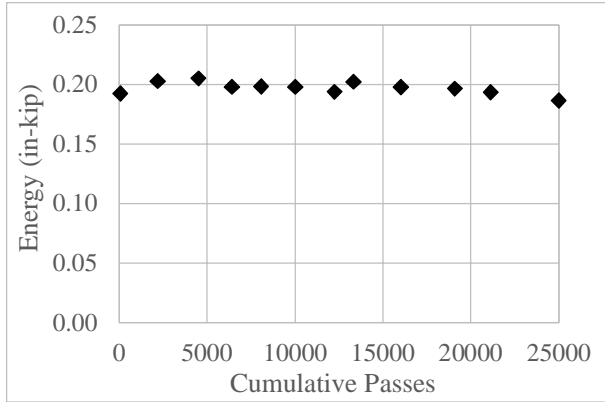


(c)

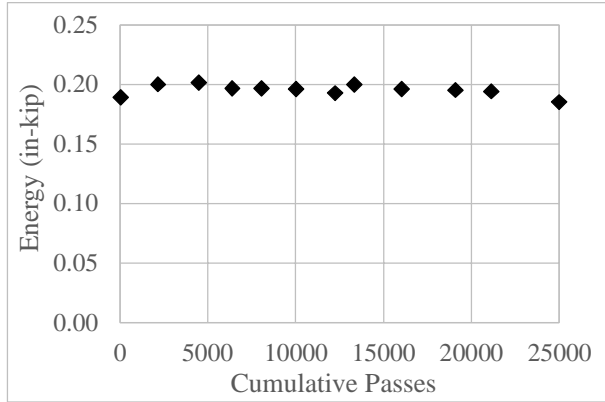


(d)

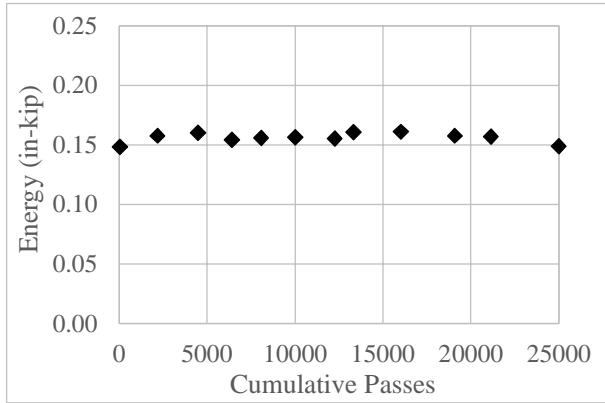
Figure 34. Pavement Deformation Energy on 12-inch Thick Slabs of South Inner Lanes: (a) SF1S, (b) SF2S, (c) SF3S, (d) SF4S



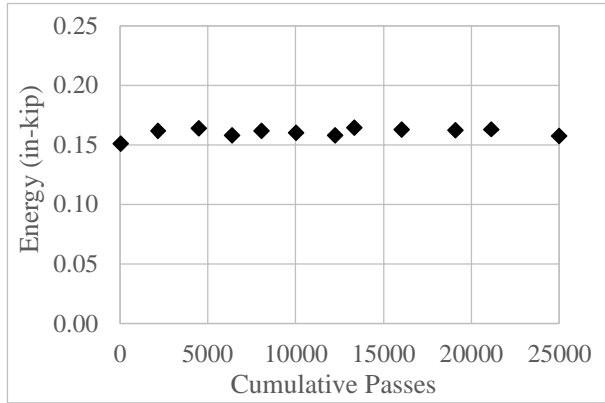
(a)



(b)

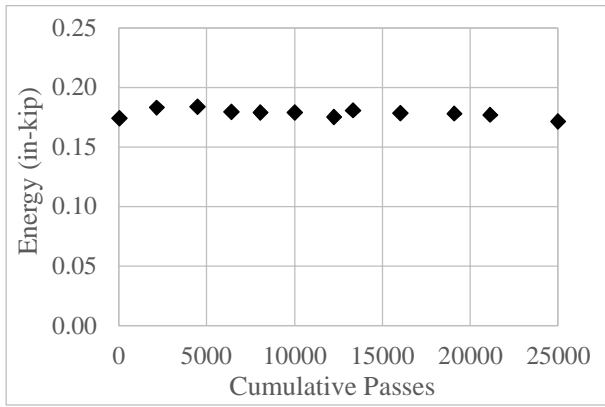


(c)

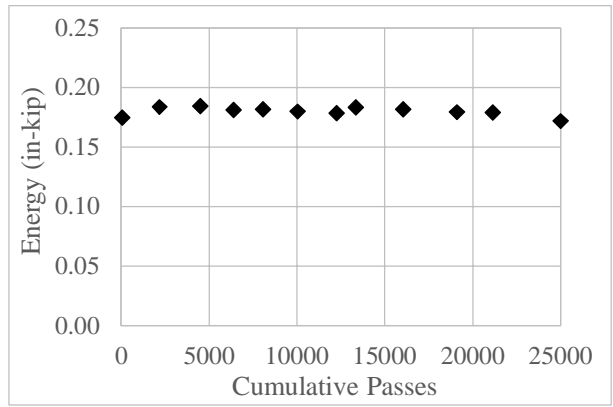


(d)

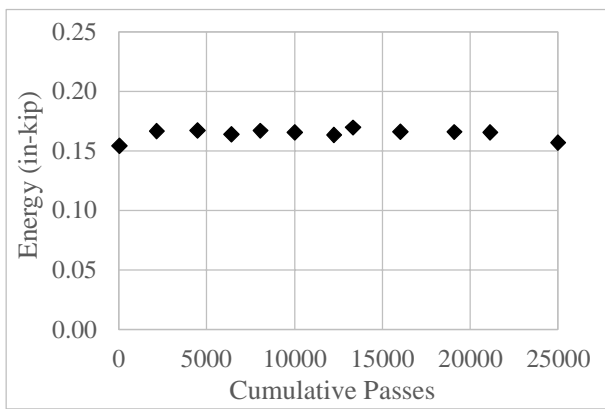
Figure 35. Pavement Deformation Energy on 9-inch Thick Slabs on North Inner Lanes: (a) SF5N, (b) SF6N, (c) SF7N, and (d) SF8N



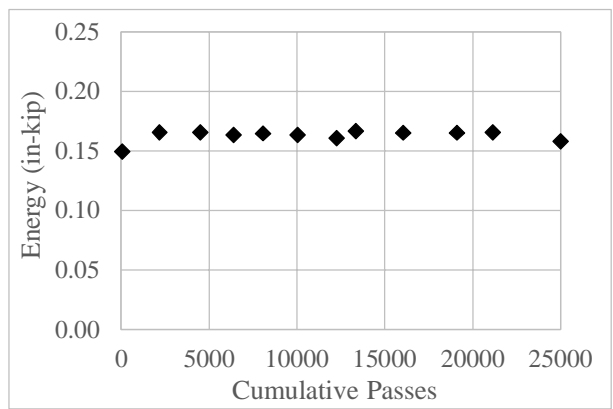
(a)



(b)



(c)



(d)

Figure 36. Pavement Deformation Energy on 9-inch Thick Slabs on South Inner Lane: (a) SF5S, (b) SF6S, (c) SF7S, (d) SF8S

7.1.2 INTERNAL STRAIN ENERGY IN PCC SLAB FOR CRACK CHARACTERIZATION

In addition to HWD load imposed pavement deformation energy, internal strain energy was computed from EG responses. The slab bending moment (M) and curvature (θ) were first determined from the strain response history under each vehicle pass.

Figure 37 illustrates the derivation of bending moment based on the strain profile. The analysis is simplified by assuming a traditional beam model. The top and bottom EGs of a loaded slab recorded both compressive (ε_c) and tensile strains (ε_t), respectively. These strains were multiplied by the slab modulus from PSPA data (E_{slab}), to determine compressive (σ_c) and tensile (σ_t) stresses.

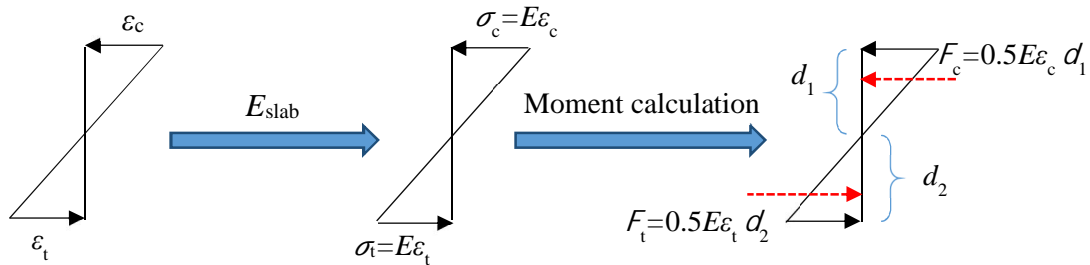


Figure 37. Derivation of Bending Moment from Strain Profile

Resultant compressive (F_c) and tensile (F_t) forces were determined based on the stress magnitudes and spacing between top and bottom EGs. The bending moment was calculated using the following equation:

$$M = \frac{2}{3}d_1F_c + \frac{2}{3}d_2F_t \quad (3)$$

where d_1 and d_2 are the depth of compressive and tensile stress zone, respectively. In this case, d_1 and d_2 (determined from the computation of NAP) are proportional to ε_c and ε_t , respectively. The curvature angle, θ , was calculated using the equation below:

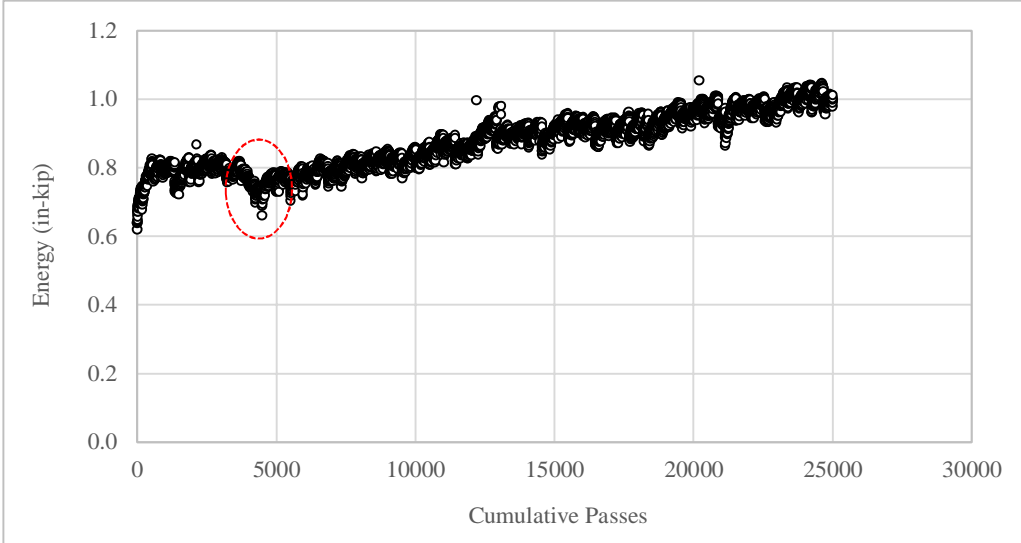
$$\theta = \varepsilon_t \times \text{bottom EG gage length}/d_2 \quad (4)$$

Finally, the strain energy was calculated as the product of moment and curvature using equation (6):

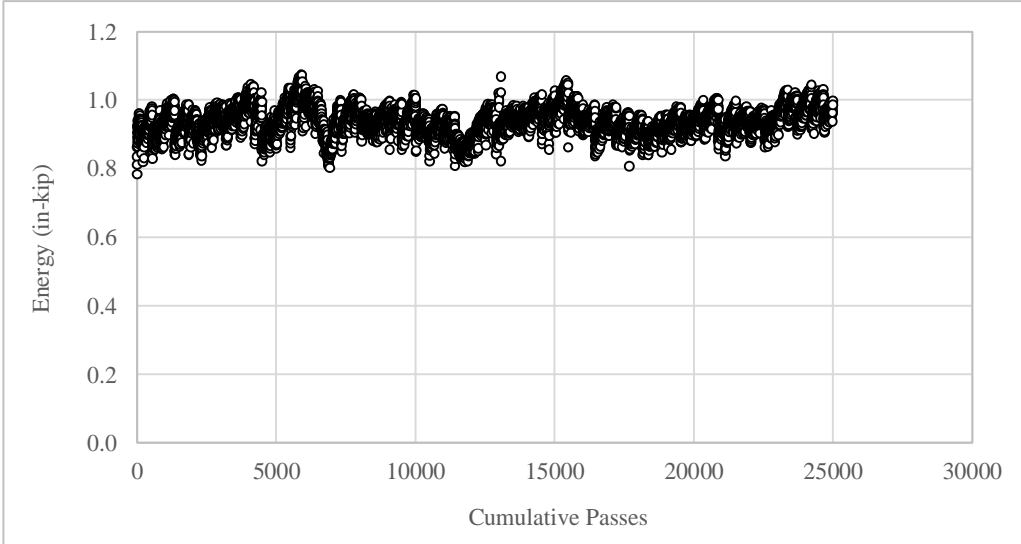
$$\text{Internal Strain Energy} = \frac{1}{2}M\theta \quad (5)$$

Initially the analysis of internal strain energy included all non-pre-cracked/unnotched slabs SF3N, SF4N, SF7N, and SF8N. Preliminary analysis of EG responses in intact slabs determined that both the top and bottom gauges were functional only in SF7N and SF8N. Therefore, SF3N and SF4N were later excluded from this analysis.

Figure 38(a) and (b) show the changes in internal strain energy over the course of trafficking for slab SF7N and SF8N, respectively. In figure 38(a), the strain energy trend for SF7N shows a clear inflection point after approximately 5,000 cumulative passes. The increasing trend observed after this inflection point may indicate the initiation of bottom-up cracks. The crack (if initiated) has not completed full-depth propagation since no sign of surface distress has been reported as of March 19, 2020. In figure 38(b), the strain energy for slab SF8N shows a relatively constant trend. No evident change of trajectory that can be associated to crack initiation is observed in the data.



(a)



(b)

Figure 38. Change in Internal Strain Energy Over the Course of Trafficking: (a) Slab SF7N, (b) Slab SF8N

7.1.3 TENSILE STRESS RATIO

It is speculated that non-load-related tensile stresses (i.e., residual stresses possibly built up in the slabs prior to initiating full-scale tests) coupled with load-induced stresses applied during static load tests, led to the initiation of bottom-up crack when exceeding the flexural strength. The residual stress was estimated for each of the slab groups tested under static load by subtracting the average maximum tensile stress at the bottom fiber from the actual flexural strength measured on laboratory-cured beams. Table 11 summarizes the estimated residual stresses.

Table 11. Summary of Estimated Residual Stresses

Group	Slab ID	Thickness (inch)	R (psi)	Crack Load (lbs)	Tensile Strain at Bottom EG (microstrain)	Compressive Strain at Top EG (microstrain)	PSPA Modulus (ksi)	Maximum Fiber Stress ¹ (psi)	Residual Stress ² (psi)
1	SF1N	12	650	107500	55.8	-84.8	4417	308.6	382.3
	SF2N			110000	55.6	-94.3	4915	346.9	
5	SF5N	9	900	85000	58.8	-81.9	4717	372.1	594.1
	SF6N			92500	68.3	-85.5	3763	339.7	

¹ Extrapolated tensile stress at the bottom fiber of inner lane slabs.

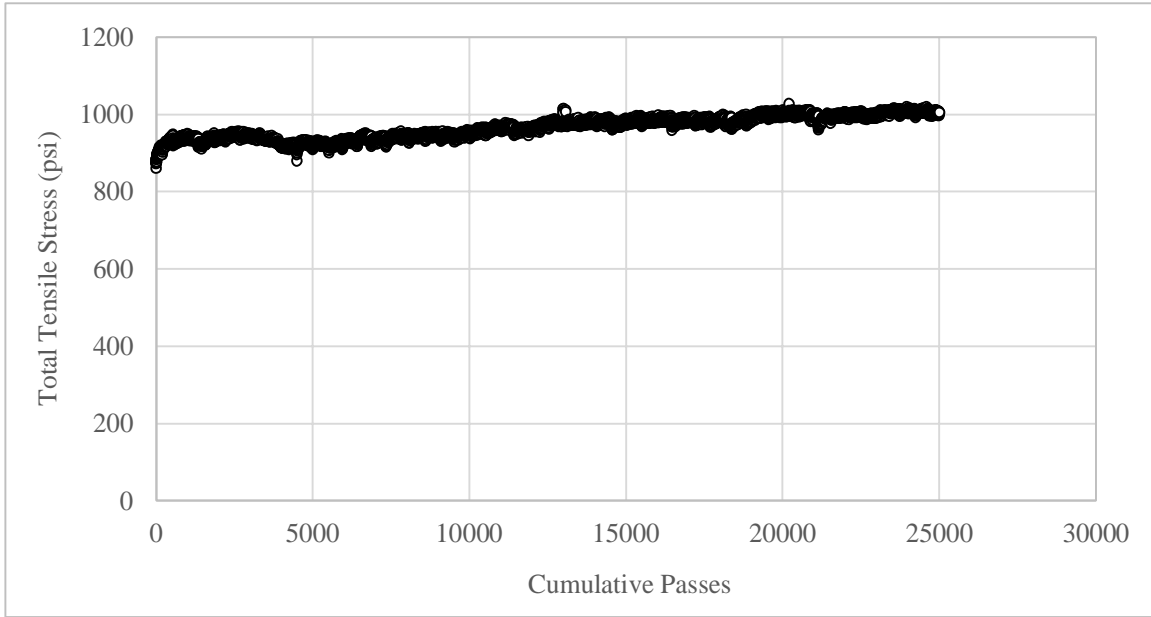
² Residual stresses determined using R of 710 and 950 psi for 12- and 9-inch slabs, respectively. These R were measured on laboratory-cured beams with an average age of 280 days.

During the moving load test, the total tensile stress (σ_{total}) at the slab bottom fiber was calculated as the sum of the load-induced tensile stress and the residual stress ($\sigma_{residual}$), as shown in the equation below (Guo et al., 2012):

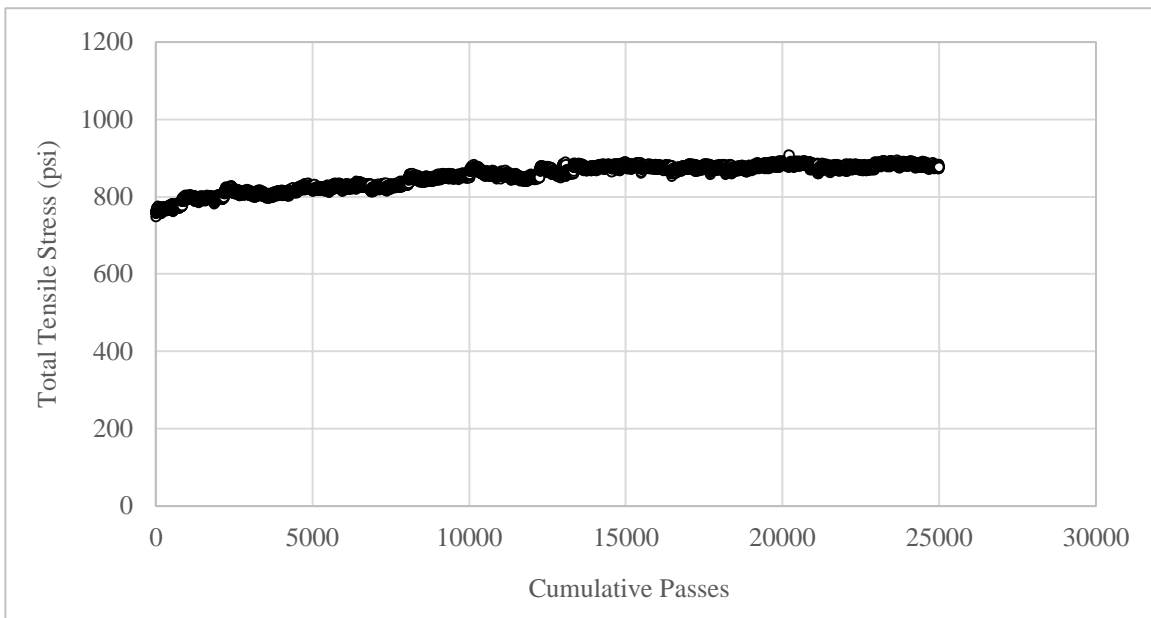
$$\sigma_{total} = E_{PSPA} \varepsilon_{load-induced} + \sigma_{residual} \quad (6)$$

where, E_{PSPA} is the slab modulus determined from PSPA testing and $\varepsilon_{load-induced}$ is the load-induced tensile strain at the slab bottom fiber. Figure 39 (a) and (b) show the change in total tensile stress over the course of trafficking for SF7N and SF8N, respectively. Note that only slabs with both top and bottom EGs operational were considered for this analysis. In both SF7N and SF8N, the initial total stress was close to 800 psi, increasing over the course of trafficking to 950 psi or above.

The ratio of total tensile stress to flexural strength (tensile stress ratio) was calculated. Figure 40 (a) and (b) show the change in tensile stress ratio over the course of trafficking for SF7N and SF8N, respectively. In the figures, the red line corresponds to the threshold tensile stress ratio of 1 (i.e., the total tensile stress equals the flexural strength of 950 psi for SF7N and SF8N). As illustrated in the figures, the total tensile stress already exceeds the flexural strength for SF7N, while the ratio remains below the threshold for SF8N. This is an indication that in both slabs a bottom-up crack may be about to initiate (if not initiated already).

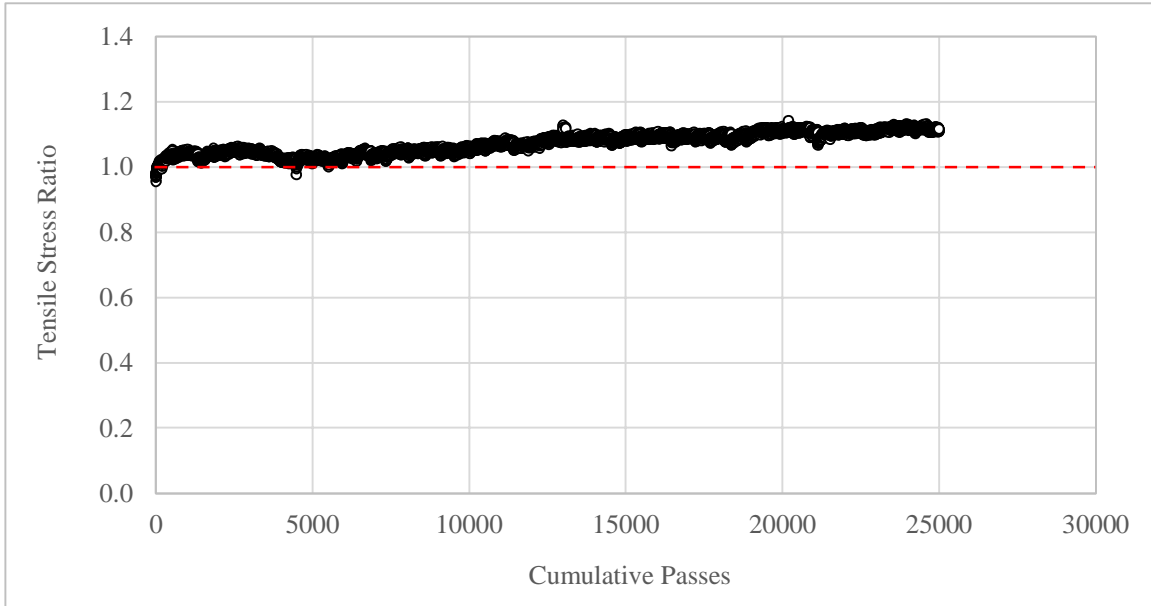


(a)

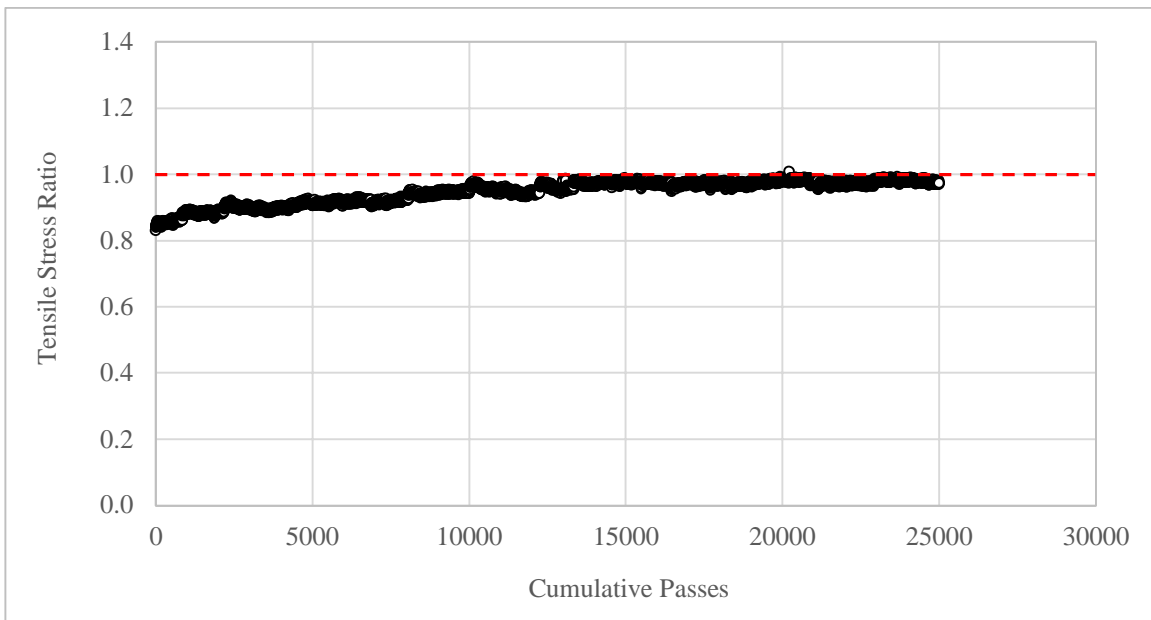


(b)

Figure 39. Change in Total Tensile Stress Over the Course of Trafficking: (a) SF7N, (b) SF8N



(a)



(b)

Figure 40. Change in Tensile Stress Ratio Over the Course of Trafficking: (a) SF7N, (b) SF8N

7.2 EFFECT OF CONCRETE FLEXURAL STRENGTH AND SLAB THICKNESS ON FATIGUE LIFE

After completing 25,000 cumulative passes with D module on March 6, 2020, the surface of CC8 S/F slabs showed no sign of deterioration. Therefore, investigating the effect of concrete flexural strength and slab thickness on fatigue life based on distress is not feasible at this point. In this section, the state of field stress in the slabs (i.e., as derived from instrumentation data) is investigated.

Table 12 summarizes the average load-induced stress, average total stress, and related stress ratios corresponding to the first pass for both 12- and 9-inch slabs. The residual stress from slab group 1 and 5 in table 11 were assumed for calculating average total stresses of 12- and 9-inch slabs. Stress ratios of 12-inch slabs are lower than 9-inch slabs. This suggests the possibility of delayed bottom-up crack initiation in 12-inch slabs which was also observed in the outer lane traffic test. The top EGs in 12-inch thick slabs were malfunctioning and therefore, the neutral axis position was assumed at the slab mid-depth for calculation of the bottom fiber strains.

Table 12. Summary of Stress Ratio Analysis

Slab ID	Thickness (inch)	R (psi)	CBR	Average Load-induced Stress (psi)	Average Total Stress (psi)	Stress Ratio ¹ (Stress / R)	
						Load-induced Stress	Total Stress
SF3N	12	650	7.5	103	485.1	0.15	0.68
SF4N							
SF7N	9	900	3.7	268	861.7	0.28	0.91
SF8N							

¹ Stress ratios were determined using R of 710 and 950 psi for 12- and 9-inch slabs, respectively. These R were measured on laboratory-cured beams with an average age of 280 days.

7.3 EFFECT OF SUBGRADE STRENGTH ON FATIGUE LIFE

The effect of subgrade strength on fatigue life is considered for the 9-inch thick inner lane slabs. Slabs SF5N and SF6N rest on subgrade of CBR 7-8, while slabs SF7N and SF8N rest on subgrade of CBR 3-4. SF5N and SF6N were pre-cracked during the static load test and therefore, the evaluation of subgrade strength effect on these slabs is only feasible for the last two stages of the failure model (i.e., full-depth and full-length crack propagation). No surface distress was observed after 25,000 cumulative passes with the D module; therefore, subgrade strength evaluation based on visual inspection data is not possible at this point.

The effect of subgrade strength is preliminarily investigated based on the load-induced stress at the bottom of slabs. Table 13 summarizes the load-induced stress in 9-inch thick slabs for two subgrade strength categories (i.e., CBR 7-8 beneath SF5N and SF6N on, and CBR 3-4 beneath SF7N and SF8N). Since SF5N and SF6N were pre-cracked slabs, the strains used for computing

load-induced stresses under intact condition were obtained from the static load test. These strains were measured during the portion of static load test conducted with the D module, at a wheel load of 35,000 lbs. The same gear configuration and wheel load were used later for the moving load test on all 9-inch slabs (i.e., SF5N-SF8N). For the case of non-pre-cracked slabs SF7N and SF8N, the strains used to derive load-induced stresses correspond to the first pass of the moving load test.

Table 13 shows that load-induced stresses in slabs built on subgrade of CBR 7-8 were lower than those in slabs built on subgrade of CBR 3-4. Therefore, longer fatigue life is expected for slabs on subgrade of CBR 7-8. This was found to be inconsistent with observations from ISM analysis which suggested the stiffness of pavement sections on subgrade of CBR 3-4 may be higher than that of sections on subgrade of CBR 7-8.

Table 13. Load-Induced Stresses (Subgrade with CBR 7-8 vs Subgrade with CBR 3-4)

Slab ID	Thickness (inch)	R-value (psi)	CBR	Maximum Fiber Strain (microstrain)	Slab Modulus (ksi)	Load-induced Stress (psi)	Average Load-induced Stress (psi)
SF5N	9	900	7-8	41.7	4717	197	161
SF6N				33.1	3763	125	
SF7N	9	900	3-4	67.2	4565	307	268
SF8N				49.7	4602	229	

7.4 COMPARISON OF NOTCHED VERSUS UNNOTCHED SLABS

The comparison of notched versus unnotched slabs is not possible at this point since no surface distress was observed after 25,000 cumulative passes with the D module.

7.5 FIELD EXPERIMENT VERSUS FAARFIELD

Prior to the initiation of full-scale tests, the coverages required for full-depth (Stage 1+2) and full-length (Stage 3) crack propagation were computed using the FAARFIELD model (HEC, 2020). The load level was assumed as 80% of the theoretical cracking load determined from FEAFAA simulations. The default 85% failure envelope was assumed regardless of subgrade strength.

The initial analysis was later updated by incorporating load-induced stresses derived from the tensile strains measured under one of the wheels of the D module. The response of bottom EGs during the ‘first pass’ of the moving load test (at 80% of the average cracking load) and the PSPA slab moduli (table 8) were used for calculating the stresses. Unlike the initial analysis, the FAARFIELD rigid failure model (Brill, 2010) coefficients *a* and *c* were interpolated to consider the effect of subgrade strength (i.e., CBR) on the failure envelop. This analysis considered only those non-pre-cracked slabs with functional EGs on the north (i.e., 12-inch slab SF4N, and 9-inch slabs SF7N and SF8N). As previously indicated, the neutral axis position was assumed at the slab mid-depth for calculation of the bottom fiber strains in slab SF4N.

Table 14 shows results of the updated FAARFIELD analysis, including the coverages allocated by the design model to each stage of the fatigue life for 12- and 9-inch thick slabs. In addition to the updated predictions, table 14 includes results from the initial analysis for comparison purposes. The updated estimates of coverages for Stage 1+2 and Stage 3 show a dramatic increase after incorporating the responses measured during the moving load test in the analysis. This is mainly attributed to the observed increase in DF values. Based on the revised analysis, no surface distress should be expected within a reasonable timeframe if trafficking is continued using the D module with 80% of the bottom-up cracking load equally distributed between the two wheels (i.e., 40% per wheel). For accelerating the occurrence of surface distress, the DF values must be lowered by increasing the wheel load.

Table 14. FAARFIELD Predicted Fatigue Life Allocated to Each Stage

Thickness (inch)	R (psi)	CBR	Analysis	$DF = R/\sigma$	FAARFIELD Prediction	
					Stage 1+2	Stage 3
12	650	7.5	initial ¹	1.25	8	20
			updated ²	6.89	unlimited	unlimited
9	900	3.7	initial ¹	1.25	8	13
			updated ²	3.55	unlimited	unlimited

¹ Initial analysis performed prior to the commencement of CC8 S/F tests

² Updated analysis incorporating load-induced stresses during the moving load test

CC8 S/F trafficking on the outer lanes concluded after 49,920 cumulative passes on the south side. The moving load test was conducted using the S module at a wheel load of 84,000 lbs and 63,500 lbs for 12- and 9-inch slabs, respectively. These wheel loads yielded DF values of 1.62 and 1.33 for 12- and 9-inch slabs, respectively. Considering this precedent, it is recommended to resume the traffic test using the S module with increased wheel load level equivalent to 80% of the average cracking load. These wheel load levels are 87,000 lbs and 71,000 lbs for 12- and 9-inch slabs, respectively.

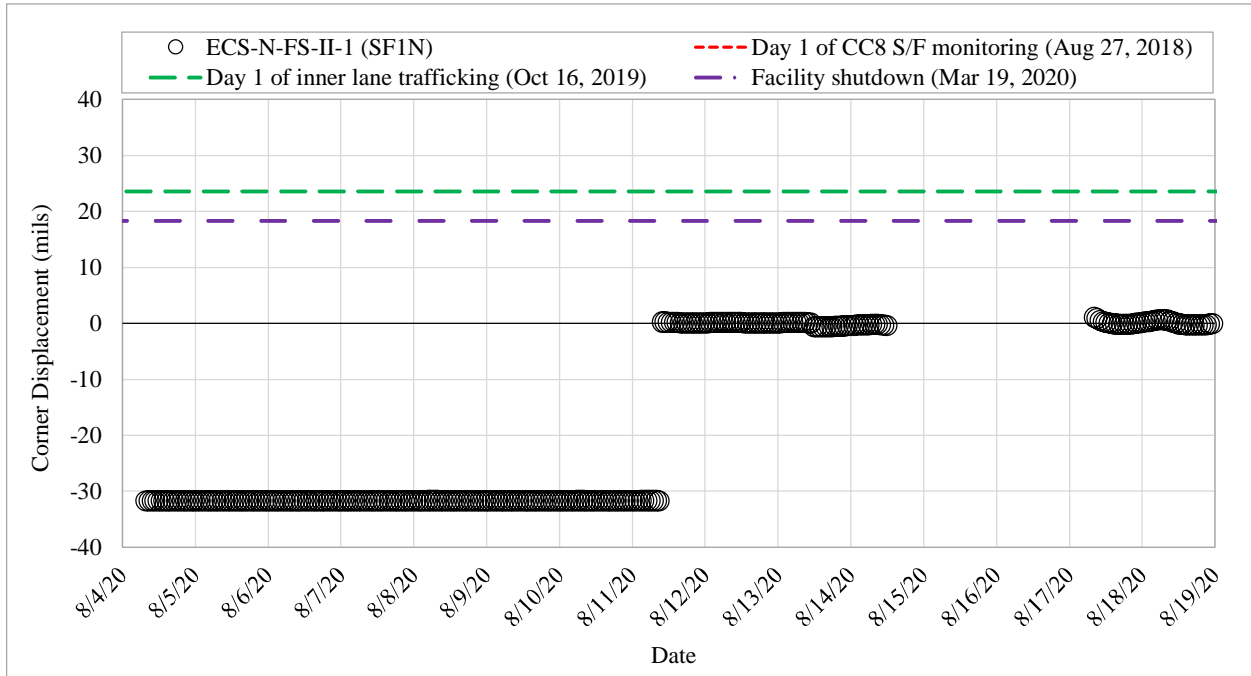
8. CC8 S/F TEST PAUSE AND TRAFFIC RESUMPTION

Trafficking on the CC8 S/F inner lanes commenced on October 16, 2019. The FAA temporarily shut down the test facilities due to the COVID-19 pandemic and therefore, trafficking had to be paused after March 19, 2020. In preparation for traffic test resumption, data collection and monitoring restarted on August 4, 2020. Also, new baseline HWD and PSPA tests, and a visual inspection of slab condition were conducted. The preparation efforts aimed at evaluating the slab curling condition and verifying the operational status of embedded instrumentation. This section documents the effort in preparation for traffic resumption.

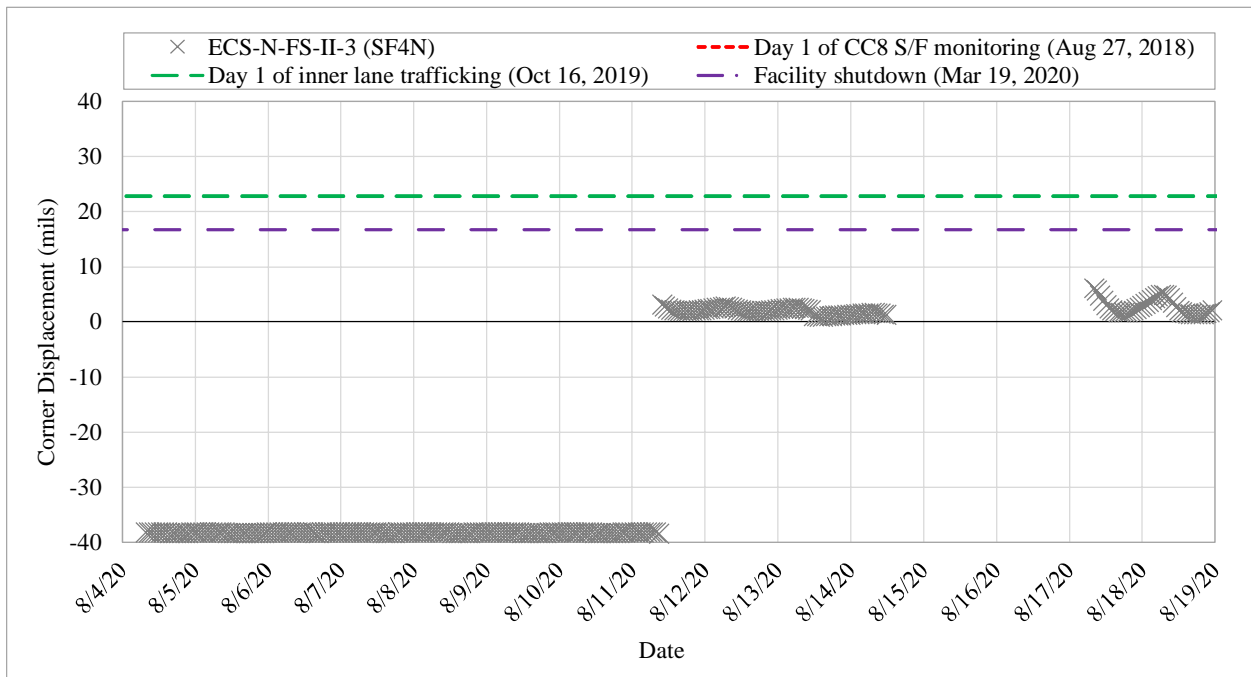
8.1 SLAB CURLING MONITORING

Figures 41 and 42 illustrate the slab corner displacement recorded by ECS. For comparison purposes, the figures include reference levels corresponding to the following events: day 1 of CC8 S/F monitoring, day 1 of inner lane trafficking, and facility shutdown. The trend of corner

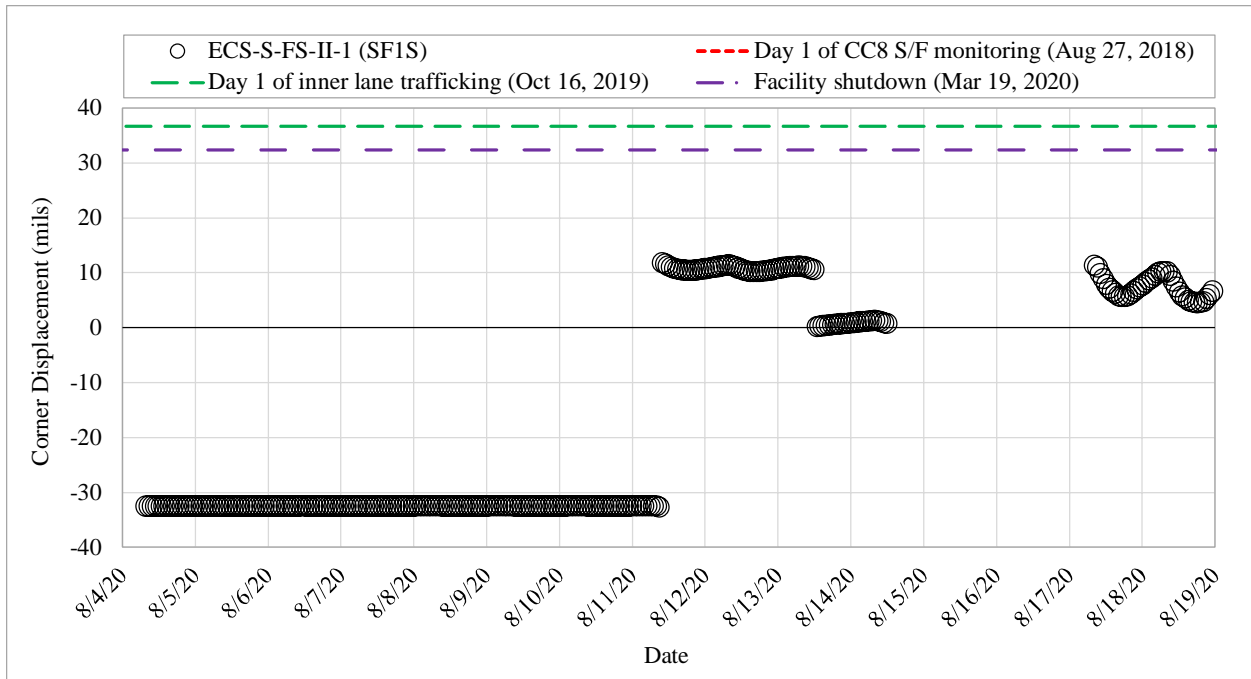
displacement for 12-inch thick slabs generally remained flat, while corners of 9-inch thick slabs show noticeable movement. During an instrumentation inspection conducted on August 11, a burnt terminal and tripped breaker in SPU 4 were reported. After SPU 4 was repaired, the high corner displacement recorded by ECS in 12-inch slabs returned to anticipated normal (lower) levels.



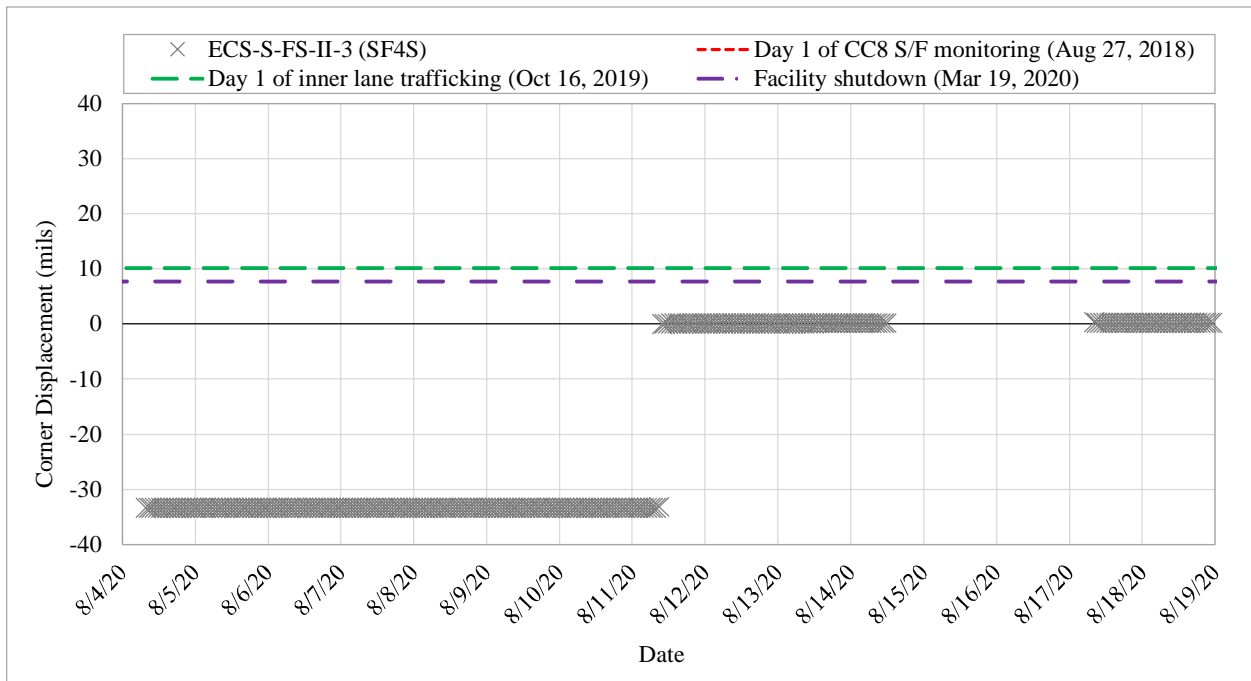
(a)



(b)

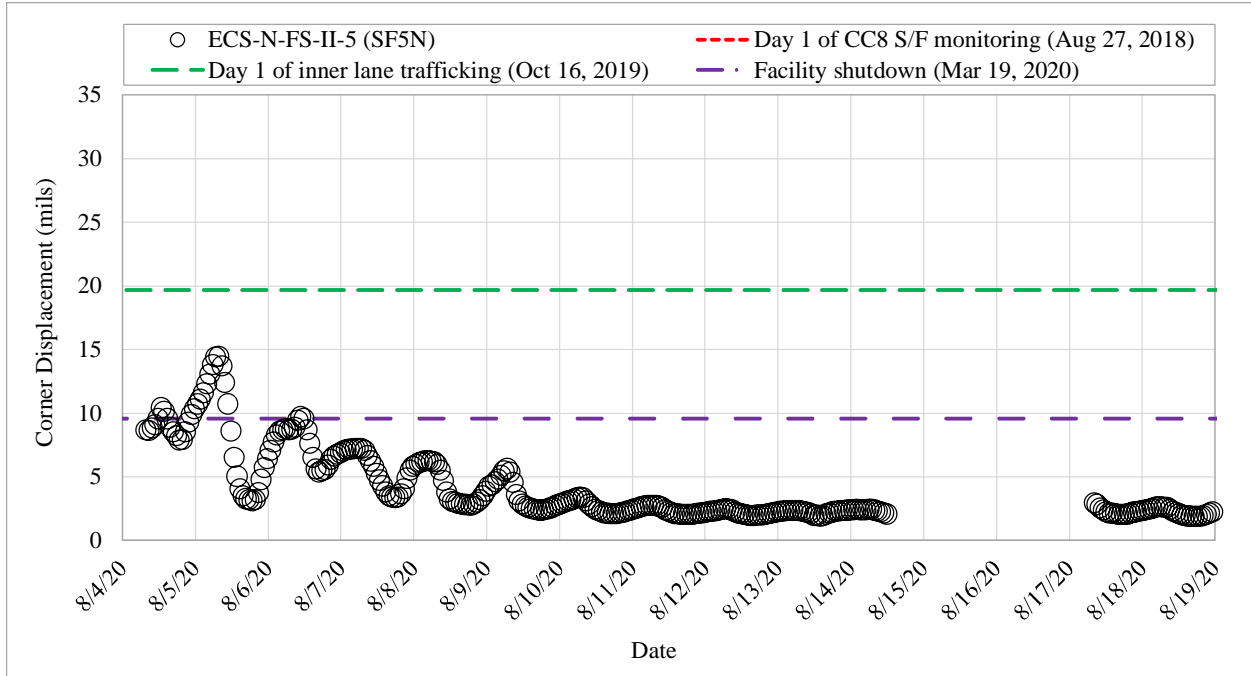


(c)

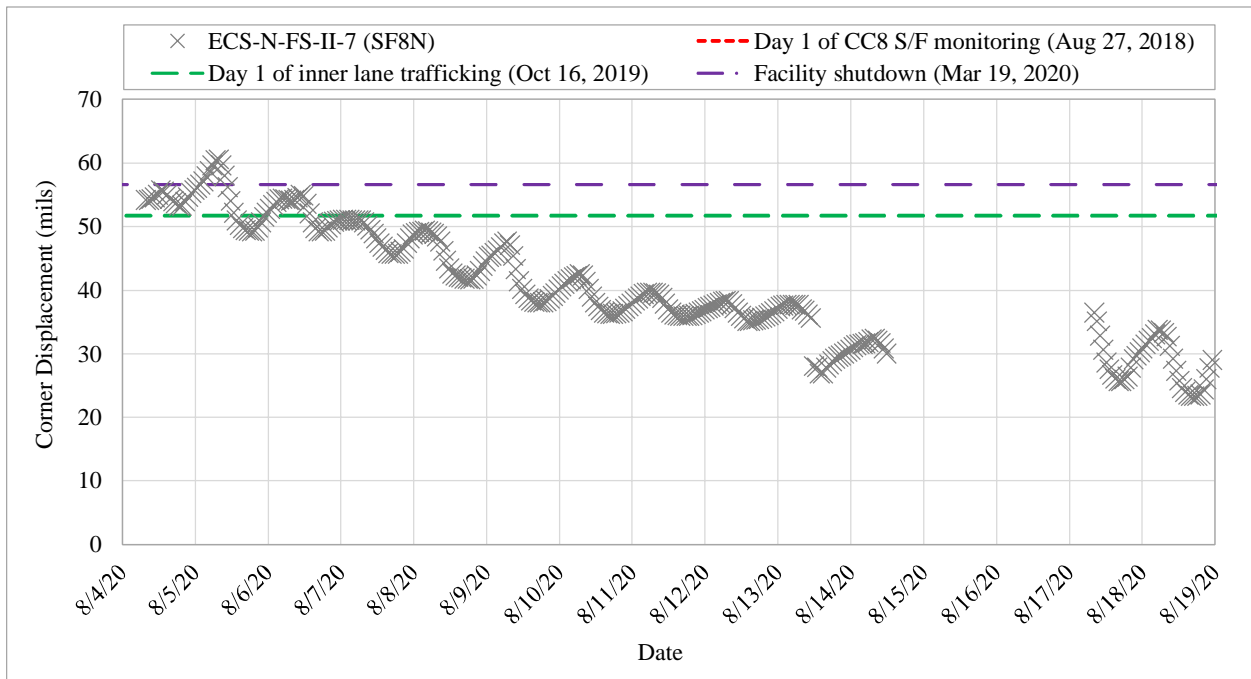


(d)

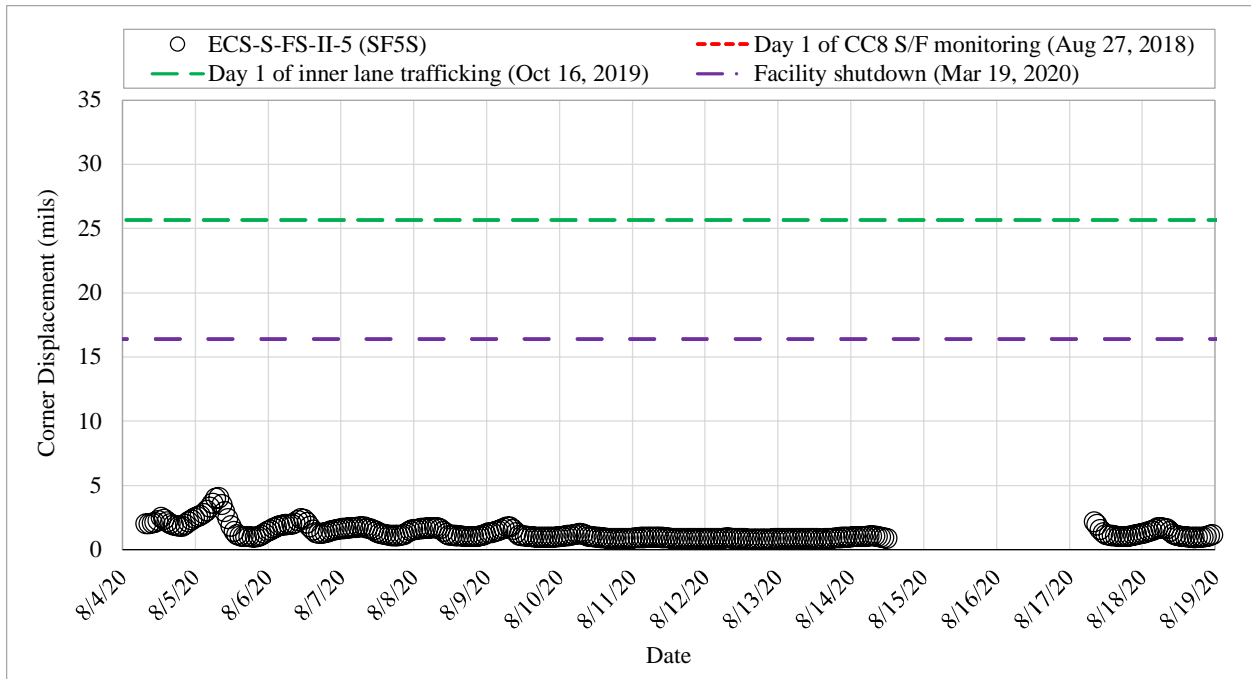
Figure 41. Corner Displacement in 12-inch Thick Slabs: (a) SF1N, (b) SF4N, (c) SF1S, (d) SF4S



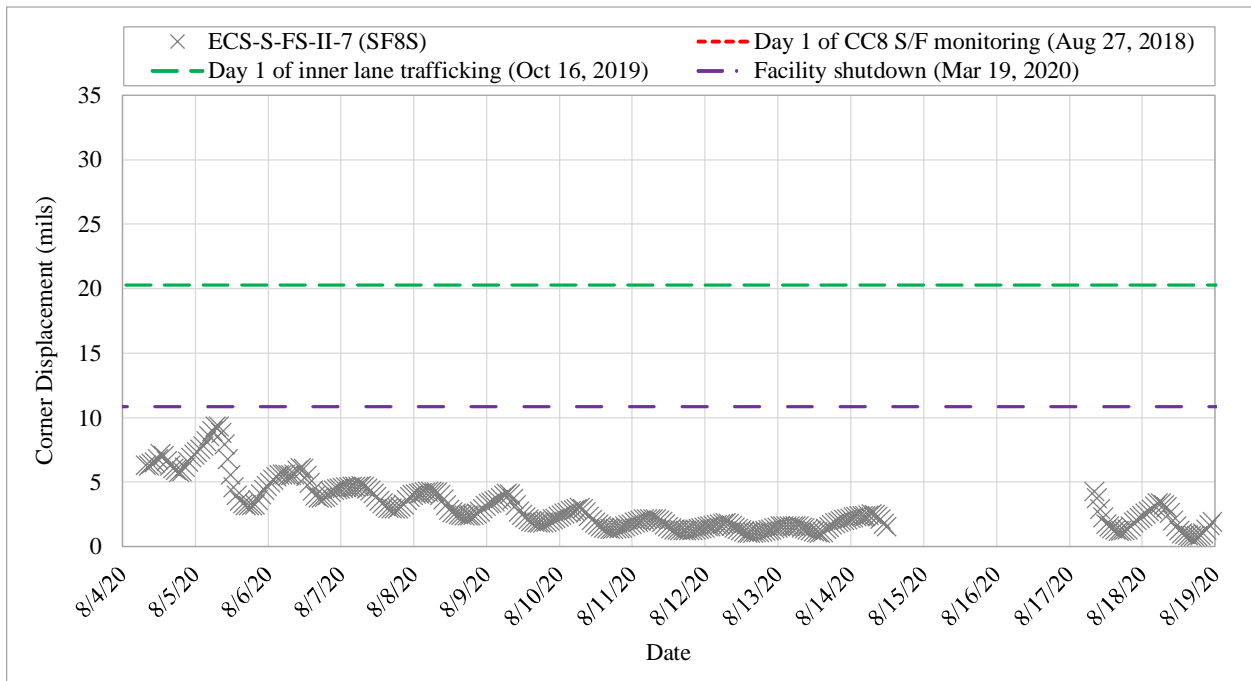
(a)



(b)



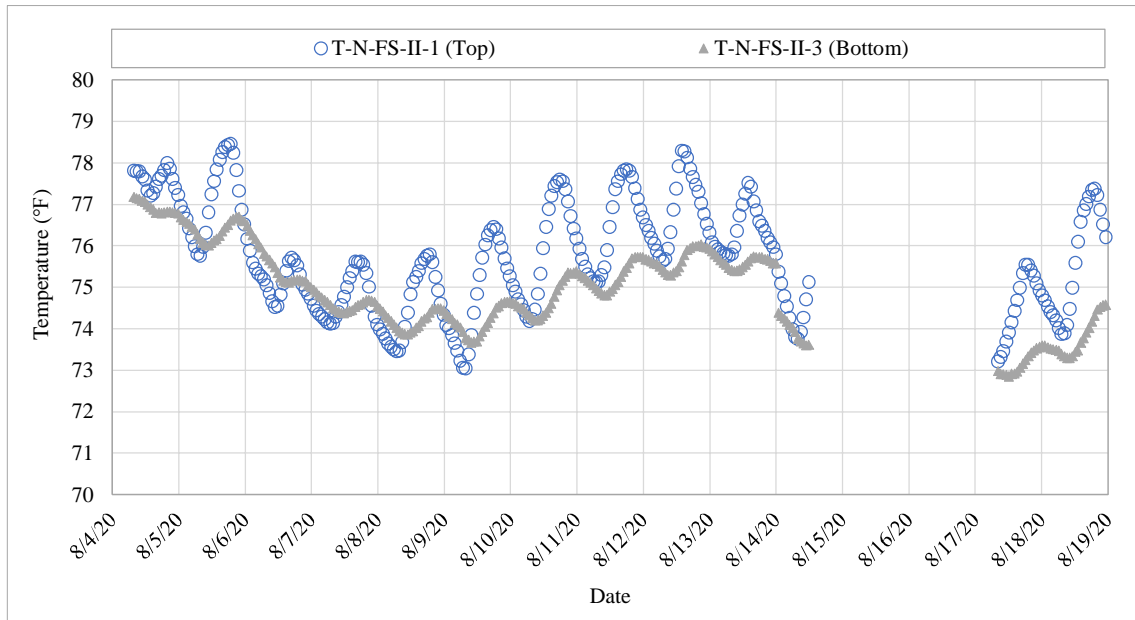
(c)



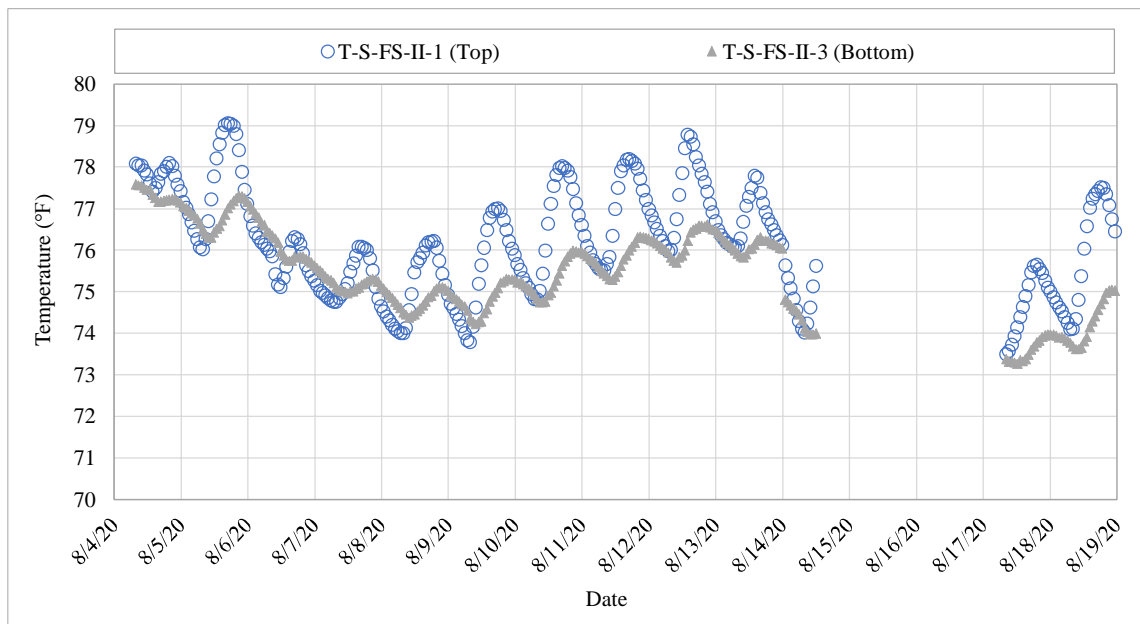
(d)

Figure 42. Corner Displacement in 9-inch Thick Slabs: (a) SF5N, (b) SF8N, (c) SF5S, (d) SF8S

Figure 43 shows that the fluctuation in temperature differential between the slab top and bottom agreed with the change in corner displacement of 9-inch thick slabs over time. Slab watering for corner displacement control started on August 4. In figure 42, the gradual attenuation of corner displacement fluctuation indicates the effectiveness of watering in controlling slab curling. Note that due to a pre-scheduled power outage in the facility, data collection was discontinued from August 14 to August 17.



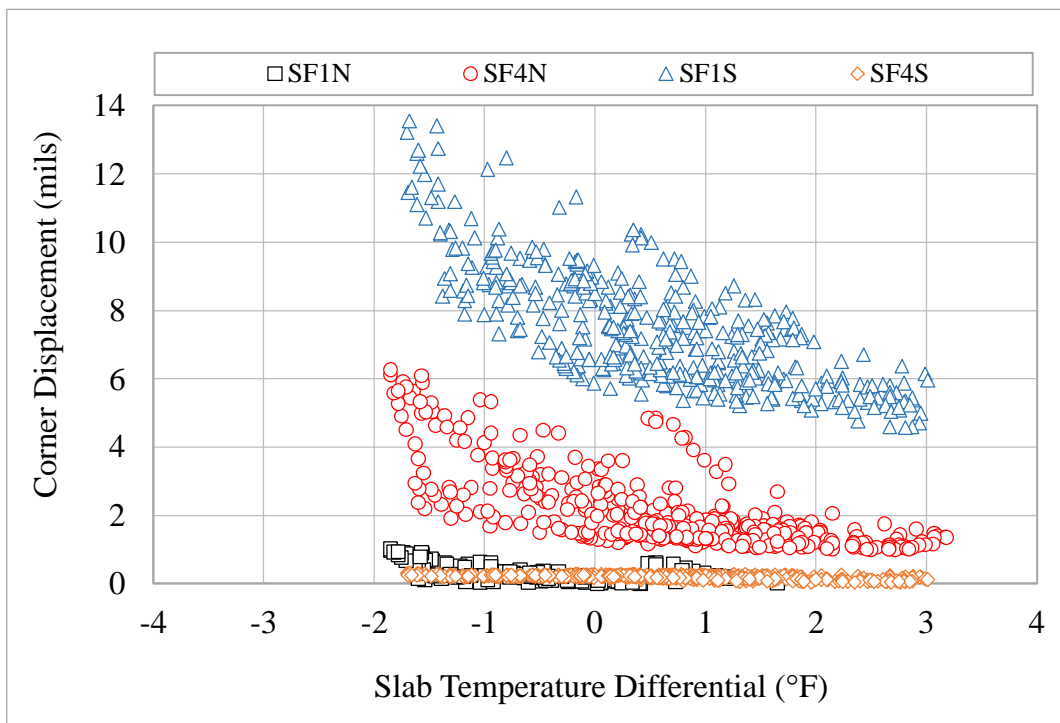
(a)



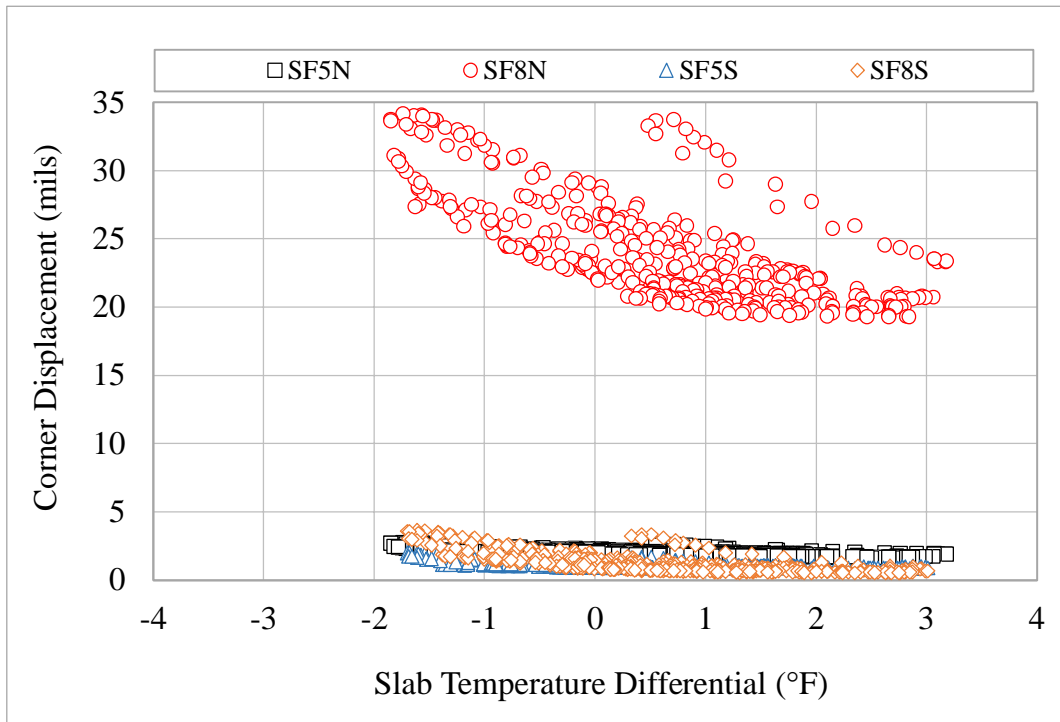
(b)

Figure 43. Daily Variation in Slab Temperature, August 18-20, 2020: (a) North, (b) South

Figure 44(a) and (b) show the slab corner displacement measured by ECS as a function of temperature differential (i.e., difference between top and bottom slab temperature) for 12- and 9-inch thick slabs, respectively. The figures plot data collected from August 18 to September 03, 2020. Negative temperature differentials indicate that the temperature at the slab top is lower than at the slab bottom, whereas the opposite applies for positive differentials. Contraction at the top of the slab resulted in the upward displacement of the corners (i.e., slab curling). Expansion of the slab top produced downward corner displacement. In both figure 44 (a) and (b), the range of corner displacement varies among the slabs. For instance, in figure 44 (a) the corner displacement for slab SF1N varies over a 10-mil range while the displacement for slab SF1S is only recorded over a 1-mil range. The upward corner displacement observed in all slabs decreases at varying rates as the negative temperature differential approaches to zero. In general, a non-uniform correlation between corner displacement and slab temperature differential was observed.



(a)



(b)

Figure 44. Corner Displacement vs. Temperature Differential: (a) 12-inch Slabs, (b) 9-inch Slabs

8.2 INSTRUMENTATION VERIFICATION

Verification of instrumentation functionality was performed after the shutdown of FAA facilities due to the COVID-19 pandemic. EG hourly static data from March 19 and August 11, 2020 were collected and reviewed. EGs are deemed ‘Functional’ if the following conditions were met: (a) EG exhibits non-zero response/reading on August 11, 2020, and (b) magnitude of the EG response on August 11, 2020 is similar to that from March 19, 2020. Otherwise, the EGs are ‘Disconnected’. Table 15 summarizes the status of EGs. Most of the EGs remained functional after the facility shut down on March 19. Monitoring of functional EGs will continue when traffic resumes.

Table 15. Assessment of Gauge Functionality for Traffic Resumption

Test Item	Slab Group	Thickness (inch)	R (psi)	Slab ID	Sensor ID	Status
North	1	12	650	SF1N	EG-N-FS-II-1	Functional
					EG-N-FS-II-2	Functional
					EG-N-FS-II-5	Functional
					EG-N-FS-II-6	Disconnected
				SF2N	EG-N-FS-II-7	Functional
					EG-N-FS-II-8	Functional
					EG-N-FS-II-13	Functional
					EG-N-FS-II-14	Functional
	SF3N	EG-N-FS-II-17	Functional			
		EG-N-FS-II-18	Disconnected			
		EG-N-FS-II-21	Disconnected			
		EG-N-FS-II-22	Disconnected			
	SF4N	EG-N-FS-II-23	Functional			
		EG-N-FS-II-24	Disconnected			
		EG-N-FS-II-29	Disconnected			
		EG-N-FS-II-30	Functional			
	5	9	900	SF5N	EG-N-FS-II-33	Functional
					EG-N-FS-II-34	Functional
					EG-N-FS-II-37	Functional
					EG-N-FS-II-38	Functional
				SF6N	EG-N-FS-II-39	Functional
					EG-N-FS-II-40	Functional
					EG-N-FS-II-45	Functional
					EG-N-FS-II-46	Functional
	SF7N	EG-N-FS-II-49	Functional			
		EG-N-FS-II-50	Functional			
		EG-N-FS-II-53	Functional			
		EG-N-FS-II-54	Functional			
SF8N	EG-N-FS-II-55	Functional				
	EG-N-FS-II-56	Functional				
	EG-N-FS-II-61	Functional				
	EG-N-FS-II-62	Functional				
7	9	900	SF8N	EG-N-FS-II-55	Functional	
				EG-N-FS-II-56	Functional	
				EG-N-FS-II-61	Functional	
				EG-N-FS-II-62	Functional	

Table 15 (continued)

Test Item	Slab Group	Thickness (inch)	R (psi)	Slab ID	Sensor ID	Status
South	2	12	650	SF1S	EG-S-FS-II-1	Functional
					EG-S-FS-II-2	Disconnected
				SF2S	EG-S-FS-II-13	Functional
					EG-S-FS-II-14	Disconnected
	SF3S			EG-S-FS-II-17	Functional	
				EG-S-FS-II-18	Disconnected	
	SF4S			EG-S-FS-II-29	Functional	
				EG-S-FS-II-30	Functional	
	4	9	900	SF5S	EG-S-FS-II-33	Functional
					EG-S-FS-II-34	Functional
				SF6S	EG-S-FS-II-45	Functional
					EG-S-FS-II-46	Functional
	SF7S			EG-S-FS-II-49	Functional	
				EG-S-FS-II-50	Functional	
8	SF8S			EG-S-FS-II-61	Functional	
				EG-S-FS-II-62	Functional	

8.3 UPDATED BASELINE HWD AND PSPA TESTS

New baseline HWD and PSPA tests were conducted on August 13-14, 2020 to evaluate the pavement condition after the temporary facility shutdown. The tests were performed at the locations indicated in the CC8 S/F test procedure, on both north and south inner lane slabs. HWD testing was conducted following the loading sequence also described in the CC8 S/F test procedure. Figure 45 compares maximum HWD deflections (D0) measured before the facility shutdown on March 09 with values measured on August 13. Deflections from both data sets are comparable. The same applies for the comparison between PSPA modulus data sets in figure 46.

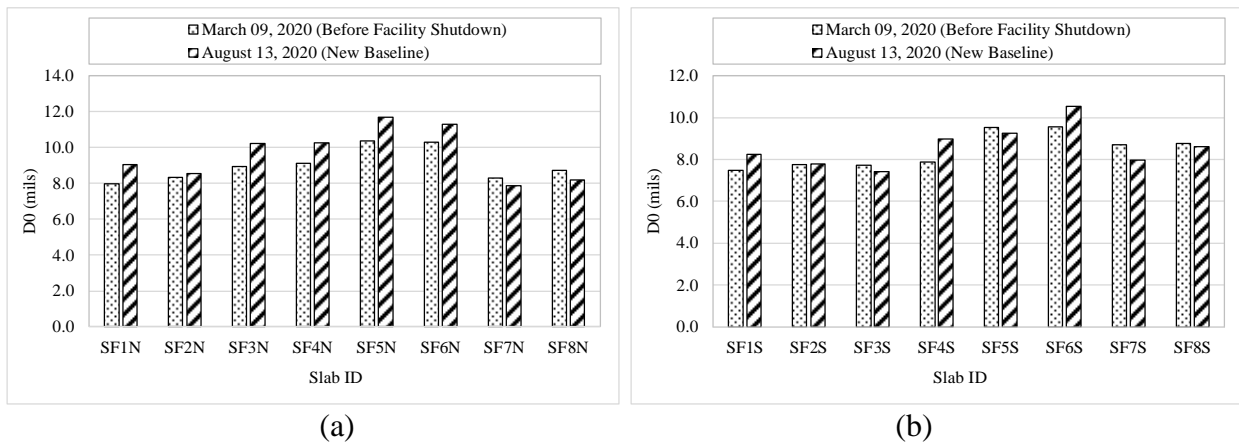


Figure 45. Maximum HWD Deflection at Center of Slabs: (a) North, and (b) South

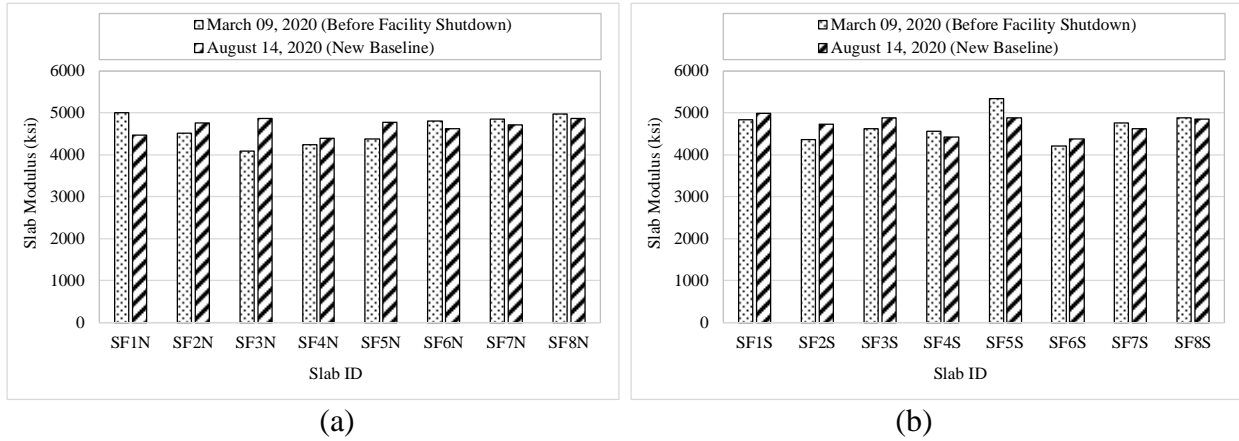


Figure 46. Slab Modulus from PSPA Testing at the Center of Slabs: (a) North, and (b) South

8.4 VISUAL INSPECTION OF SLAB CONDITION

The initial slab visual inspection conducted after reopening the facility reported: hairline cracks, joint faulting, corner displacement, and undulated slab surface. Slabs SF3N, SF4N, SF5S, and SF6S were further evaluated on August 17, 2020. Non-load related shrinkage cracks were observed on the surface of slab SF4N, close to the north edge as shown in figure 47.

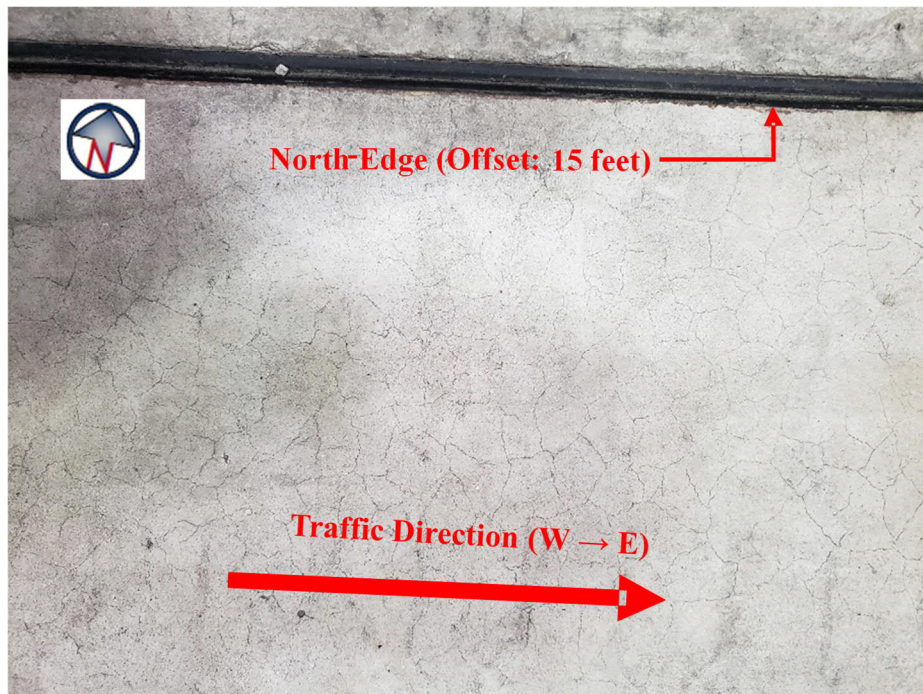


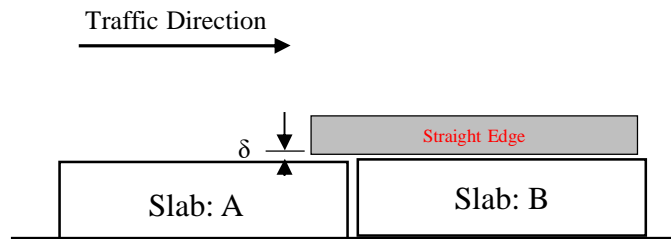
Figure 47. Shrinkage Cracks on Slab SF4N

During inspection of transverse joints, differences in the surface elevation of slabs SF4N and SF6S relative to SF3N and SF5S, respectively, were reported. As illustrated in figure 48(a) and (b), joint

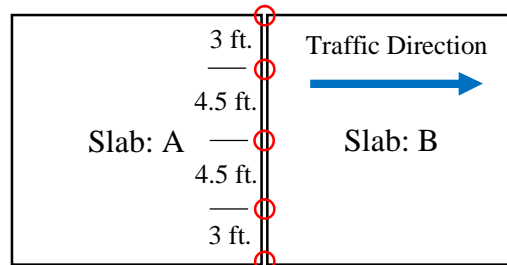
faulting is obtained by measuring the vertical difference (δ) between the bottom of a straight edge placed on top of the elevated slab and the top of the adjacent slab. Figure 48 (c) indicates the measurement locations along transverse joints. Table 16 summarizes the faulting measurements. Note that faulting of 0.0625 inch is reported at a +/-12 ft. offset from the centerline. This measurement location is the nearest to the wheel track (i.e., +/-10 ft. offset)



(a)



(b)



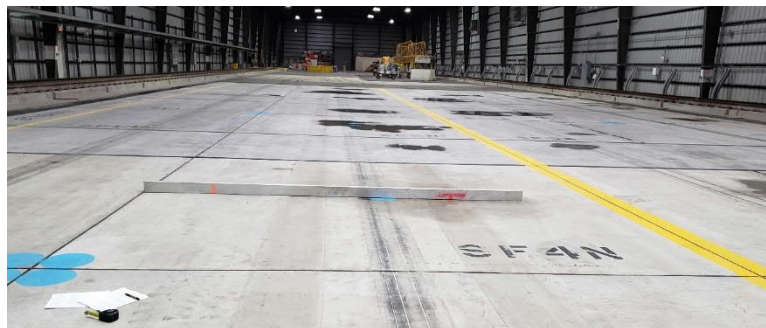
(c)

Figure 48. Joint Faulting Measurement: (a) Field Measurement, (b) Faulting Interpretation, (c) Measurement Locations

Table 16. Summary of Joint Faulting Measurement

Joint	Offset (ft.)	Faulting (inch)
Transverse (SF3N-SF4N)	-15	0.1250
	-12	0.0625
	-7.5	0.1250
	-3	0
	0	0.0625
Transverse (SF5S-SF6S)	0	0.1250
	3	0.0625
	7.5	0.0625
	12	0.0625
	15	0.0313

The slab surface elevation was mapped using the straight edge as shown in figure 49. Figure 49(a) illustrates the straight edge placed transversely across the middle of slab SF4N, aligned with the slab north edge at one of its ends (i.e., offset -15 ft.). The surface depression (i.e., vertical difference between the straight edge bottom and the slab surface) was measured at different locations, as shown in figure 49 (b). Contours of the surface elevation were generated for slabs SF3N, SF4N, SF5S, and SF6S as shown in figure 50 (a) and (b). The interior of the slabs exhibited higher depression.

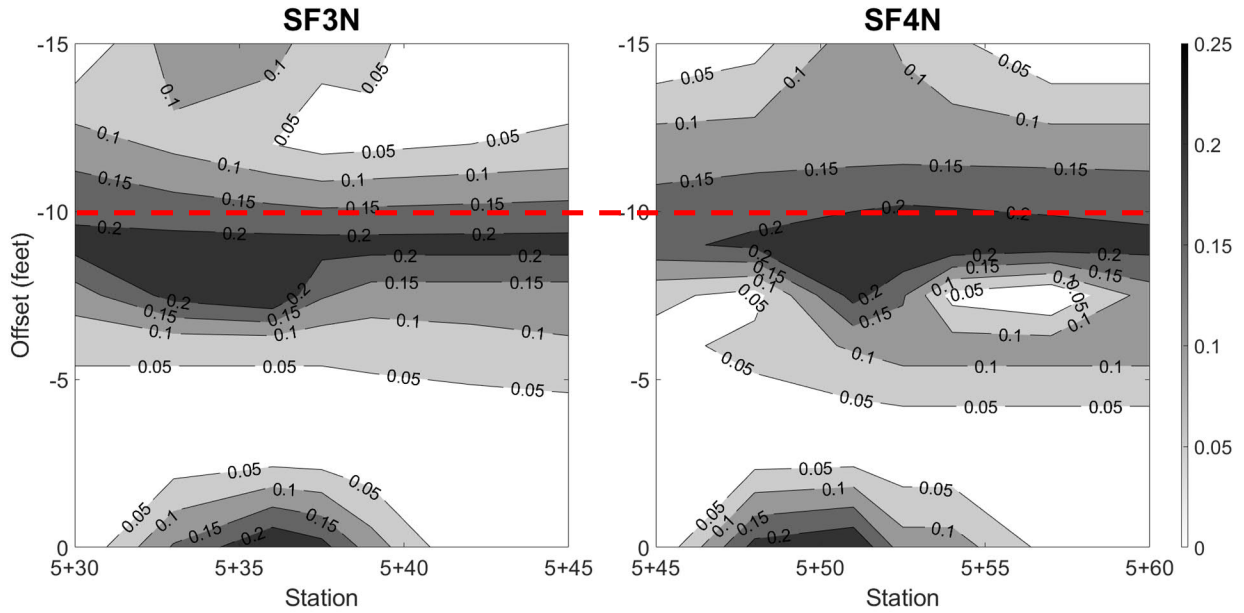


(a)

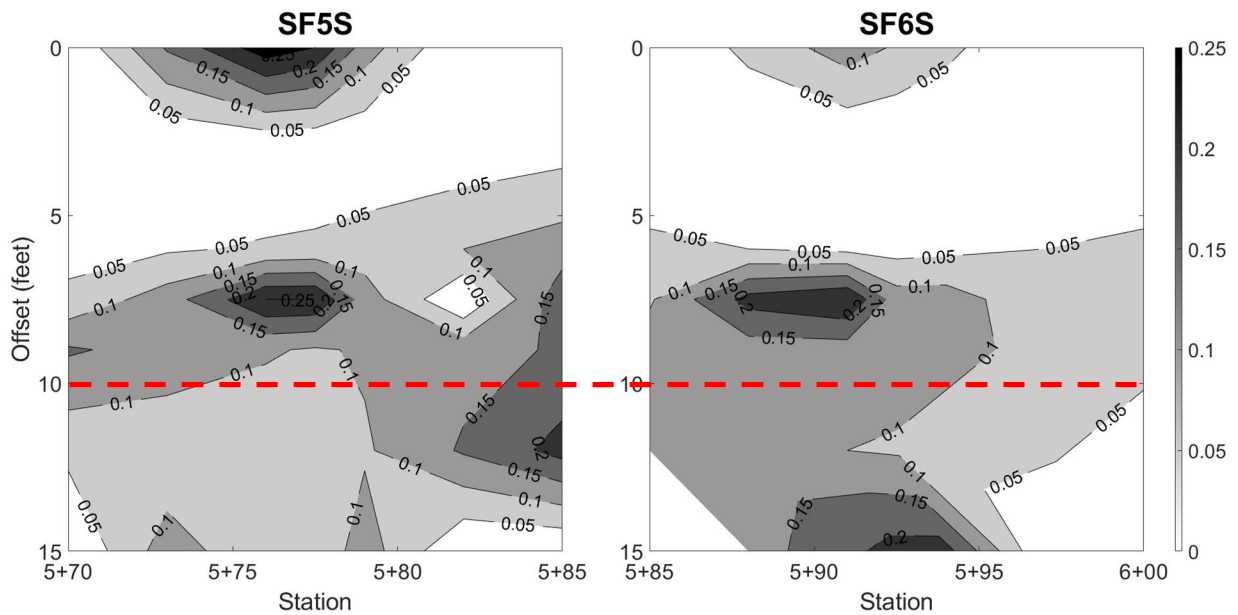


(b)

Figure 49. Surface Elevation Mapping: (a) Placement of Straight Edge, (b) Surface Measurement



(a)



(b)

Figure 50. Slab Surface Elevation Map: (a) North (SF3N and SF4N), (b) South (SF5S and SF6S)

8.5 RECOMMENDATION ON TRAFFIC RESUMPTION

Watering effectively reduced slab corner displacement. The assessment of instrumentation condition concluded that all the ECS and most of the EGs that were operational at the time the facility shut down (March 19, 2020), remain functional to date. Both HWD maximum deflection and PSPA slab modulus showed minimum changes since the facility shutdown. No major issue

was identified during visual inspections on the surface, joints, and corners of selected slabs. Based on the outcome of the pre-traffic assessment, resumption of CC8 S/F traffic test and related activities in compliance with the test plan is recommended.

9. CONCLUSIONS

The CC8 S/F full-scale tests are aimed at determining the cracking strength and fatigue life of concrete slabs. Data from individual slabs are obtained regarding: (1) slab cracking strength for comparison to ASTM C78; (2) crack initiation and propagation in unnotched slabs (Stages 1 and 2); (3) the trade-off between concrete flexural strength and slab thickness; and (4) the effect of subgrade strength. Traffic tests on the inner lanes were paused after March 19, 2020 due to the COVID-19 pandemic. This report documents the static load test results and preliminary findings of the moving load tests based on the 25,000 cumulative vehicle passes completed prior to the facility shutdown. Distress, instrumentation, and field-testing data collected were reviewed and analyzed. Preliminary conclusions of this study are summarized in the following sections.

9.1 INSTRUMENTATION AND FIELD TESTING

- The strain response of EGs installed at the top and bottom of slabs was used to monitor crack initiation, full-depth, and full-length propagation. Throughout the 25,000 cumulative passes completed on March 19, 2020, EG strain responses did not provide any clear indication of bottom-up crack initiation in the intact unnotched slabs.
- PSPA tests were conducted throughout the trafficking period to determine the change in concrete modulus. After 25,000 passes, the average modulus for 12 inch thick slabs was less than that for 9 inch thick slabs. There was a positive correlation between R and concrete modulus. PSPA data showed no overall decrease in modulus that would indicate degradation in the structural integrity of slabs.
- In general, the ISM derived from HWD test data indicated no degradation in slab integrity. Test items on subgrade with CBR 3-4 had higher ISM than those on subgrade with CBR 7-8 on both the north and south sides. This suggests that the effect of subgrade strength may be offset by the variability in material strength of shallower layers (e.g., higher compressive strength of P-306MR observed for slab groups on subgrade with CBR 3-4 compared to groups on subgrade with CBR 7-8).

9.2 CRACKING STRENGTH

- The load-related stress, causing rupture of the PCC slabs, were determined under static loads. These CC8 load-related stress levels were below 55% of the concrete flexural strength of field cured beams. In the previous CC6 strength tests (Yin, 2011), the estimated rupture stress at the bottom extreme fiber (as derived from EG response data) was close to the concrete flexural strength. This discrepancy between CC8 and CC6 is most likely due to the presence of non-load-related built-in stresses in the slab.

9.3 MOVING LOAD TESTS

- Moving loads were applied to the inner lane slabs for full-depth and full-length crack propagation (and crack initiation in the case of not pre-cracked slabs). However, no surface

distress was observed on the slabs after 25,000 cumulative passes. Therefore, the effect of concrete flexural strength and thickness as well as subgrade strength cannot be evaluated at this point. The comparison of notched versus unnotched slabs was also unfeasible due to the lack of performance data.

- The effect of concrete flexural strength and thickness based on the state of stress was investigated. Current stress ratios were calculated as the ratio of the stress at the slab bottom fiber to R . It was observed that stress ratios on 12-inch slabs were smaller than 9-inch slabs, indicating a possible delay in crack initiation (i.e., Stage 1) for 12-inch slabs as it observed during the traffic tests on outer lanes.
- The effect of subgrade strength was preliminarily investigated based on the state of stress. Load-induced stresses were estimated at the bottom of intact slabs over subgrade of CBR 7-8 (SF5N and SF6N), and subgrade of CBR 3-4 (SF7N and SF8N). The load-induced stress in slabs over subgrade of CBR 7-8 was lower than those over subgrade of CBR 3-4. Therefore, longer fatigue life for slabs on subgrade of CBR 7-8 may be anticipated.

9.4 FIELD EXPERIMENT VERSUS FAARFIELD

- The initial FAARFIELD predictions were updated using load-induced stress derived from EG strain responses during the moving load test. The revised predictions showed an extreme increase in the number of coverages required to complete Stage 1+2 and Stage 3. This is mainly attributed to the observed increase in DF values. Based on the revised analysis indicated that no surface distress should be expected within a reasonable timeframe if trafficking is continued using the D module with 80% of the bottom-up cracking load equally distributed between the two wheels (i.e., 40% per wheel).
- For accelerating the occurrence of surface distress, the DF values must be lowered by increasing the wheel load. Considering both fatigue life and DF values reported during CC8 S/F traffic test on the outer lanes, it is recommended to resume traffic on the inner lanes using the S module with increased wheel load level equivalent to 80% of the cracking load. These wheel load levels are 87,000 lbs and 71,000 lbs for 12- and 9-inch slabs, respectively.

10. REFERENCES

ASTM International Standard C78. 2018. Standard Test Method for Flexural Strength of Concrete (Using Simple Beam with Third-Point Loading), West Conshohocken, PA, 2018.

ASTM International Standard D5340-12. 2012. Standard Test Method for Airport Pavement Condition Index Surveys, West Conshohocken, PA.

Brill, D. R., Calibration of FAARFIELD Rigid Pavement Design Procedure, Report No. DOT/FAA/AR-09/57, Federal Aviation Administration, New Jersey, 2010.

Federal Aviation Administration. 2017. AC 150/5320-6F, Airport Pavement Design and Evaluation.

Federal Aviation Administration. 2018. AC 150/5370-10H, Standard Specifications for Construction of Airports.

Guo, E. H., Brill, D. R., and Yin, H. 2012. Concrete Pavement Strength Investigations at the FAA National Airport Pavement Test Facility. Proc., 7th RILEM International Conference on Cracking in Pavements, 337-346.

CC8 Phase 4 Strength/Fatigue Traffic Test Report – Outer Lane. Delivery Order 005: NAPTF Support.

Rollings, R.S. 1988. Design of Overlays for Rigid Airport Pavements, Report No. DOT/FAA/PM87/19, Federal Aviation Administration, Washington, D.C.

Tomlinson, C., Aponte, R., Gawrysiak, J., Mahaffay, B., and Flynn, M. Construction Cycle 8 (CC8) Construction Report. 2018. CSRA, Inc., Delivery Order 050: Construction Support.

Yin, H. 2011. CC6 Traffic Test Part I - Concrete Pavement Failure Investigations of MRS1-N.